ABSTRACT

CANTY, NICHOLAS KÖNIG. Deoxypodophyllotoxin Synthase – Investigating the Pivotal Carbon-Carbon Bond Formation in Aryltetralin Lignan Biosynthesis
(Under the direction of Dr. Wei-chen Chang).

Lignans constitute a large and diverse class of phenylpropanoids widely distributed throughout the plant kingdom.[1] They exhibit a wide range of pharmaceutically relevant biological activities and consequently have attracted widespread research interest. One of the most well-known and commercially relevant lignans is podophyllotoxin from mayapple species (*Podophyllum peltatum, Sinopodophyllum hexandrum*).[2] It exhibits potent antineoplastic, antiviral, and antimalarial properties and as such has become a lead compound for drug development.[3,4] In fact, podophyllotoxin and semi-synthetic structural analogs etoposide and teniposide are listed on the World Health Organization's List of Essential Medicines, and dozens more have entered clinical trials.[5,6] Unsurprisingly, the pharmacological importance of podophyllotoxin has elicited numerous synthetic approaches over the years. Nonetheless, current production requires isolation of key precursors from producing plants.[7–10]

Deoxypodophyllotoxin synthase, a non-heme iron enzyme, catalyzes the oxidative cyclization of its substrate (-)-yatein to (-)-deoxypodophyllotoxin, thereby completing the aryltetralin lignan scaffold via stereo- and regioselective $C(sp^2)$-$C(sp^3)$ bond formation.[11] Deeper insight into how DPS facilitates this synthetically challenging transformation may provide a foundation for developing sustainable and economical chemoenzymatic methods to access this important molecular scaffold.

Deoxypodophyllotoxin Synthase – Investigating the Pivotal Carbon-Carbon Bond Formation in Aryltetralin Lignan Biosynthesis

by
Nicholas König Canty

A thesis submitted to the Graduate Faculty of
North Carolina State University
in partial fulfillment of the
requirements for the degree of
Master of Science

Chemistry

Raleigh, North Carolina
2023

APPROVED BY:

Dr. Wei-chen Chang Committee Chair	Dr. Vincent Lindsay
Dr. Reza Ghiladi	

BIOGRAPHY

Nicholas König Canty was born in 1997 in New York City to an American father and a German mother before moving to Germany with his family, at the age of two. Nicholas grew up and attended school in Frankfurt, Germany and moved to Munich to begin his studies in Chemistry and Biochemistry at the Ludwig Maximilian University. After completing a bachelor's thesis on the topic of palladium-catalyzed acylations of organozinc compounds in the research group of Dr. Paul Knochel, he received his B.S. degree in 2020.

Nicholas moved to Raleigh to pursue a graduate degree at North Carolina State University in 2021. He joined the research group of Dr. Wei-chen Chang where his research involved the study of enzymatic transformations and their use for the synthesis of natural products.

ACKNOWLEDGMENTS

First and foremost, I would like to express my sincere gratitude to my advisor, Dr. Wei-chen Chang, for his invaluable guidance and mentorship. He provided me with a fascinating research project and encouragement to succeed. His enthusiasm and immense knowledge have been a constant source of motivation and inspiration throughout my time at NC State.

In addition, I would like to thank Dr. Vincent Lindsay, whose class on reaction mechanisms helped me see chemistry with new eyes. I am also grateful to Dr. Reza Ghiladi for his heartfelt dedication to the program and personal advocacy on behalf of its students.

Furthermore, I would like to say thank you to my fellow labmates, past and present, for countless hours sharing great conversations, good food, and many late nights. A special debt of gratitude is owed to Tzu-Yu Chen and Lide Cha for making me feel so welcome right from the start and for never hesitating to interrupt their own work to lend their thoughtful advice and guidance. This thesis would not have been possible without you.

Lastly, I am forever grateful to my parents, Thomas and Anne, and my brother, Christopher, for their endless love, support, and encouragement.

TABLE OF CONTENTS

LIST OF FIGURES

LIST OF SCHEMES

LIST OF TABLES

LIST OF ABBREVIATIONS

2OG – 2-oxoglutarate

4CL – 4-coumarate-CoA-ligase

AD – anno domini

aq. – aqueous

Ar – aryl

Bn – benzyl

C4H/C3H/C3'H – cinnamate 4-hydroxylase/cinnamate 3-hydroxylase/cinnamate 3'-hydroxylase

CA – coniferyl alcohol

CAD – cinnamyl alcohol dehydrogenase

cat. – catalytic

CCoAOMT – caffeoyl-CoA-*O*-methyltransferase

CCR – cinnamoyl-CoA-reductase

CoA – coenzyme A

COMT – caffeate 3-*O*-methyltransferase

CYP – cytochrome P450

DBU – 1,8-Diazabicyclo[5.4.0]undec-7-ene

DCM – dichloromethane

DG – directing group

DIR – dirigent protein

DMP – Dess-Martin periodinane

DPS – deoxypodophyllotoxin synthase

dr – diastereomeric ratio

E. coli – *Escherichia coli*

EA – ethyl acetate

EDTA – ethylenediamine

eq. – equivalent

et al. – et alia

FDA – Food and Drug Administration

HAT – hydrogen atom transfer

HCT – hydroxycinnamoyl-CoA: shikimate/quinate hydroxycinnamoyl transferase

HMPA – hexamethylphosphoramide

HPV – human papillomavirus

IPTG – isopropyl β-D-1-thiogalactopyranoside

LB – Luria-Bertani

LDA – lithium diisopropylamide

LHMDS – lithium hexamethyldisilazide

MDO – methylenedioxy

NADPH – nicotinamide adenine dinucleotide phosphate

NAD(P)H – nicotinamide adenine dinucleotide phosphate or nicotinamide adenine dinucleotide

Ni-NTA – Nickel nitriloacetic acid

NMR – nuclear magnetic resonance

o.n. – overnight

OD600 – optical density

OMT – *O*-methyltransferase

PAL – phenylalanine ammonia lyase

PDB – protein data bank

PLR – pinoresinol lariciresinol reductase

Pp – Podophyllum peltatum

r.t. – room temperature

Sh – Sinopodophyllum hexandrum

S. hexandrum – Sinopodophyllum hexandrum

SAM – *S*-adenosyl methionine

SDH – secoisolariciresinol dehydrogenase

SDS-PAGE – sodium dodecyl sulfate-polyacrylamide gel electrophoresis

S_N – nucleophilic substitution

TAL – tyrosine ammonia lyase

TB – Terrific Broth

TFA – trifluoroacetic acid

THF – tetrahydrofuran

TLC – thin layer chromatography

Tris – tris(hydroxymethyl)aminomethane

UV-Vis – ultraviolet-visible

wt – wild-type

CHAPTER 1: Introducing Non-Heme Iron Enzyme Deoxypodophyllotoxin Synthase (DPS)

1.1 Introduction: Fe/2OG Dependent Oxygenases

Mononuclear non-heme iron and 2-oxoglutarate (Fe/2OG) dependent oxygenases constitute a diverse superfamily of enzymes ubiquitous in both eukaryotes and prokaryotes. They are involved in numerous vital biological processes, including primary metabolism and the biosynthesis secondary metabolites, oxygen sensing, and controlling metal homeostasis and epigenetic regulation.[12]

While most characterized Fe/2OG enzymes have been shown to catalyze hydroxylation, the enzyme family exhibits impressively diverse reactivity, facilitating a range of oxidative transformations. Other known transformations include halogenation, desaturation, epoxidation and C-C/O/N bond formation (Figure 1.1).[13] Unsurprisingly, Fe/2OG dependent enzymes are particularly well represented in natural product biosynthesis.[14] Furthermore, their unique ability to selectively functionalize inert C-H bonds is of high interest to the synthetic community, as selective C-H activation presents one of the major challenges and current limitations of organic synthesis.[15] Though numerous powerful organometallic reactions have been developed in pursuit of overcoming this challenge, they often require the use of toxic and expensive reagents, as well as the presence of directing groups in close proximity to the targeted C-H bond.[16] In enzymatic catalysis, selectivity is instead imparted by the precise alignment of a substrate in the enzyme's active site.

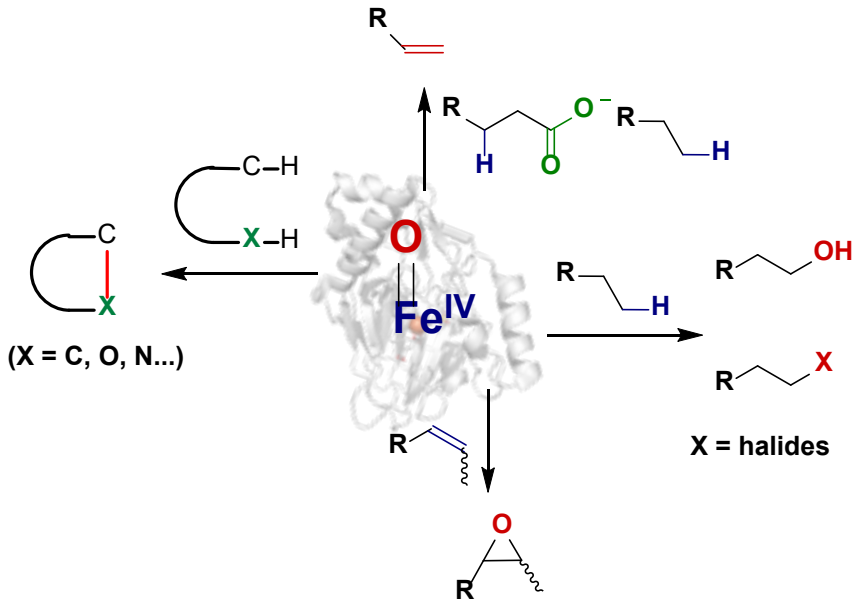

Figure 1.1: Functional diversity of Fe/2OG enzymes.

Despite their functional diversity, Fe/2OG enzymes share common mechanistic principles. In 1982, Hanauske-Abel and Günzler first proposed a comprehensive mechanism for Fe/2OG hydroxylases (Scheme 1.1). Though the reaction mechanism was based on little experimental data, it has since been largely validated.[17]

In the resting state, the mononuclear Fe(II)-center is coordinated by a 2-His, 1-Glu/Asp motif (hence termed the facial triad) and three water molecules in octahedral geometry. Bidentate coordination of co-substrate, 2-oxoglutarate (2OG), displaces two water ligands, and binding of the primary substrate in the active site displaces the final water ligand. This results in square-pyramidal geometry and leaves an open coordination in axial position. Oxidative addition of molecular oxygen to the open coordination site yields a reactive Fe(III)-superoxo intermediate. Subsequent attack of the distal oxygen on C2 of 2OG triggers O-O bond cleavage and decarboxylation of 2OG to succinate, thereby forming a short lived, high-valent (S = 2) Fe(IV)-oxo (ferryl) complex. The reactive ferryl complex then abstracts a hydrogen atom from the

substrate, resulting in a substrate radical and reduced Fe(III)-OH (ferric-hydroxide) complex. This process is commonly referred to as hydrogen atom transfer or hydrogen atom abstraction. “Rebound” of the coordinated hydroxyl ligand on the substrate radical produces the hydroxylated product and regenerates Fe(II). The catalytic cycle is completed by release of the product and succinate (Scheme 1.1). The general mechanism up until C-H bond cleavage is broadly applicable to members of the Fe/2OG family, however the fate of the substrate radical is dependent on the specific chemical environment of the respective enzyme’s active site (Scheme 1.1).[18,19]

Scheme 1.1: Conserved mechanism of Fe/2OG hydroxylases.

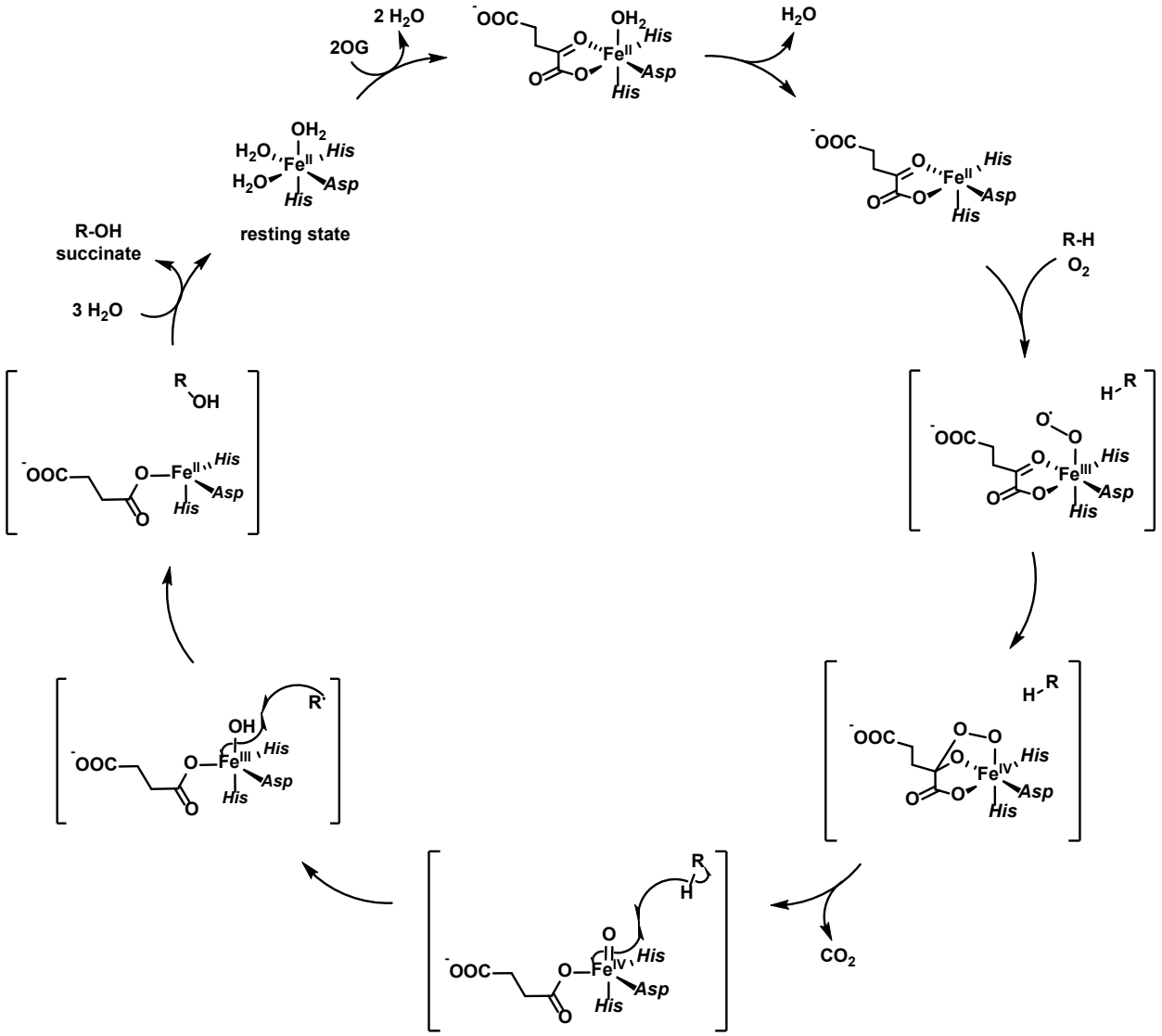

1.2 Structure and Relevance of Lignan Natural Products

Lignans are a large and diverse class of natural products widely distributed in the plant kingdom and are found in roots, rhizomes, stems, leaves, seeds and fruits.[1] They are derived from the stereoselective oxidative coupling of two phenylpropanoid monomers, also termed monolignols, at the olefin of the propenyl moiety. The resulting β-β' (C8-C8') bond defines the substance class. Another defining characteristic of lignans is that oxygen represents the only heteroatom incorporated into the scaffold. Despite this rather narrow definition and common origin, lignans exhibit a vast structural diversity. A highly divergent biosynthesis leads to different patterns in cyclization, dividing lignans into structural subtypes: furofurans, furans, dibenzylbutanes, dibenzyllactones, dibenzylcyclooctadienes, aryltetralins and arylnaphtalenes (Figure 1.2).[20] Lignans exhibit a broad range of biological activities including antioxidant, antimicrobial, antiviral and antineoplastic properties, making them a rich source of lead compounds for drug development .[4,21–24] In fact, many lignan-rich plants have been known to humans for their therapeutic properties and potential health benefits and have a long history of use in traditional medicine and diet. Prominent examples include flax (*Linum usitatissimum*), sesame (*Sesamum indicum*), forsythia (*Forsythia suspensa*), olive (*Olea europaea*) and schisandra (*Schisandra chinensis*).[25]

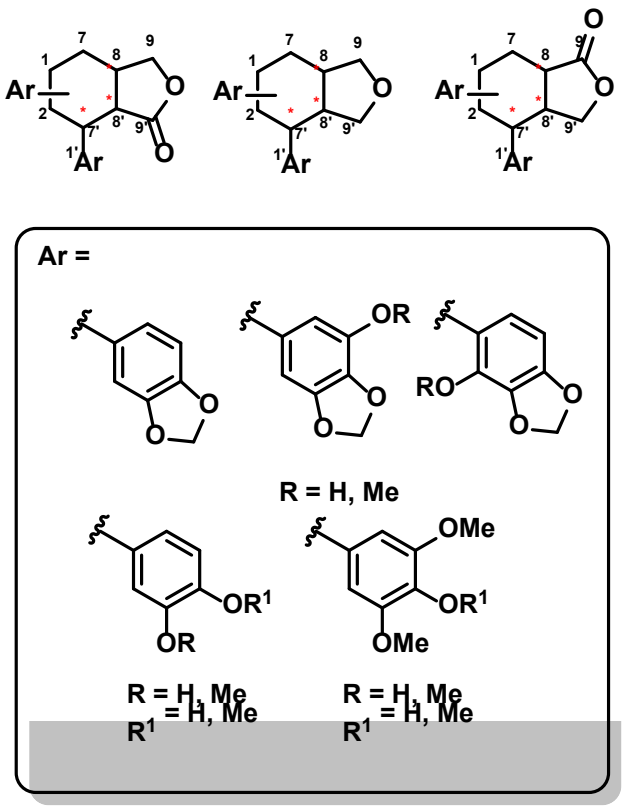

Figure 1.2: Structural features of aryltetralin lignans.

One of the most well-known lignans is podophyllotoxin, an aryltetralin lignan found in mayapple species (*Podophyllum peltatum, Sinopodophyllum hexandrum*). Aryltetralin lignans are characterized by a core scaffold comprised of 4 ring systems connected by 3 consecutive chiral systems, as depicted in Figure 1.2. Podophyllotoxin is a potent anti-cancer and anti-viral agent that prevents cell division by destabilizing microtubules. It was FDA-approved for the treatment of external warts caused by human papillomavirus (HPV) in 1990, but has been used since 1942.[2,26] Medicinal use of *Podophyllum* was reported as early as 900 AD in The Leech Book of Bald, an English pharmaceutical reference book.[26] Since the 1970s, dozens of podophyllotoxin derived drugs have entered clinical trials. Deoxypodophyllotoxin, a biosynthetic precursor to podophyllotoxin, was approved for phase I trials by the National Medical Products

Administration in China in 2017.[27] Its semi-synthetic glycosylated congeners etoposide and teniposide were approved for medical use in the United States in 1983 and 1992 respectively. Both are used for the treatment of several cancer types, including lung cancer, lymphoma, leukemia, neuroblastoma and testicular cancer. Etoposide is listed in the World Health Organization's List of Essential Medicines.[5,6,28] Structures of deoxypodophyllotoxin, podophyllotoxin, as well as etoposide, teniposide and etopophos are depicted in Figure 1.3.

However, natural occurrence of podophyllotoxin and its structural analogs (podophyllotoxins) in producing organisms is often very low. Podophyllotoxin accounts for 0.3-1.0% (w/w) of rhizome mass, making extraction laborious and uneconomical.[29,30] As a result, an estimated 300,000 lbs. of mayapple roots are harvested per year to cover the demand of podophyllotoxin and epipodophyllotoxin, the precursor to etoposide and teniposide.[7] As mayapple species are not suitable to farm, wild *S. hexandrum* has become an endangered species.[31,32]

Therefore, gaining insight into the biosynthesis of podophyllotoxins can provide a foundation for developing sustainable and economical methods of production and for guiding the search for new pharmaceutically relevant structural analogs.

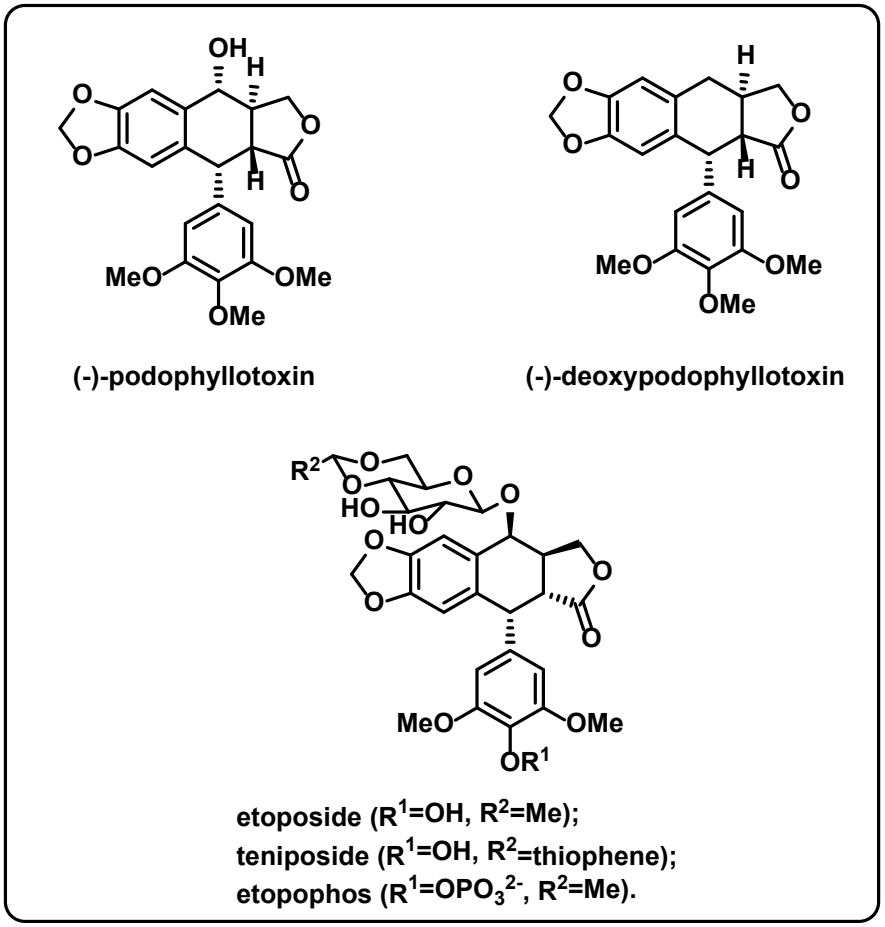

Figure 1.3: Structures of deoxypodophyllotoxin, podophyllotoxin, and analogs etoposide, teniposide and etopophos.

1.3 Current Understanding of Lignan Biosynthesis

1.3.1 Podophyllotoxin Biosynthesis

Coniferyl alcohol (CA) serves as the common precursor to all lignans known to date. It is a product of phenylpropanoid metabolism, a highly important metabolic pathway in plants giving rise to not only lignans, but also flavanones, chalcones, stilbenes and various other classes of natural products, diverting a significant flux of phenylalanine and tyrosine from protein synthesis to produce *para*-hydroxy-cinnamyl alcohols.[33,34]

Initial extrusion of ammonia is facilitated by phenylalanine ammonia lyase (PAL)/tyrosine ammonia lyase (TAL) to produce the corresponding cinnamic acid. Subsequent hydroxylation and *O*-methylation are catalyzed by cyctochrome P450 monooxygenases and SAM-dependent *O*-methyltransferases respectively, while reduction to the alcohol is enabled via CoA-ligation by 4-coumarate-CoA-ligase (4CL) to produce the corresponding activated CoA-ester followed by successive reductions by NADPH-dependent cinnamoyl-CoA reductase (CCR) and cinnamyl alcohol dehydrogenase (CAD) (Scheme 1.2).[35–40]

Scheme 1.2: Biogenesis of coniferyl alcohol.

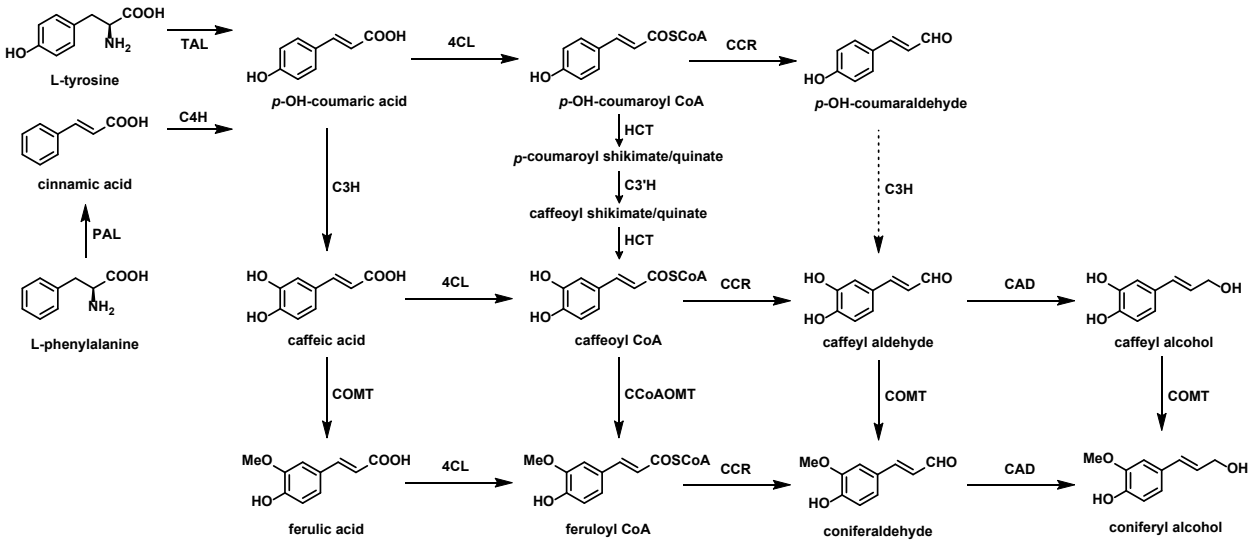

Dimerization of CA proceeds in a phenolic oxidative coupling reaction facilitated by an oxidase, e.g. laccase, and dirigent protein (DIR), in which the oxidase generates a phenoxy radical and DIR induces stereo- and regio-selective coupling of two monolignol radical species (Scheme 1.3).[41–43]

The regioselective coupling mediated by DIR facilitates the formation of the lignan-defining C8-C8’ bond yielding pinoresinol. This step is also the source of chirality in lignan biosynthesis. Overall, three new bonds (including one C-C and two C-O bonds) and four new stereocenters are generated in this single-step coupling – a feat unachievable by synthetic methods. Notably, DIR-mediated polymerization of CA yields the structural polymer lignin, the second most abundant biopolymer on earth.[44–47]

Scheme 1.3: Formation of matairesinol in the scaffold-generating pathway in lignan biosynthesis.

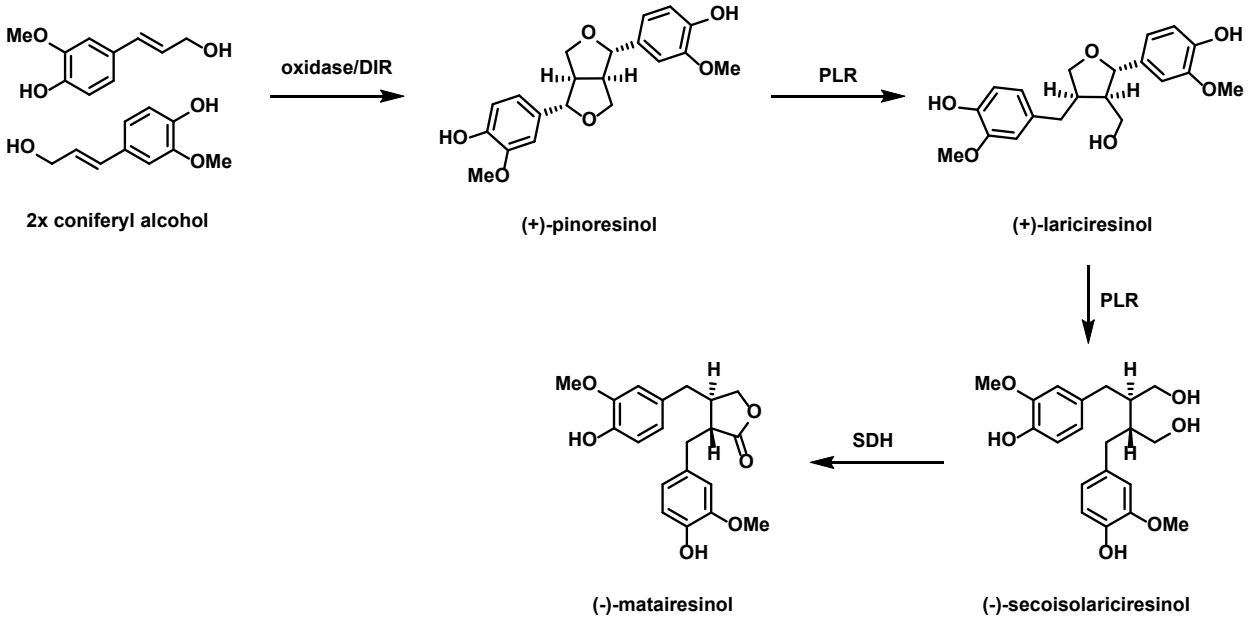

Following dimerization, pinoresinol is subjected to consecutive reduction by pinoresinol lariciresinol reductase (PLR), producing lariciresinol and secoisolariciresinol. Secoisolariciresinol in turn is oxidized by secoisolariciresinol dehydrogenase (SDH) to form matairesinol. Overall, four different lignan scaffolds are produced: furofuran (pinoresinol), furan (lariciresinol), dibenzylbutane (secoisolariciresinol) and dibenzyllactone (matairesinol). A vast majority of lignan natural products originate from either one of the four intermediates. At each step, some intermediate flux is diverted from the general pathway and subjected to scaffold-tailoring transformations, which ultimately is the key to complexity generation in lignan biosynthesis.[48–50]

The pathway from matairesinol to podophyllotoxin is no exception. A series of scaffold-tailoring transformations on the dibenzylbutyrolactone scaffold of matairesinol eventually generate yatein, the immediate precursor to the aryltetralin lignan scaffold (Scheme 1.4). Due to

the pharmacological importance of podophyllotoxin, its biosynthesis has been the subject of extensive research, and responsible genes have been largely identified.[51]

The conversion of (-)-matairesinol to (-)-pluviatolide proceeds via methylenedioxy (MDO) bridge formation. In plants, such transformations are commonly associated with the cytochrome P450 monooxygenase family (CYP). Leveraging massively parallel sequencing of *Sinopodophyllum hexandrum* and *Podophyllum peltatum* transcriptomes, two P450s involved in (-)-pluviatolide formation were identified, *Sh*CYP719A23 and *Pp*CYP719A24.[52] Unlike Fe/2OG enzymes, CYPs utilize heme as a cofactor and require an external reductant like NAD(P)H, but both utilize activation of molecular oxygen to generate a reactive, high-valent iron complex to perform oxidative transformations on their primary substrates.[53]

In the next step, (-)-pluviatolide is converted to (-)-bursehernin via *O*-methylation at C4'. Subsequent C5'-hydroxylation yields (-)-5'-desmethyl-yatein, followed by C5'-*O*-methylation to yield (-)-yatein.[54] This alternating pattern of hydroxylation and subsequent *O*-alkylation represents a common scaffold-tailoring strategy in lignan biosynthesis.[55] Like MDO-bridge formation, aryl-hydroxylations in lignan biosynthesis are generally associated with CYPs. *O*-Methylations are catalyzed by (*S*)-adenosyl-L-methionine (SAM) dependent *O*-methyltransferases. In 2015, Lau and Sattely identified the remaining four enzymes responsible for the conversion of (-)-pluviatolide to (-)-deoxypodophyllotoxin in *Sinopodophyllum hexandrum*. SAM-dependent *O*-methyltransferases *Sh*OMT3 and *Sh*OMT1 were implicated in (-)-bursehernin and (-)-yatein formation respectively, while C-5' hydroxylation was shown to be catalyzed by *Sh*CYP71CU1.[8] Finally, iron and 2-oxoglutarate (Fe/2OG) dependent deoxypodophyllotoxin synthase *Sh*DPS (also known as *Sh*2-ODD) facilitates cyclization of (-)-yatein to (-)-deoxypodophyllotoxin, completing the aryltetralin lignan scaffold.[8,56] To date,

the gene responsible for the conversion of deoxypodophyllotoxin to podophyllotoxin remains elusive.[27]

Scheme 1.4: Biosynthetic route to aryltetralin scaffold.

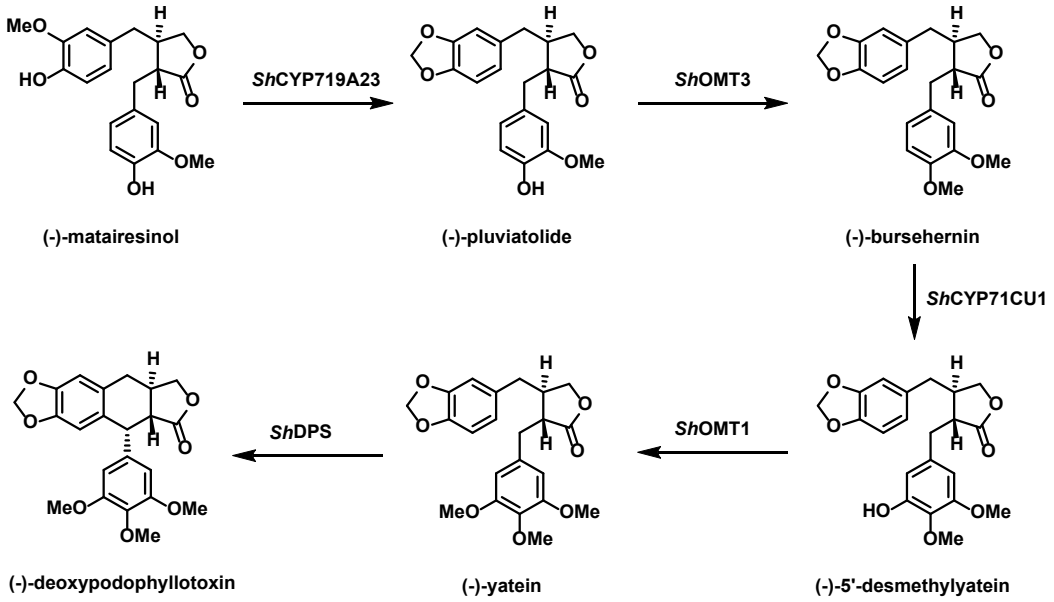

1.3.2 Deoxypodophyllotoxin Synthase

Scheme 1.5: DPS-catalyzed stereo- and regioselective carbon-carbon bond formation.

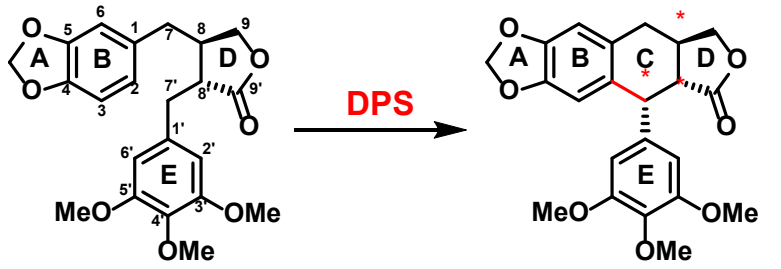

(-)-yatein (-)-deoxypodophyllotoxin

From a synthetic chemist's perspective, the DPS-catalyzed cyclization is quite remarkable. Overall, DPS facilitates a two-electron oxidation (on substrate (-)-yatein), forging a $C(sp^2)$-$C(sp^3)$ bond and a stereocenter in the process (Scheme 1.5). Performing an analogous coupling reaction using organic synthetic methodology would require the prior installation of an orthogonal pair of functional groups at C2 and C7' (and/or the presence of directing groups to guide reactivity), as well as the use of a suitable catalyst. The introduction of such compatible functional group pairs is often far from trivial. Late-stage installation is usually hampered by inherent molecular steric and electronic constraints, while introducing them early in the synthesis necessitates their compatibility with subsequent transformations.[57] Additionally, the strict control of chirality presents a further obstacle thus far limiting the commercial use of producing podophyllotoxins by pure total synthesis.[58]

The mechanism of the DPS-catalyzed transformation was elucidated by our lab in 2022 using substrate-bound structural analysis, biochemical assays with substrate analogs and chemical model studies (Scheme 1.6).[11] Initial hydrogen atom abstraction of the pro-*R* hydrogen atom at C7' by a presumptive Fe(IV)-oxo species generates a substrate radical and Fe(III)-

hydroxo intermediate. Instead of canonical hydroxyl-rebound, electron transfer from the substrate radical to the ferric metal center generates Fe(II)-OH and results in a secondary carbocation at C7'. Subsequently, C-C bond formation is likely induced by rotation of the benzodioxole moiety, positioning its C6 in close proximity to the C7'-centered carbocation.

Scheme 1.6: Proposed mechanism of DPS-mediated cyclization.

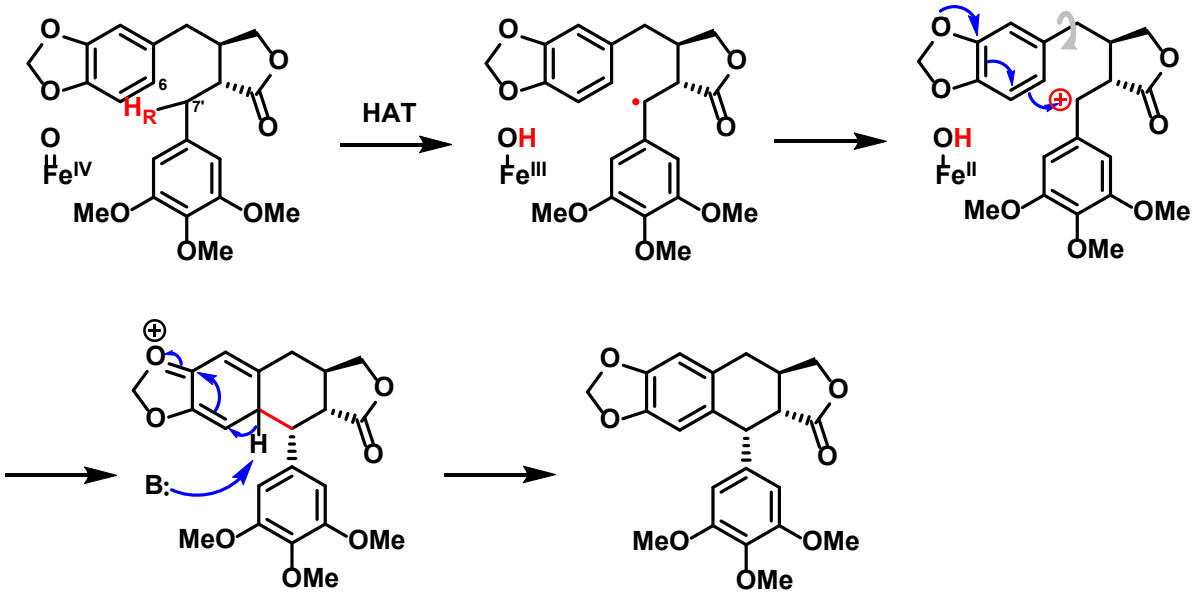

1.4 Developments in the Preparation of Podophyllotoxins

The clinical importance of podophyllotoxin and structural analogs (podophyllotoxins) has elicited numerous synthetic approaches in recent years. A brief overview of notable reports is provided in the following, more details on chemical and biological syntheses can be found in reviews by Shen,[27] and Zhang.[58]

1.4.1 Chemical Synthesis

A concise total synthesis of racemic podophyllotoxin employing a C(sp^3)-H arylation strategy was reported in 2014 by Maimone et al. (Scheme 1.7).[59] The corresponding arylation precursor was prepared via diastereoselective cycloaddition, positioning an acetonide-directing group adjacent to the desired arylation site. Subsequent Pd(II)-catalyzed coupling with 3,4,5-trimethoxyphenyl iodide was followed by a one-pot cleavage of the acetonide directing group and the acetal group, products (±)-podophyllotoxin and (±)-epipodophyllotoxin were obtained in 43% and 33% respectively. Notably, this late-stage arylation strategy enables rapid access to podophyllotoxin analogs with varied E-ring substitution.

Scheme 1.7: Total synthesis of racemic (epi)-podophyllotoxin reported by Maimone et al.[59]

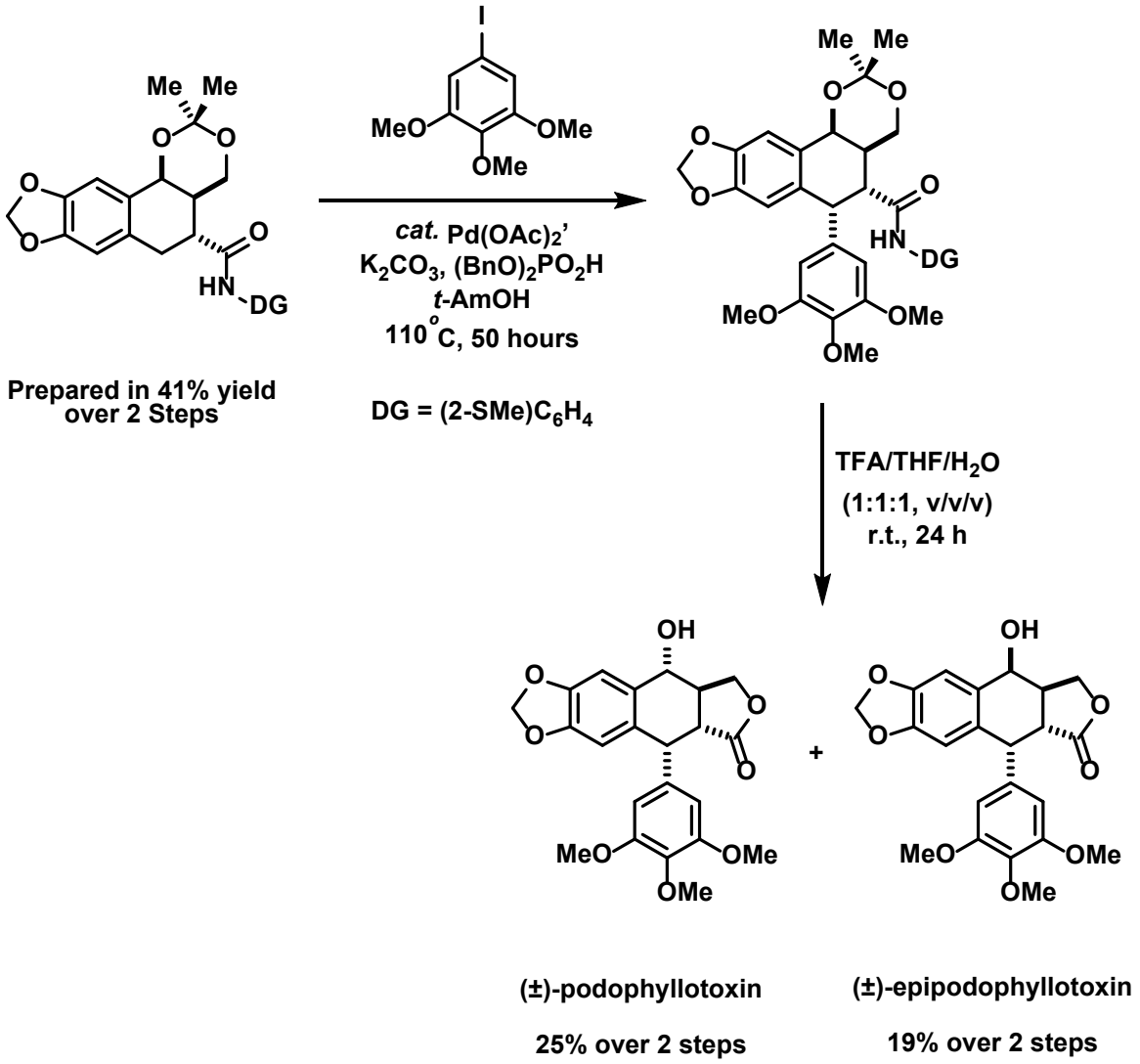

1.4.2 Synthetic Biology

In a 2019 study, Sattely and co-workers reconstituted the entire biosynthetic pathway from coniferyl alcohol to (-)-deoxypodophyllotoxin by transient co-expression of 16 genes from *Sinopodophyllum hexandrum* in *Nicotiana benthamiana* (tobacco).[60] Accumulation of 4.3 mg/g dry plant weight (-)-deoxypodophyllotoxin was detected, and 0.71 mg/g dry plant weight (-)-

deoxypodophyllotoxin were obtained following isolation. As shown in Scheme 1.8, several enzymes are utilized to convert L-phenylalanine to products (-)-deoxypodophyllotoxin and (-)-4'-desmethylepipodophyllotoxin (not isolated) *in planta*. Notably, exogenous addition of on-pathway intermediates was not required due to the native presence of L-phenylalanine. For more detail, please refer to the original publication.[60]

Scheme 1.8: Biological synthesis of (-)-deoxypodophyllotoxin via plant chassis reported by Sattely et al.[60]

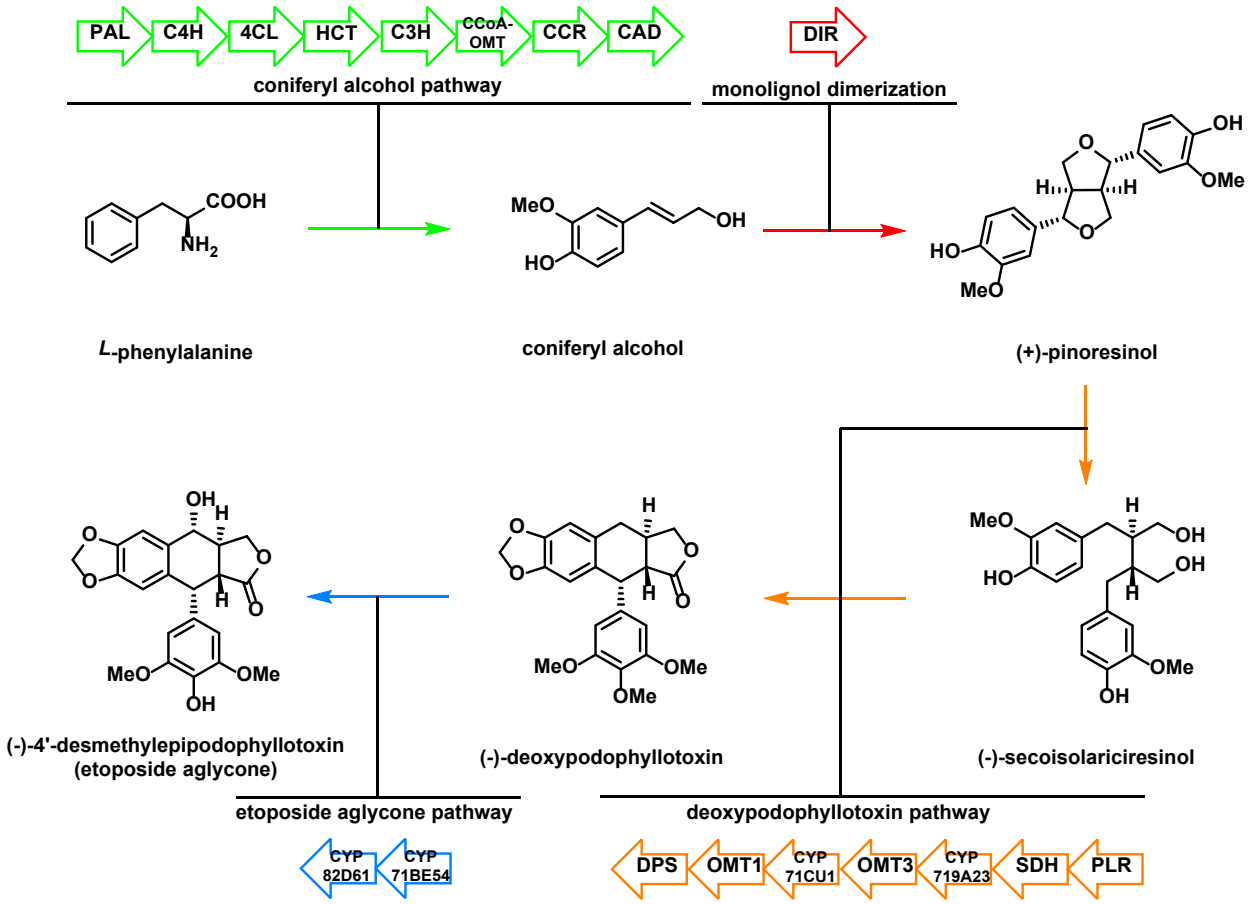

1.4.3 Chemoenzymatic Synthesis

An asymmetric chemoenzymatic synthesis of (-)-podophyllotoxin was reported by Renata and co-workers. Key intermediate (-)-yatein was produced in a copper-mediated

oxidative enolate coupling of a chiral oxazolidinone with an ester.[61] DPS was then leveraged to forge the critical C-C bond, producing (-)-deoxypodophyllotoxin. Completion of the synthesis was achieved via benzylic oxidation with CrO_3 and subsequent diastereoselective reduction with L-selectride, yielding (-)-podophyllotoxin (Scheme 1.9).

Scheme 1.9: Chemoenzymatic synthesis of (-)-podophyllotoxin leveraging DPS.[61]

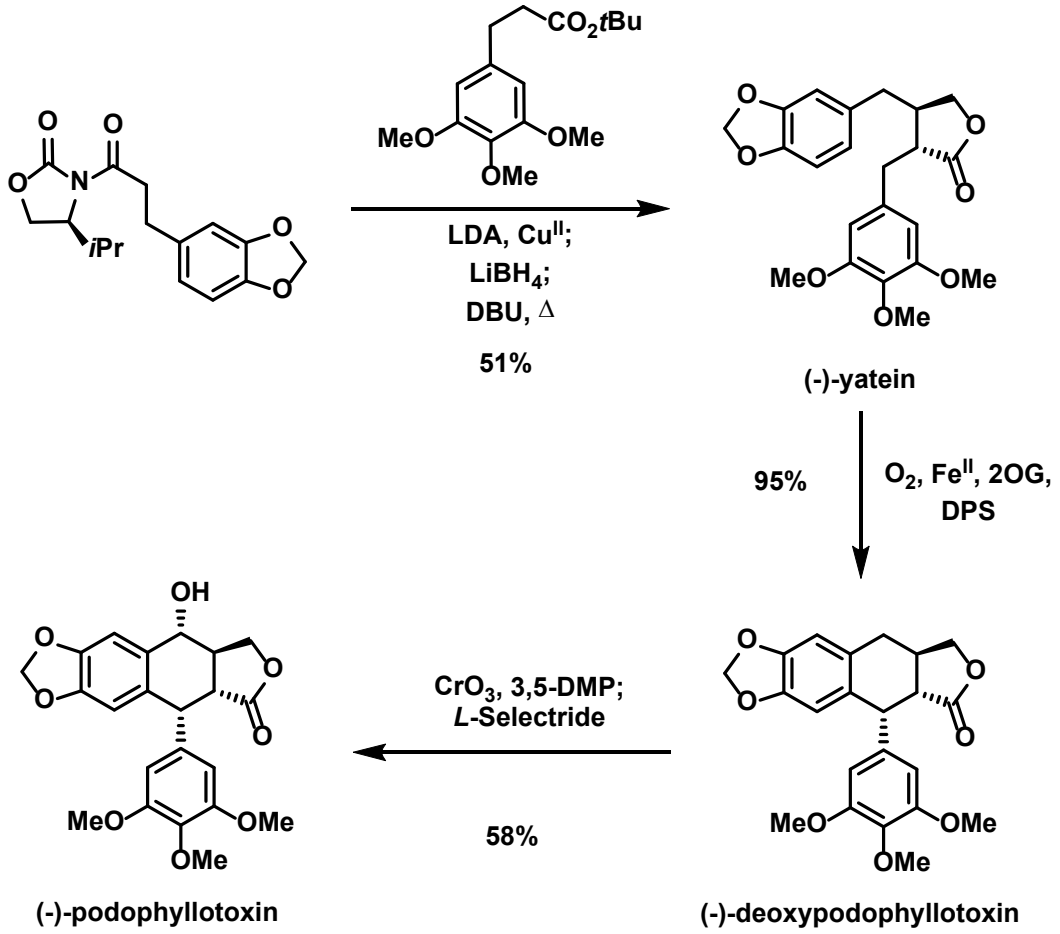

1.5 Outlook

Despite this significant progress, extraction of key precursors from producing plants such as *Sinopodophyllum hexandrum* and *Podophyllum peltatum* still remains the main method of obtaining podophyllotoxins. On the other hand, while synthetic and biotechnological approaches are emerging as promising alternatives, their economic viability is still limited.[8–10,61–63]

The advantages and disadvantages of organic and biological synthesis seem to complement each other. The precision and complex machinery of enzymatic catalysis can provide unmatched selectivity, allowing for chemistry thus far unavailable to synthetic chemists, but is often highly substrate specific. By contrast, the development of organic synthesis has given rise to an enormous arsenal of reactions to address inherent limitations in selectivity, thus making them more applicable to a broader range of substrates.

Chemoenzymatic synthesis has the potential to combine advantages of both, making use of the efficiency, scalability, and broader scope of organic synthesis, while leveraging the precision and chemical finesse of enzymatic catalysis to circumvent inherent limitations.

CHAPTER 2: Investigations into the Mechanism and Substrate Scope of DPS

2.1 Introduction: Scope of Thesis

A deeper understanding of how DPS catalyzes completion of the tetracyclic core may be the key to realizing efficient access to the aryltetralin lignan scaffold. Furthermore, it may provide a foundation for developing sustainable and economical chemoenzymatic methods of producing podophyllotoxins.

In pursuit of this goal, I will address the synthesis of mechanistic probes to evaluate and access the promiscuity of DPS. Additionally, this study will provide insight into its underlying catalytic mechanism and active-site residues essential to substrate recognition. Together, these observations may aid in applying strategies such as structure-guided and semi-rational site-selective mutagenesis, and bioinformatics approaches toward ultimately harnessing the synthetic potential of DPS.

2.2 Results and Discussion

2.2.1 Synthetic Preparation of Substrate Analogs

With the overarching goal of probing, and ultimately expanding, the substrate scope of DPS to access a library of natural and non-natural aryltetralin lignans, (particularly podophyllotoxin and the etoposide aglycone (-)-4'-desmethylepipodophyllotoxin), using a single enzymatic transformation, I initially set out to devise a synthetic route to the native substrate of DPS, yatein.

Ideally, the synthesis would: (i) provide a concise and efficient route to yatein, (ii) be suitable to rapid diversification and (iii) be readily amendable to introducing asymmetric conditions at a later stage to produce enantio-enriched target compounds.

Scheme 2.1: Preparation of lactone intermediate **3**.

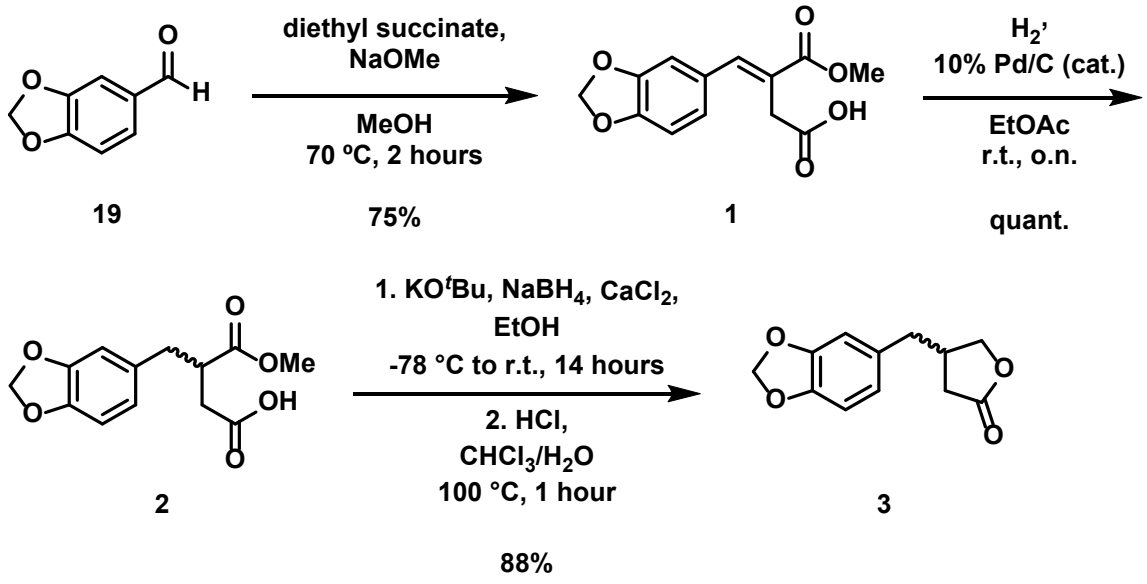

A suitable method adhering to the criteria above was identified (Scheme 2.1). Starting from piperonal **19**, condensation with a succinate ester would generate the corresponding

α/β-unsaturated acid intermediate **1**, followed by reduction of the olefin to form **2** and subsequent lactonization to give **3**, the direct precursor to yatein **11**.[56,64–66] Finally, enolization of the lactone intermediate and S_N2-reaction with 3,4,5-trimethoxybenzyl bromide **7** would yield yatein **11** (Scheme 2.2).[11,64,67] For clarity, structures of numbered compounds are provided in Appendix A.18.

Scheme 2.2: Completing the synthesis of native substrate yatein.

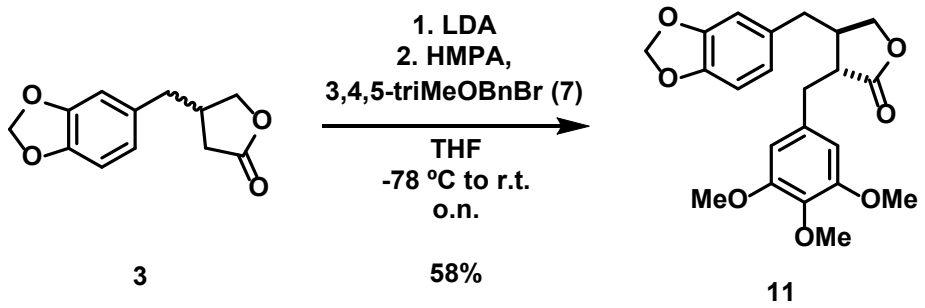

In the first step, piperonal **19** is subjected to Stobbe condensation under basic conditions. Initial attempts were conducted using dimethyl succinate and, though successful, resulted in poor yields. Interestingly, a significant increase in yield (~20%) was observed under identical conditions using diethyl succinate instead.[64,66] The condensation product **2** was first purified according to literature precedent by recrystallization in methanol.[66] However, this proved to be inefficient and time-consuming due to decent solubility of the condensation product in methanol. I found trituration in diethyl ether to be less prone to product loss, while also avoiding the slow turnaround of recrystallization.

The next step in the synthesis involves Pd/C-catalyzed hydrogenation to reduce the olefin of intermediate **2**. The reaction readily proceeds under atmospheric pressure and room temperature to produce the product in quantitative yield. The reaction generally reached

completion after approximately 6h as indicated by TLC but was generally left to stir overnight. The product **3** is obtained as a colorless oil that can be used in the next step without further purification.[64] For easier handling, trituration in diethyl ether yields colorless crystals.

Scheme 2.3: Unsuccessful asymmetric hydrogenation attempt.

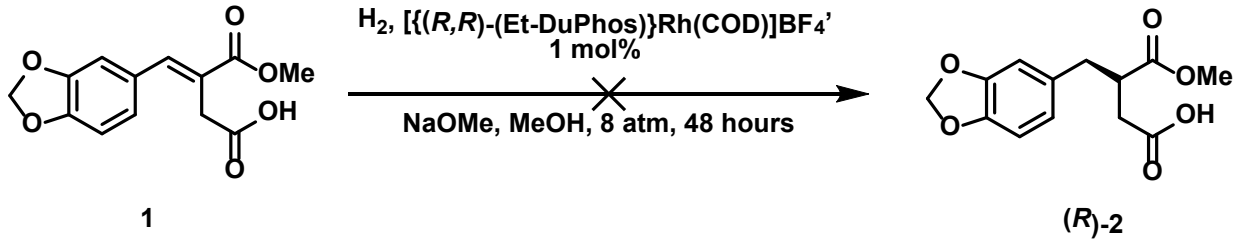

Additionally, asymmetric hydrogenation according to literature precedent (Scheme 2.3) was attempted. The reported pressure of 8 atm could not be attained using our hydrogenation apparatus, and full recovery of the starting material was observed. Therefore, screening attempts were abandoned.[64]

Next, the lactone intermediate **3** was obtained in excellent yield (88%) via calcium borohydride reduction. Calcium borohydride is a suitable reductant in this case, as it provides chemoselectivity in reducing the ester moiety in the hemiester intermediate **2** over the carboxylate moiety. Notably, the use of a bulky base like potassium *tert*-butoxide over potassium hydroxide significantly increases the yield of this transformation (~30%).[56,65] Purification by column chromatography can be omitted. Instead, a simple wash with sodium bicarbonate prior to removal of the solvent also resulted in pure product.

As shown in Scheme 2.2, the lactone **3** is subjected to enolization using lithium diisopropylamide (LDA) and hexamethylphosphoramide. The resulting enolate subsequently reacts with benzyl bromide **7** in an S_N2-reaction to finish installation of the E-ring. LDA is

prepared *in situ* by addition of *n*-butyl lithium to diisopropylamine in THF and must be used fresh.[68] Initial attempts produced very low yields (<10%), likely due to moisture contamination resulting in lower LDA concentration than expected. Omission of HMPA was also accompanied by a significant drop in yield.[67,69] Likely, HMPA increases the nucleophilicity of the corresponding enolate by solvating lithium cations. Purification by column chromatography gave yatein **11** in reasonable yield (58%).

With the native substrate in racemic form in hand, I set out to design a set of yatein analogs to serve as initial probes for investigating the substrate scope and necessary conditions for DPS-mediated C-C bond formation. I first identified suitable substitution sites based on the mechanistic findings and structural analysis previously reported by our lab.[70] The proposed mechanism of DPS likely undergoes cation-induced C-C bond formation (Scheme 1.6). This implicates the electronic properties of the E-ring to potentially play a role in the reaction outcome by stabilizing or destabilizing the carbocation intermediate. Therefore, I chose the *para*-position of the E-ring as one suitable modification site.

Structural analysis of the substrate-bound structure of DPS (PDB: 7E37) revealed that the substrate adopts a U-shaped conformation in the active site, with the E ring located in a tight hydrophobic pocket (Figure 2.1). Specifically, residues L181, K187, F290 and V298 impose steric constraints via hydrophobic interactions and hydrogen bonding, and along with π-π stacking to H184 position the substrate in the active site. No obvious interactions with the two *meta*-methoxy substituents can be identified. Therefore, in addition to the *para*-position, the two *meta*-MeO-substituents were selected as suitable modification sites.

Notably, investigations into the bioactivities of aryltetralin lignans have indicated that subtle changes in the substitution pattern of the aromatic rings, in particular ring E, could

significantly alter their mechanism of action, further supporting the choice in modification sites.[61]

Lastly, the benzodioxole moiety was selected due to its direct involvement in cyclization. It forms π-π interactions with H165 and van-der-Waals interactions with T86, M167, L181 and F290, effectively forming a barrier between the relatively hydrophobic active site and a polar surface made up of the carbonyl oxygen atoms of P80, E81, Y82 and G84 (Figure 2.1). This raised the question if the near planarity of the bicyclic benzodioxole moiety may also be important to DPS-activity, in addition to its electronic properties.

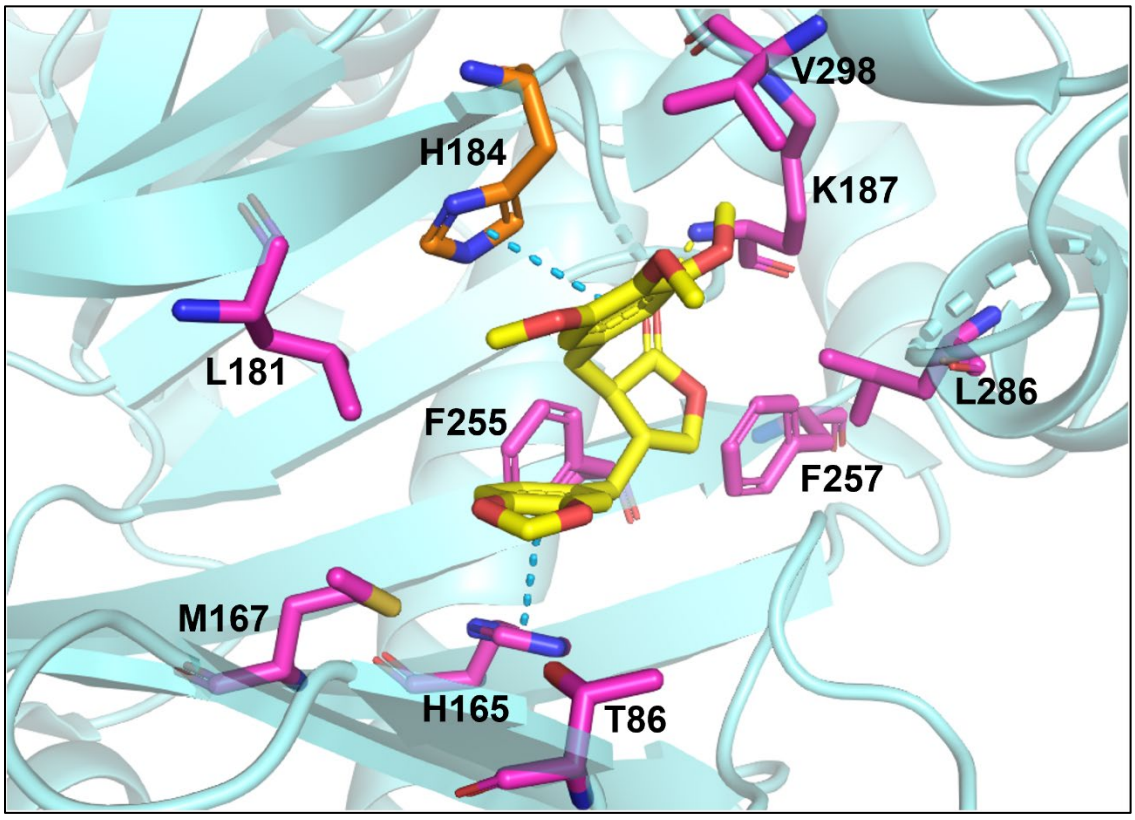

Figure 2.1: Substrate-bound X-ray structures provide insight into key interactions involved in substrate recognition. Polar interactions and π–π interactions are represented by yellow and cyan dashes, respectively. (PDB: 7E37).

Having chosen my target modification sites, the next step involved choosing appropriate modifications. Initially, I planned to install a range of electron donating to electron withdrawing groups in the *para*-position to investigate the tolerance of DPS-activity to varied electronic properties in the E-ring. However, due to the limited commercial availability of corresponding benzyl bromides or suitable precursors, I chose to take inventory of those available to me and selected suitable candidates (Figure 2.2).

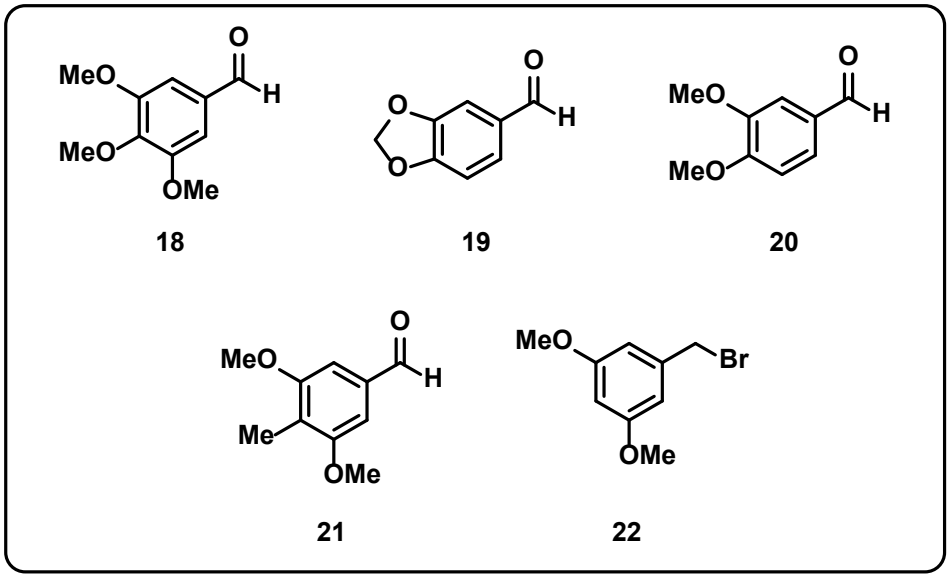

Figure 2.2: Selected candidates for preparation of benzyl bromides. **20** was used as the precursor to lactone intermediate **6**.

In addition, analogous synthesis of the lactone intermediate **3** was repeated with 3,4-dimethoxybenzaldehyde **20** as the precursor instead of piperonal **19**. Similar yields were obtained and are summarized in Table 2.1.

Table 2.1: Obtained yields in the preparation of lactone intermediates **3** and **6.**

Precursor	**Product**	**Step 1**	**Step 2**	**Step 3**
19	**3**	75%	Quant.	88%
20	**6**	77%	Quant.	81%

The benzyl bromides **7-10** were readily prepared in near quantitative yield, requiring no further purification, from the corresponding benzaldehydes (Figure 2.2) via reduction with sodium borohydride and subsequent bromination with phosphorus tribromide (Scheme 2.5).[71,72] As 3,5-dimethoxybenzyl bromide **22** was commercially available, it was selected to prepare my first substrate analog.

I attempted the transformation using my optimized conditions described above but was not able to obtain the desired product. Based on previous experience, I suspected moisture-contamination in LDA to be the likely culprit. Similar results were observed in subsequent attempts. Screening other strong bases like *n*-butyl lithium, LHMDS, potassium *tert*-butoxide produced the same results. Finally, I decided to go back and retry the original reaction with 3,4,5-trimethoxybenzyl bromide **7** to identify the source of the problem, whether it be moisture contamination in my LDA, my hands, or unsuitable reaction conditions for conversion of 3,5-dimethoxybenzyl bromide **22**. To my relief, the reaction with **7** proceeded as expected. These results indicate an electron-rich benzyl bromide is necessary for successful product formation under the chosen conditions.

Benzyl bromides **8-10** were readily added to lactone intermediates **3** and **6** to yield the corresponding dibenzyl butyrolactone substrate analog in comparable yields, as summarized in the table below (Table 2.2). Notably, varying diastereoselectivity was observed in the final

coupling reactions. Diastereoselectivity was noticeably greater with LDA when compared to other screened bases (LHMDS, *n*-BuLi, KO*t*Bu). The diastereomeric ratio (*dr*) values were determined by ^{1}H-NMR and are provided in the table below (Table 2.2). Interestingly, the choice of solvent system had a significant impact on the extent of separation during purification. While varying ratios of ethyl acetate/hexanes resulted in poor or unsuccessful separation, coeluting as a single spot on TLC, diastereomers were readily separated when using acetone/hexanes instead.

Table 2.2: Final products with respective yields and diastereomeric ratio. [a]Single diastereomer, [b]determined by ^{1}H-NMR.

Entry	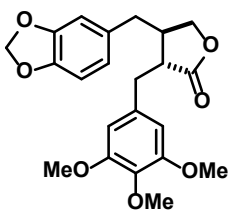 **11**	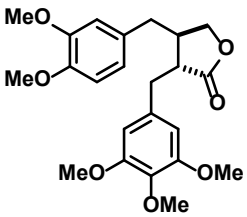 **12**	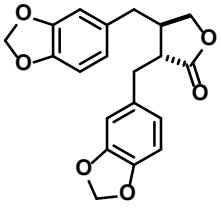 **13**	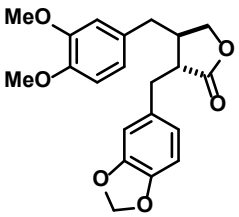 **14**
Yield[a]	58%	48%	42%	46%
dr[b]	≥ 20:1	≥ 20:1	4:1	4:1

Entry	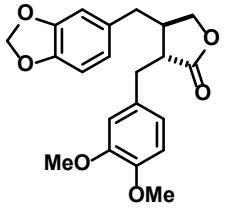 **15**	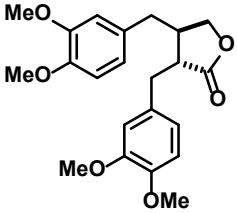 **16**	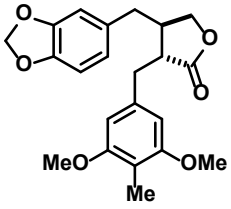 **17**
Yield[a]	46%	48%	52%
dr[b]	5:1	5:1	≥ 20:1

Overall, the native substrate and 6 analogs were prepared for use as mechanistic probes to test the substrate promiscuity of DPS. A current limitation of the outlined conditions is the need

of an electron-rich benzyl bromide for the introduction of the E-ring. Further optimization may be required to expand the substrate analog library. Nonetheless, this method provides a foundation for future preparation of further structural analogs.

2.2.2 Overexpression and Purification of DPS

To evaluate the substrate scope of DPS, the protein needed to be purified for subsequent evaluation of activity via biochemical assays. The *E. coli* (BL21) cell line was chosen as an appropriate host for overexpression. In addition to wild-type (wt) DPS, an F255V mutant was also overexpressed and purified. The F255V mutation was introduced by previous post-doctoral researcher in the Chang lab, Dr. Haoyu Tang. F255 is located above C7 of yatein. To accommodate functionality in this position, for example a C7-hydroxyl group to enzymatically produce epipodophyllotoxin or podophyllotoxin, valine was incorporated instead to create a larger pocket (Figure 2.3).

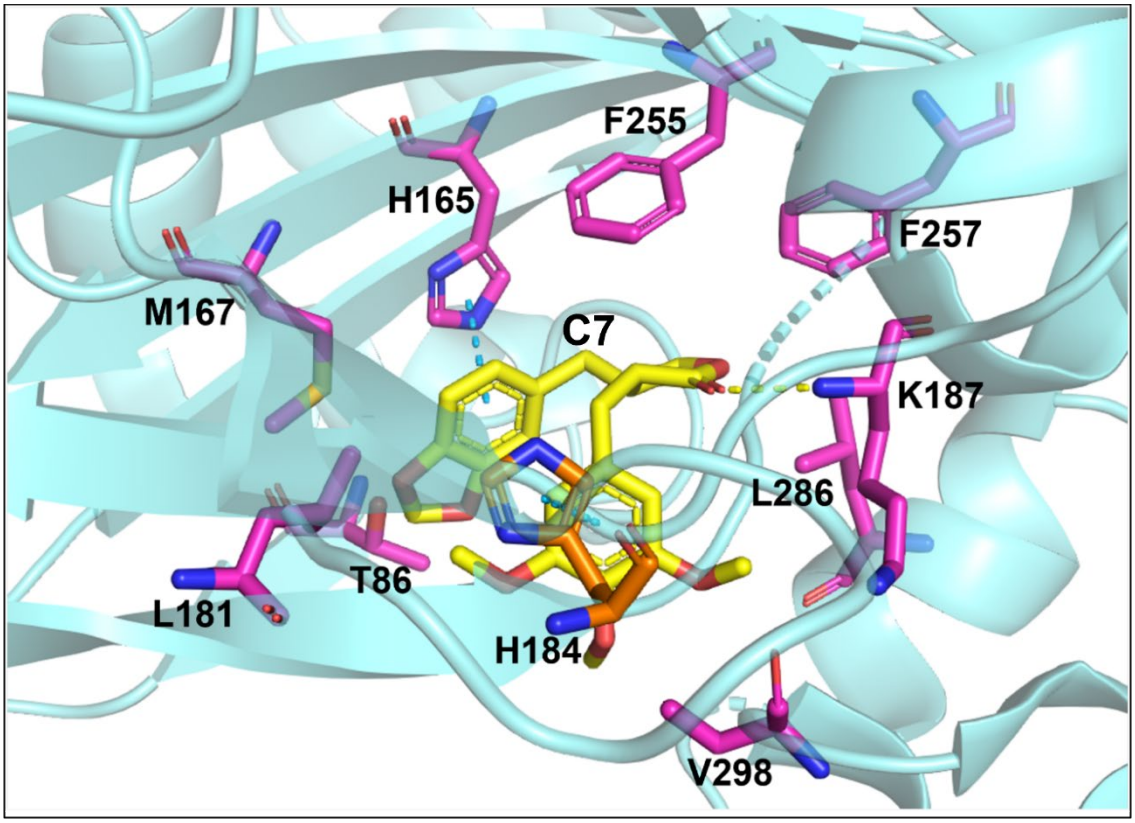

Figure 2.3: A closer look at the DPS active site. The location of residue F255 may prevent accommodation of pre-installed functionality on the C7 of yatein.

Plasmids containing the genes of wt- and F255V-*dps*, were transformed into *E. coli* (BL21). 6L scale overexpression using Terrific Broth (TB) and subsequent purification using nickel-nitrilotriacetic acid (Ni-NTA) affinity chromatography were performed using the experimental procedure described in Chapter 2.4. Both wt- and F255V-DPS were successfully obtained in concentrations of 1.83 mM (4 mL) and 0.93 mM (3 mL) respectively.

Reduced yields are common in protein overexpression and purification of variants, as mutations may result in reduced solubility or improper folding. No solubility concerns were observed in the case of DPS-F255V, however additional bands visualized by sodium dodecyl sulfate-polyacrylamide gel electrophoresis (SDS-PAGE) are more prominent in F255V-DPS (Figures 2.4 and 2.5, Chapter 2.4). Nonetheless, both wild-type and variant are readily obtained using the procedure delineated in Chapter 2.4. Furthermore, wt-DPS was demonstrated to be catalytically active, as results obtained from *in vitro* biochemical assays were consistent with those previously described by our lab in 2022.[70]

2.3 Conclusion

The results presented herein provide a foundation for developing an efficient, convergent chemoenzymatic strategy to produce diversified aryltetralin lignans. Utilizing a combinatorial chemo-enzymatic approach allows for facile, large-scale production and diversification of the key dibenzylbutyrolactone intermediate via organic synthesis, while harnessing the unique and powerful chemistry enabled by DPS to complete the aryltetralin lignan scaffold via $C(sp^3)$-$C(sp^2)$ bond formation.

To this end, I have outlined a synthetic strategy for access to analogs of yatein, the native substrate of DPS, allowing for rapid diversification by introducing a functionalized benzyl bromide in the final coupling step. Using this method, I have prepared 7 compounds for use as mechanistic probes. Additionally, I have overexpressed and purified both wild-type DPS and variant F255V-DPS, providing a platform ready for *in vitro* biochemical assays for investigations into its native substrate promiscuity. Taken together with the current mechanistic and structural understanding, this may provide rationale for structure-guided site-selective mutagenesis in explorations into the chemoenzymatic potential of DPS.

2.4 Materials and Methods

General Materials

All chemicals (used without purification unless specifically mentioned) were purchased from Fisher Chemical (Fair Lawn, NJ), Acros Organics (Geel, Belgium), or Chem-Impex Int'l Inc. (Wood Dale, IL). Deuterated solvents were acquired by Cambridge Isotope Laboratories Inc. (Andover, MA). Analytical thin layer chromatography (TLC) was carried out on pre-coated TLC aluminum sheets (silica gel, grad 60, F254, 5 x 20 cm) acquired from EMD chemicals (Billevica, MA). Flash column chromatography was performed using silica gel (230-400 mesh, grade 60) obtained from Fisher Scientific (Hanover Park, IL). Nuclear magnetic resonance (NMR) spectra were recorded using Bruker 500, 600 or 700 MHz spectrometer at the nuclear magnetic resonance facility of the Department of Chemistry, North Carolina State University. Chemical shifts were reported in parts per million (δ) relative to the internal standard of tetramethylsilane (TMS). The signals observed were described as follows: s (singlet), d (doublet), t (triplet), q (quartet), dd (doublet of doublets), m (multiplet). The number of protons (n) for a given resonance was indicated as nH.

Enzymes, molecular weight marker, isopropyl β-D-1-thiogalactopyranoside (IPTG), antibiotics, Luria-Bertani (LB), and *E. coli* BL21 star (DE3) are products of New England Biolabs (Beverly, MA), BioBasic (Ontario, Canada), or Bio-Rad (Hercules, CA). Protein concentrations were recorded by ultraviolet visible (UV-Vis) spectra on Agilent Technologies UV-Vis 8454 system.

2.4.1 Preparation of Lactone Intermediate

Scheme 2.4: Preparation of lactone intermediates **3** and **6**.

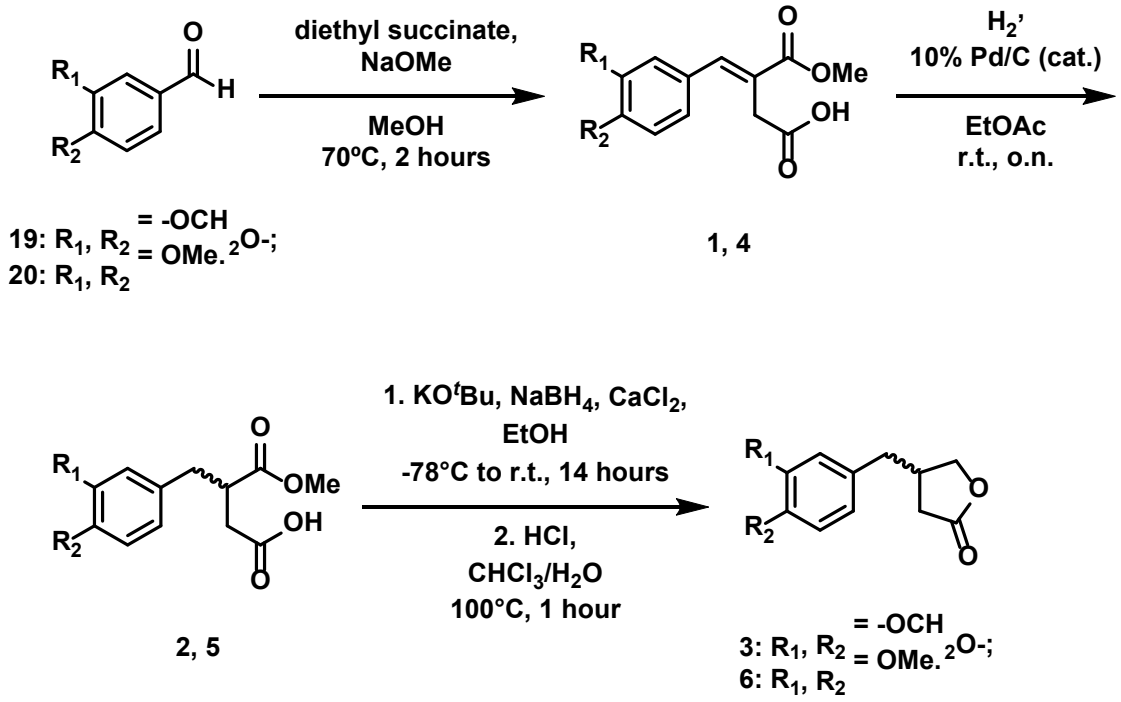

Step I:

To a solution of benzaldehyde **19 (20)** (1.0 eq.) stirring in methanol (~0.67 M) was added diethyl succinate (1.2 eq.), followed by sodium methoxide (1.5 eq.). The reaction mixture was brought to reflux by heating an oil bath to 70 ºC and stirred at that temperature for 2 hours. Upon cooling, the solvent was removed under reduced pressure before acidifying to pH ≤ 3 with 6 M aqueous hydrochloric acid. The mixture was extracted with diethyl ether or ethyl acetate. The combined organic layers were extracted with saturated sodium bicarbonate (*aq*.) and the combined aqueous layers acidified to pH ≤ 3 with 6 M HCl and subsequently extracted with dichloromethane. The combined organic layers were washed with brine and dried over $MgSO_4$.

After removal of the solvent *in vacuo*, the residue was triturated in diethyl ether to afford **1 (4)** as a pale yellow/white solid (75-77%).[65,66]

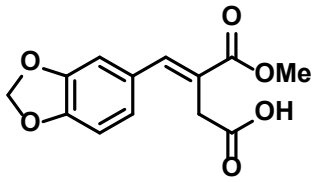

Compound **1** (77% yield; (*E*)-4-(benzo[d][1,3]dioxol-5-yl)-3-(methoxycarbonyl)but-3-enoic acid). ^{1}H NMR (500 MHz, $CDCl_3$): δ = 7.82 (s, 1H), 6.89 (d, *J* = 7.5 Hz, 1H), 6.88 (s, 1H), 6.85 (d, *J* = 7.5 Hz, 1H), 6.00 (s, 2H), 3.83 (s, 3H), 3.60 (s, 2H). ^{13}C NMR (126 MHz, $CDCl_3$): δ = 176.8, 168.3, 148.7, 148.2, 142.6, 128.7, 124.2, 123.8, 109.3, 108.8, 101.6, 52.6, 33.8. **(Appendix A.1)**

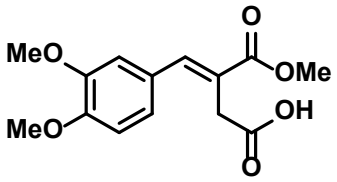

Compound **4** (75% yield; (*E*)-4-(3,4-dimethoxyphenyl)-3-(methoxycarbonyl)but-3-enoic acid) ^{1}H NMR (500 MHz, $CDCl_3$): δ = 7.86 (s, 1H), 7.00 (dd, *J* = 8.2, 2.0 Hz, 1H), 6.98 (d, *J* = 2.0 Hz, 1H), 6.90 (d, *J* = 8.2 Hz, 1H), 3.91 (s, 3H), 3.89 (s, 3H), 3.85 (s, 3H), 3.63 (s, 2H). ^{13}C NMR (126 MHz, $CDCl_3$): δ = 176.5, 168.7, 150.2, 149.1, 143.0, 127.4, 123.0, 122.9, 112.4, 111.2, 56.1, 52.6, 34.1. **(Appendix A.4)**

Step II:

A solution of **1 (4)** in ethyl acetate (~0.5 M) was degassed with nitrogen. 10% Pd/C (cat.) was added, followed by introduction of hydrogen. The mixture was agitated under a hydrogen atmosphere (1 atm) for 12 hours. The catalyst was removed by filtration through celite/celite filtration and the filtrate concentrated *in vacuo* to afford **2 (5)** as a colorless, viscous oil in quantitative yield.[64]

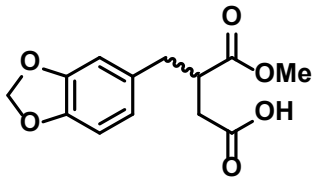

Compound **2** (quant. yield; 3-(benzo[d][1,3]dioxol-5-ylmethyl)-4-methoxy-4-oxobutanoic acid). ^{1}H NMR (500 MHz, $CDCl_3$): δ =6.72 (d, *J* = 7.9 Hz, 1H), 6.64 (d, *J* = 1.7 Hz, 1H), 6.59 (dd, *J* = 7.9, 1.7 Hz, 1H), 5.92 (s, 2H), 3.67 (s, 3H), 3.04 (m, 1H), 2.97 (dd, *J* = 13.6, 6.2 Hz, 1H), 2.69 (dd, *J* = 17.3, 8.8 Hz, 1H), 2.68 (dd, *J* = 13.6 Hz, 8.8, 1H), 2.44 (dd, *J* = 17.3, 4.8 Hz, 1H). ^{13}C NMR (126 MHz, $CDCl_3$): δ = 177.9, 174.6, 147.9, 146.5, 131.7, 122.2, 109.3, 108.4, 101.1, 52.2, 43.0, 37.4, 34.7. **(Appendix A.2)**

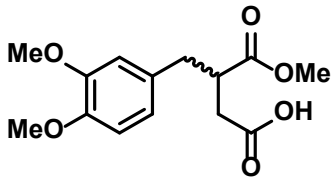

Compound **5** (quant. yield; 3-(3,4-dimethoxybenzyl)-4-methoxy-4-oxobutanoic acid). ^{1}H NMR (500 MHz, $CDCl_3$): δ = 6.78 (d, *J* = 8.1 Hz, 1H), 6.68 (dd, *J* = 8.1, 2.0 Hz, 1H), 6.66 (d, *J* = 2.0 Hz, 1H), 3.85 (s, 3H), 3.85 (s, 3H), 3.67 (s, 3H), 3.07 (td, *J* = 9.0, 4.1 Hz, 1H), 3.00 (dd, *J*

= 13.6, 6.1 Hz, 1H), 2.72 (d, *J* = 8.8 Hz, 1H), 2.69 (dd, *J* = 8.8, 4.0 Hz, 1H), 2.44 (dd, *J* = 17.2, 4.8 Hz, 1H). ^{13}C NMR (126 MHz, $CDCl_3$): δ = 177.7, 174.7, 149.1, 148.0, 130.5, 121.2, 112.1, 111.3, 56.0, 56.0, 52.2, 43.1, 37.4, 34.8. **(Appendix A.5)**

Step III:

Potassium *tert*-butoxide (1.1 eq.) was added to a solution of intermediate **2** (**5**) in ethanol (0.5 M). The resulting mixture was stirred at room temperature for 30 min. To a suspension of calcium chloride in ethanol (1.15 M) was slowly added a solution of $NaBH_4$ in ethanol (1 M) at 0 ºC. The mixture was stirred at 0 ºC for 1 hour, then cooled to -78 ºC. The solution of **2** (**5**) was slowly added at -78 ºC and the resulting mixture was stirred at -78 ºC for 2 hours. After 2 hours, the mixture was allowed to warm to room temperature and stirred for an additional 12 hours. The solvent was evaporated, and the resulting residue was partitioned between chloroform and water. Concentrated hydrochloric acid (excess) was added and the mixture was refluxed at 100 ºC for 1 hour. Upon cooling, the mixture was extracted with chloroform. The combined organic layers were washed with saturated sodium bicarbonate (*aq.*) followed by water and brine. The organic layers were dried over anhydrous $MgSO_4$. The product **3** (**6**) was obtained as a yellow, viscous oil after removal of the solvent under reduced pressure in good yields (81-88%).[56,64]

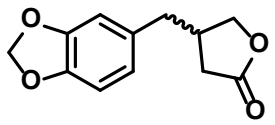

Compound **3** (88% yield; 4-(benzo[d][1,3]dioxol-5-ylmethyl)dihydrofuran-2(3H)-one). ^{1}H NMR (500 MHz, $CDCl_3$): δ = 6.75 (d, *J* = 7.9 Hz, 1H), 6.63 (d, *J* = 1.8 Hz, 1H), 6.60 (dd, *J* = 7.9, 1.8 Hz, 1H), 5.95 (s, 2H), 4.33 (dd, *J* = 9.2, 7.1 Hz, 1H), 4.02 (dd, *J* = 9.2, 6.2 Hz, 1H), 2.84 – 2.75 (m, 1H), 2.71 (dd, *J* = 12.6, 6.1 Hz, 1H), 2.67 (dd, *J* = 12.7, 7.1 Hz, 1H), 2.60 (dd, *J* = 17.5, 8.1 Hz, 1H), 2.27 (dd, *J* = 17.5, 7.1 Hz, 1H). ^{13}C NMR (126 MHz, $CDCl_3$): δ = 176.9, 148.1, 146.6, 132.1, 121.8, 109.0, 108.6, 101.2, 72.7, 38.8, 37.5, 34.3. **(Appendix A.3)**

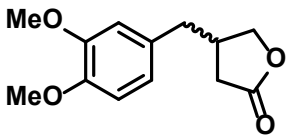

Compound **6** (81% yield; 4-(3,4-dimethoxybenzyl)dihydrofuran-2(3H)-one). ^{1}H NMR (500 MHz, $CDCl_3$): δ = 6.81 (d, *J* = 8.1 Hz, 1H), 6.69 (dd, *J* = 8.1 Hz, 1.5 Hz, 1H), 6.65 (d, *J* = 1.5 Hz, 1H), 4.33 (dd, *J* = 9.0, 7.1 Hz, 1H), 4.03 (dd, *J* = 9.1, 6.1 Hz, 1H), 3.87 (s, 3H), 3.86 (s, 3H), 2.83 (m, 1H), 2.72 (dd, *J* = 12.6, 6.1 Hz, 1H), 2.71 (dd, *J* = 12.6, 8.2 Hz, 1H), 2.60 (dd, *J* = 17.5, 8.2 Hz, 1H), 2.29 (dd, *J* = 17.5, 7.1 Hz, 1H). ^{13}C NMR (126 MHz, $CDCl_3$): δ =177.0, 149.2, 148.0, 130.9, 120.8, 111.9, 111.5, 72.8, 56.0, 38.7, 37.4, 34.4. **(Appendix A.6)**

2.4.2 Preparation of Benzyl Bromides

Scheme 2.5: Synthesis of benzyl bromides **7-10**.

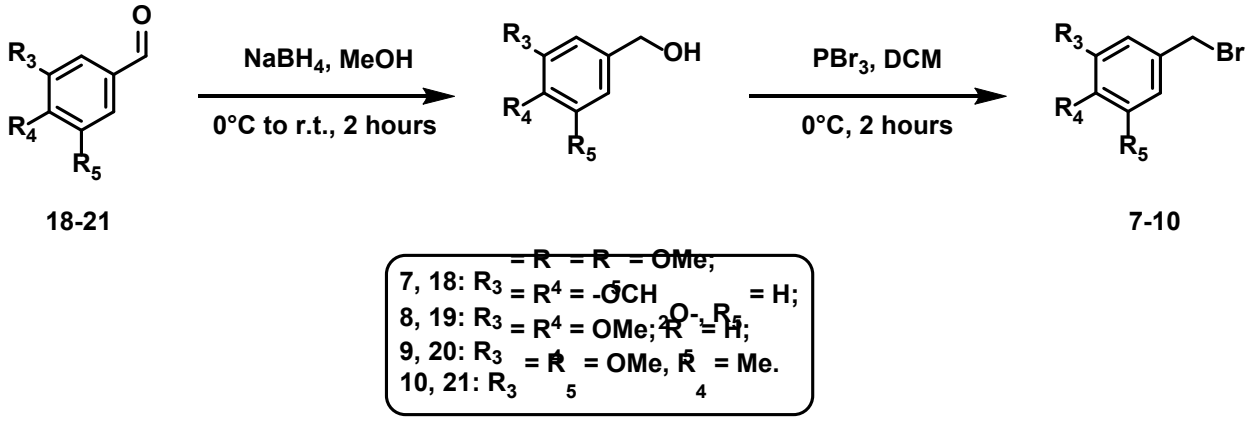

Step I:

A solution of benzaldehyde **18-21** (1.0 eq.) in methanol (0.25 M) was cooled to 0 ºC, followed by addition of $NaBH_4$ (2.0 eq.) in portions. After addition, the mixture was allowed to slowly warm to room temperature. The reaction was followed by TLC (EA:hexanes = 1:2) until full substrate consumption was observed (~ 1-2 hours). The solvent was removed under reduced pressure and the residue was partitioned between dichloromethane and water. The aqueous layer was extracted with dichloromethane. The combined organic layers were washed with brine and dried over anhydrous magnesium sulfate. Removal of the solvent under reduced pressure afforded the corresponding benzyl alcohol, which was used in the next step without further purification.[71,72]

Step II:

The benzyl alcohol (1.0 eq.) from the previous step was dissolved in dichloromethane (0.2 M) and cooled to 0 ºC. Phosphorus tribromide (1.1 eq.) was added dropwise and the resulting solution was stirred at 0 ºC until full consumption of the starting material. The reaction was quenched by addition of saturated ammonium chloride (*aq.*) and extracted with dichloromethane. The combined organic layers were washed with water and brine and dried over anhydrous magnesium sulfate. The drying agent was removed by gravity filtration and the solvent removed under reduced pressure, affording the benzyl bromide **7-10** as a white to tan solid in (93-96%).[71,72]

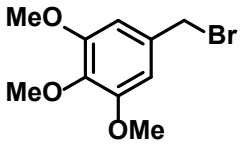

Compound **7** (95% yield; 5-(bromomethyl)-1,2,3-trimethoxybenzene). ^{1}H NMR (500 MHz, $CDCl_3$): δ = 6.62 (s, 2H), 4.46 (s, 2H), 3.87 (s, 6H), 3.84 (s, 3H). ^{13}C NMR (126 MHz, $CDCl_3$): δ = 153.4, 138.3, 133.3, 106.2, 61.0, 56.3, 34.4. **(Appendix A.7)**

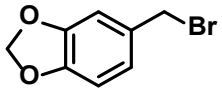

Compound **8** (96% yield; 5-(bromomethyl)benzo[d][1,3]dioxole). ^{1}H NMR (500 MHz, $CDCl_3$): δ = 6.88 (d, J = 1.8 Hz, 1H), 6.86 (dd, J = 7.8, 1.7 Hz, 1H), 6.75 (d, J = 7.8 Hz, 1H), 5.97 (s, 2H), 4.46 (s, 2H). ^{13}C NMR (126 MHz, $CDCl_3$): δ = 148.1, 148.0, 131.7, 122.9, 109.6, 108.5, 101.5, 34.3. **(Appendix A.8)**

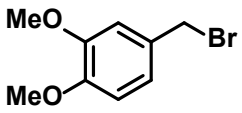

Compound **9** (95% yield; 4-(bromomethyl)-1,2-dimethoxybenzene). ^{1}H NMR (500 MHz, $CDCl_3$): δ = 6.95 (dd, *J* = 8.2, 2.0 Hz, 1H), 6.91 (d, *J* = 2.0 Hz, 1H), 6.81 (d, *J* = 8.2 Hz, 1H), 4.50 (s, 2H), 3.90 (s, 3H), 3.88 (s, 3H). ^{13}C NMR (126 MHz, $CDCl_3$): δ = 149.4, 149.2, 130.4, 121.7, 112.2, 111.2, 56.1, 56.0, 34.5. **(Appendix A.9)**

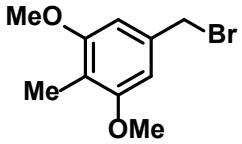

Compound **10** (93% yield; 5-(bromomethyl)-1,3-dimethoxy-2-methylbenzene). ^{1}H NMR (500 MHz, $CDCl_3$): δ = 6.57 (s, 2H), 4.49 (s, 2H), 3.83 (s, 3H), 3.83 (s, 3H) 2.07 (s, 3H). ^{13}C NMR (126 MHz, $CDCl_3$): δ = 158.5, 136.0, 115.2, 104.5, 55.9, 34.8, 8.3. **(Appendix A.10)**

2.4.3 Preparation of Substrate Analogs

Scheme 2.6: Synthesis of substrate analogs **11-17.**

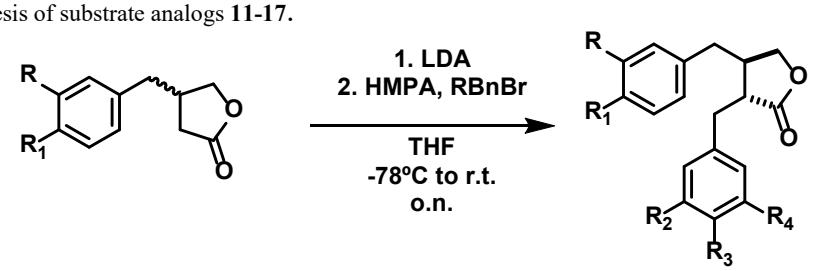

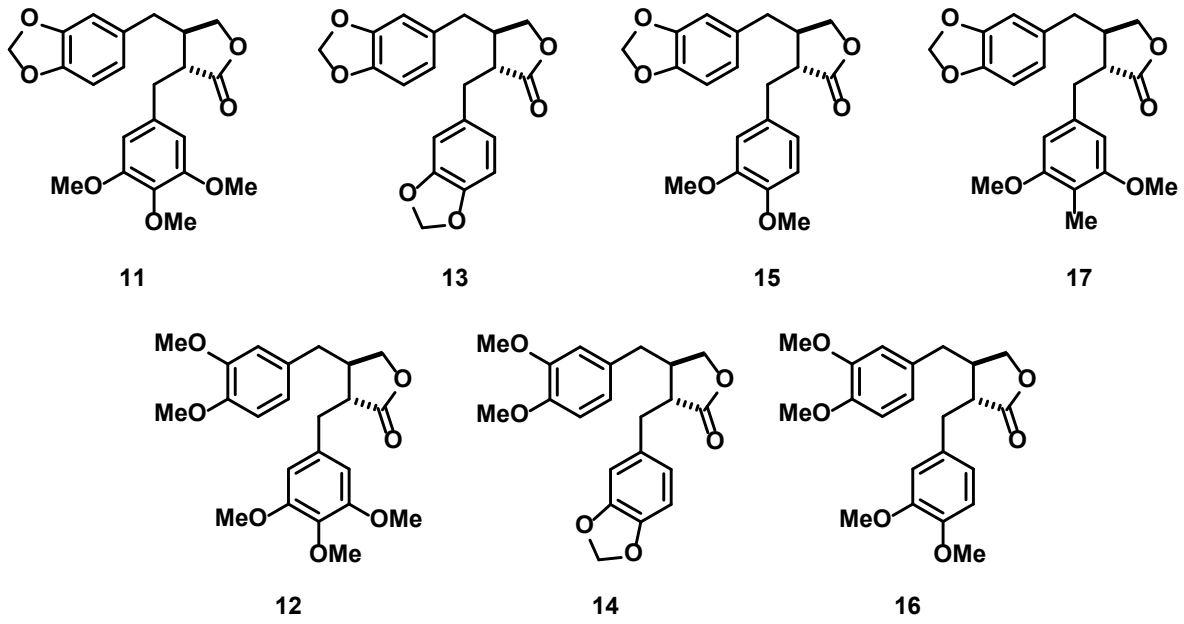

A dry flask was charged with diisopropylamine (1.6 eq.) and THF (1 M) and the solution was cooled to -78 ºC under inert atmosphere. *n*-Butyllithium (1.5 eq.) was added dropwise over 10 minutes, upon which the solution was stirred for 30 minutes. Hexamethylphosphoramide (1.1 eq.) was added dropwise, and the mixture stirred for an additional 15 minutes, followed by dropwise addition of a solution of benzyl bromide **7-10** (1.85 eq.) in THF (0.5 M). The solution was stirred for 2 hours at -78 ºC, then allowed to warm to room temperature and stirred for an additional 3-12 hours. The reaction was quenched with saturated ammonium chloride (*aq.*) and extracted with ethyl acetate. The combined organic layers were washed with 1 M HCl, then with

water and brine and dried over magnesium sulfate. The solvent was removed under reduced pressure and the crude product was obtained as a set of diastereomers. Following purification by silica-gel column chromatography using acetone and hexanes, the final product **11-17** was obtained as a single diastereomer (42-59%) as a colorless to tan viscous oil.[11,56,73]

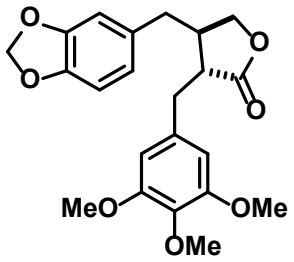

Compound **11** (58% yield; (3*R*,4*R*)-4-(benzo[d][1,3]dioxol-5-ylmethyl)-3-(3,4,5-trimethoxybenzyl)dihydrofuran-2(3H)-one). ^{1}H NMR (500 MHz, $CDCl_3$): δ = 6.69 (d, *J* = 7.6 Hz, 1H), 6.47 (d, *J* = 1.8 Hz, 1H), 6.47 (dd, *J* = 7.6, 1.8 Hz, 1H), 6.35 (s, 2H), 5.93 (d, *J* = 3.1 Hz, 1H), 5.93 (d, *J* = 3.1 Hz, 1H), 4.18 (dd, *J* = 9.0, 7.6 Hz, 1H), 3.87 (dd, *J* = 9.0, 7.6 Hz, 1H), 3.83 (s, 9H), 2.93 (dd, *J* = 14.0, 7.5 Hz, 1H), 2.91 (dd, *J* = 14.1, 8.6 Hz, 1H), 2.65 – 2.56 (m, 2H), 2.55 – 2.46 (m, 2H). ^{13}C NMR (126 MHz, $CDCl_3$): δ = 178.7, 153.4, 148.1, 146.6, 137.0, 133.5, 131.7, 121.7, 108.9, 108.5, 106.4, 101.3, 71.3, 61.0, 56.3, 46.6, 41.2, 38.5, 35.4. **(Appendix A.11)**

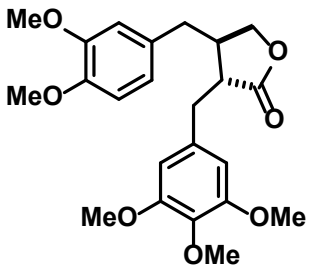

Compound **12** (58% yield; (3*R*,4*R*)-4-(3,4-dimethoxybenzyl)-3-(3,4,5-trimethoxybenzyl)dihydrofuran-2(3H)-one). ^{1}H NMR (500 MHz, $CDCl_3$): δ = 6.75 (d, *J* = 7.7 Hz, 1H), 6.55 (d, *J* = 7.5 Hz, 1H), 6.50 (s, 1H), 6.36 (s, 2H), 4.20 – 4.14 (m, 1H), 3.92 – 3.86 (m, 1H), 3.85 (s, 3H), 3.82 (s, 12H), 2.98 – 2.88 (m, 2H), 2.72 – 2.64 (m, 1H), 2.63 – 2.55 (m, 2H), 2.55 – 2.51 (m, 1H). ^{13}C NMR (126 MHz, $CDCl_3$): δ = 178.7, 153.4, 149.1, 148.0 137.0, 133.5, 130.5, 120.6, 112.0, 111.4, 106.4, 71.5, 61.0, 56.3, 56.1, 46.7, 41.2, 38.3, 35.2. **(Appendix A.12)**

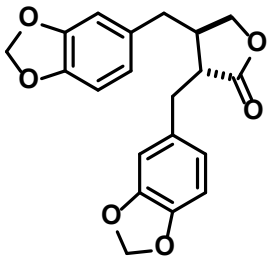

Compound **13** (42% yield; (3*R*,4*R*)-3,4-bis(benzo[d][1,3]dioxol-5-ylmethyl)dihydrofuran-2(3H)-one. ^{1}H NMR (500 MHz, $CDCl_3$): δ = 6.71 (dd, *J* = 15.7, 8.0 Hz, 2H), 6.63 (s, 1H), 6.60 (d, *J* = 7.9 Hz, 2H), 6.46 (m, 2H), 5.94 (d, *J* = 3.0 Hz, 2H), 5.93 (d, *J* = 3.0 Hz, 2H), 4.13 (dd, *J* = 8.9, 6.4 Hz, 1H), 3.86 (dd, *J* = 8.9, 6.4 Hz, 1H), 2.98 (dd, *J* = 14.0, 4.5 Hz, 1H), 2.84 (dd, *J* = 14.0, 6.9 Hz, 1H), 2.62 – 2.51 (m, 2H), 2.50 – 2.43 (m, 2H). ^{13}C NMR (126 MHz, $CDCl_3$): δ = 178.6, 148.0, 148.0, 146.6, 146.5, 131.7, 131.5, 122.4, 121.7, 109.6, 109.0, 108.5, 108.4, 101.2, 71.3, 46.6, 41.4, 38.5, 35.0. **(Appendix A.13)**

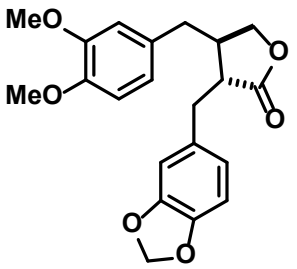

Compound **14** (46% yield; (3*R*,4*R*)-3-(benzo[d][1,3]dioxol-5-ylmethyl)-4-(3,4-dimethoxybenzyl)dihydrofuran-2(3H)-one. ^{1}H NMR (500 MHz, $CDCl_3$): δ = 6.76 (d, *J* = 7.7 Hz, 1H), 6.71 (d, *J* = 7.6 Hz, 1H), 6.60 (s, 1H), 6.59 (d, *J* = 8.8 Hz, 1H), 6.58 (d, *J* = 8.8 Hz, 1H), 6.48 (s, 1H), 5.93 (d, *J* = 3.3 Hz, 1H), 5.92 (d, *J* = 3.3 Hz, 1H), 4.20 – 4.11 (m, 1H), 3.92 – 3.87 (m, 1H), 3.85 (s, 3H), 3.83 (s, 3H), 2.96 (d, *J* = 12.8 Hz, 1H), 2.85 (d, *J* = 12.8 Hz, 1H), 2.63 – 2.45 (m, 4H). ^{13}C NMR (126 MHz, $CDCl_3$): δ = 178.6, 149.2, 148.0, 146.6, 131.5, 130.5, 122.4, 120.8, 111.8, 111.4, 109.6, 108.3, 101.2, 71.5, 56.1, 56.0, 46.6, 41.3, 38.4, 34.9. **(Appendix A.14)**

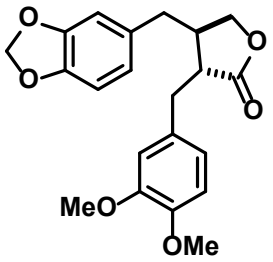

Compound **15** (46% yield; (3*R*,4*R*)-4-(benzo[d][1,3]dioxol-5-ylmethyl)-3-(3,4-dimethoxybenzyl)dihydrofuran-2(3H)-one). ^{1}H NMR (500 MHz, $CDCl_3$): δ = 6.79 (d, *J* = 8.0 Hz, 1H), 6.69 (d, *J* = 7.8 Hz, 2H), 6.67 (s, 1H), 6.45 (d, *J* = 7.9 Hz, 1H), 6.43 (s, 1H), 5.93 (d, *J* = 1.2 Hz, 1H), 5.93 (d, *J* = 1.2 Hz, 1H), 4.15 – 4.09 (m, 1H), 3.92 – 3.88 (m, 1H), 3.86 (s, 3H), 3.84 (s, 3H), 2.97 (dd, *J* = 14.0, 6.7 Hz, 1H), 2.89 (dd, *J* = 14.0, 6.7 Hz, 1H), 2.63 – 2.53 (m, 1H), 2.59 (m, 1H), 2.52 – 2.41 (m, 1H). ^{13}C NMR (126 MHz, $CDCl_3$): δ = 178.7, 149.2, 148.1,

148.0, 146.5, 131.7, 130.2, 121.7, 121.5, 112.3, 111.2, 108.9, 108.4, 101.2, 71.3, 56.0, 56.0, 46.7, 41.2, 38.5, 34.8. **(Appendix A.15)**

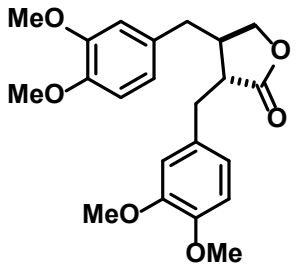

Compound **16** (48% yield; (3*R*,4*R*)-3,4-bis(3,4-dimethoxybenzyl)dihydrofuran-2(3H)-one). ^{1}H NMR (500 MHz, $CDCl_3$): δ = 6.79 – 6.72 (m, 2H), 6.68 (s, 1H), 6.65 (d, *J* = 8.1 Hz, 1H), 6.55 (d, *J* = 8.1 Hz, 1H), 6.48 (s, 1H), 4.12 (m, 1H), 3.92 – 3.88 (m, 1H), 3.85 (s, 3H), 3.85 (s, 3H), 3.83 (s, 3H), 3.82 (s, 3H), 2.95 (m, 2H), 2.65 (m, 1H), 2.58 (m, 1H), 2.52 (m, 1H). ^{13}C NMR (126 MHz, $CDCl_3$): δ = 178.8, 149.2, 149.1, 148.1, 148.0, 130.6, 130.3, 121.5, 120.7, 112.5, 112.0, 111.4, 111. 2, 71.4, 56.0, 56.0, 56.0, 56.0, 46.7, 41.2, 38.3, 34.6. **(Appendix A.16)**

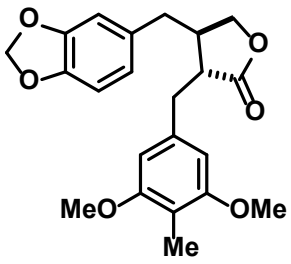

Compound **17** (52% yield; (3*R*,4*R*)-3,4-bis(benzo[d][1,3]dioxol-5-ylmethyl)dihydrofuran-2(3H)-one). ^{1}H NMR (500 MHz, $CDCl_3$): δ = 6.69 (d, *J* = 7.6 Hz, 1H), 6.45 (d, *J* = 10.3 Hz, 2H), 6.32 (s, 2H), 5.93 (s, 2H), 4.18 – 4.10 (m, 2H), 3.87 (dd, *J* = 9.2, 7.3 Hz, 2H), 3.79 (s, 6H), 2.97 (dd, *J* = 13.9, 5.0 Hz, 1H), 2.91 (dd, *J* = 13.9, 7.1 Hz, 1H), 2.63 – 2.56 (m, 2H), 2.51 – 2.48 (m, 2H), 2.05 (s, 3H). ^{13}C NMR (126 MHz, $CDCl_3$): δ = 178.8, 158.5,

148.0, 146.5, 136.1, 131.8, 121.7, 113.1, 108.9, 108.4, 104.7, 101.2, 71.4, 55.9, 46.7, 41.2, 38.5, 35.6, 8.1. **(Appendix A.17)**

2.4.4 Protein Overexpression and Purification

Wild-type- and F255V-DPS were overexpressed in *E. coli* BL21 (DE3). A single cell colony was used for the inoculation of a start culture in 250 mL Terrific Broth (TB) solution containing 50 μg/μL kanamycin. The start culture was incubated at 37 ºC and shaken at 220 rpm for approximately 14 hours and subsequently used to inoculate 1 L x 6 of cells in TB medium. The cell LB (1 L x 6) was incubated at 37 ºC and 220 rpm until reaching an optical density (OD600) of ~ 0.6. Protein overexpression was then induced with isopropyl β-D-1-thiogalactosidase (IPTG) and subsequently shaken at 18 ºC for an additional 14-16 hours. The cells were harvested by centrifuging for 30 minutes at 18 ºC and 6000 rpm. The obtained cell weight was approximately 47 g and 30 g for wt- and F255V-DPS respectively.

The resulting cell paste was lysed via sonication (12 cycles with each cycle being 30 sec induction and 60 sec delay) for 6 min and then centrifuged for 30 minutes at 20,000 rpm 8 ºC. The supernatant was loaded onto a nickel-nitrilotriacetic acid (Ni-NTA) column and washed with 3 column equivalents of lysis buffer (100 mM tris(hydroxymethyl)aminomethane (Tris) at pH = 7.8). The N-His_6-tagged proteins were eluted with the elution buffer containing 250 mM imidazole and 100 mM Tris at pH = 7.8. Elution fractions containing the proteins were visualized by SDS-PAGE analysis using 10% Coomassie Blue Staining (Figures 2.4 and 2.5) and concentrated using Macrosep Advance Centrifugal Devices (Pall, NY). The proteins were concentrated to a final volume of 4 and 3 mL and subjected to dialysis overnight with 2 L buffer containing 10 mM EDTA and 100 mM Tris (pH = 7.8), followed by twice with 2 L buffer containing 100 mM Tris (pH = 7.8). The concentrations of wt- and F255V-DPS were determined using UV-Vis spectroscopy and calculated to be 1.83 mM and 0.93 mM respectively, using the

molar absorptivity (calculated from https://ca.expasy.org) of wt-DPS (35597.5 $M^{-1}cm^{-1}$) and DPS-F255V (35597.5 $M^{-1}cm^{-1}$).

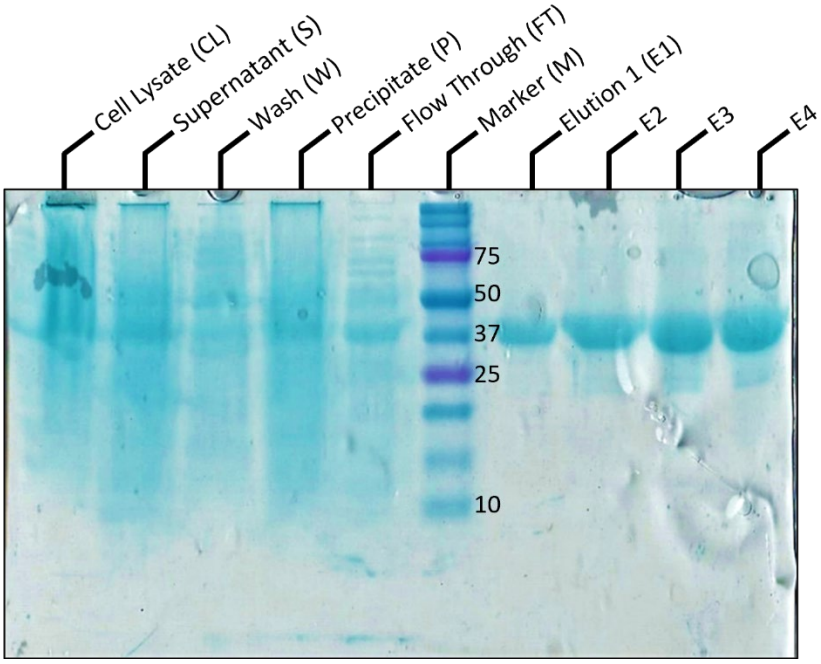

Figure 2.4: Sodium dodecyl sulfate-polyacrylamide gel electrophoresis (SDS-PAGE) analysis of wild-type DPS. Marker descriptors in kDa. DPS has an approximate mass of ~ 37 kDa.

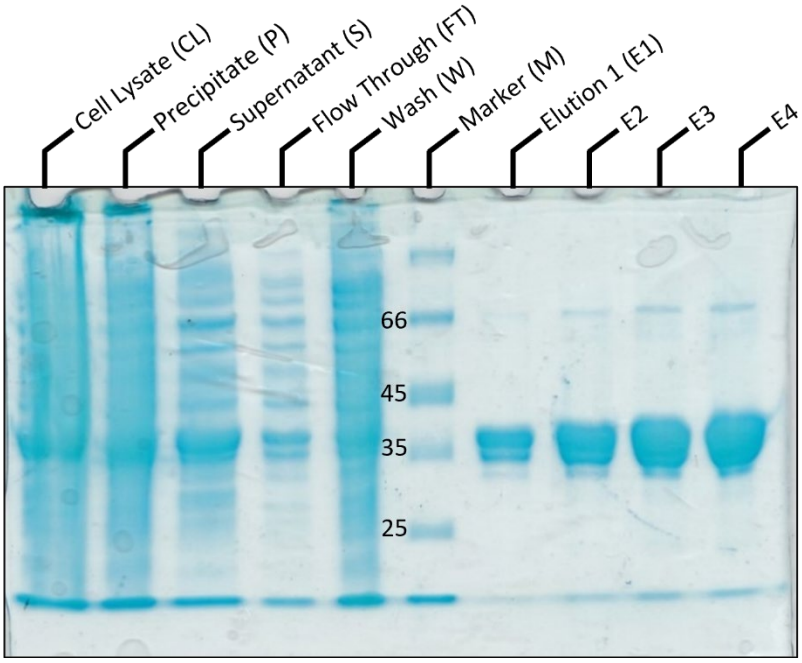

Figure 2.5: Sodium dodecyl sulfate-polyacrylamide gel electrophoresis (SDS-PAGE) analysis of F255V-DPS variant. Marker descriptors in kDa.

REFERENCES

(1) Umezawa, T. Phylogenetic Distribution of Lignan Producing Plants. *Wood Res. Bull. Wood Res. Inst. Kyoto Univ.* **2003**, *90*, 27–110.

(2) Newman, D. J.; Cragg, G. M.; Snader, K. M. Natural Products as Sources of New Drugs over the Period 1981−2002. *J. Nat. Prod.* **2003**, *66* (7), 1022–1037. https://doi.org/10.1021/np030096l.

(3) Cui, Q.; Du, R.; Liu, M.; Rong, L. Lignans and Their Derivatives from Plants as Antivirals. *Molecules* **2020**, *25* (1), 183. https://doi.org/10.3390/molecules25010183.

(4) Wang, L. X.; Wang, H. L.; Huang, J.; Chu, T. Z.; Peng, C.; Zhang, H.; Chen, H. L.; Xiong, Y. A.; Tan, Y. Z. Review of Lignans from 2019 to 2021: Newly Reported Compounds, Diverse Activities, Structure-Activity Relationships and Clinical Applications. *Phytochemistry*. Elsevier Ltd October 1, 2022. https://doi.org/10.1016/j.phytochem.2022.113326.

(5) Utsugi, T.; Shibata, J.; Sugimoto, Y.; Aoyagi, K.; Wierzba, K.; Kobunai, T.; Terada, T.; Oh-hara, T.; Tsuruo, T.; Yamada, Y. Antitumor Activity of a Novel Podophyllotoxin Derivative (TOP-53) against Lung Cancer and Lung Metastatic Cancer. *Cancer Res.* **1996**, *56* (12), 2809–2814.

(6) Hande, K. . Etoposide: Four Decades of Development of a Topoisomerase II Inhibitor. *Eur. J. Cancer* **1998**, *34* (10), 1514–1521. https://doi.org/10.1016/S0959-8049(98)00228-7.

(7) Walsh, C. T.; Tang, Y. *Natural Product Biosynthesis: Chemical Logic and Enzymatic Machinery*; The Royal Society of Chemistry, 2017.

(8) Lau, W.; Sattely, E. S. Six Enzymes from Mayapple That Complete the Biosynthetic

Pathway to the Etoposide Aglycone. *Science (80-.).* **2015**, *349* (6253), 1224–1228. https://doi.org/10.1126/science.aac7202.

(9) Liang, Z.; Zhang, J.; Zhang, X.; Li, J.; Zhang, X.; Zhao, C. Endophytic Fungus from Sinopodophyllum Emodi (Wall.) Ying That Produces Podophyllotoxin. *J. Chromatogr. Sci.* **2015**, *54* (2), 175–178. https://doi.org/10.1093/chromsci/bmv124.

(10) Liu, Q.; Yu, T.; Li, X.; Chen, Y.; Campbell, K.; Nielsen, J.; Chen, Y. Rewiring Carbon Metabolism in Yeast for High Level Production of Aromatic Chemicals. *Nat. Commun.* **2019**, *10* (1), 4976. https://doi.org/10.1038/s41467-019-12961-5.

(11) Tang, H.; Wu, M.-H.; Lin, H.-Y.; Han, M.-R.; Tu, Y.-H.; Yang, Z.-J.; Chien, T.-C.; Chan, N.-L.; Chang, W. Mechanistic Analysis of Carbon–Carbon Bond Formation by Deoxypodophyllotoxin Synthase. *Proc. Natl. Acad. Sci.* **2022**, *119* (1), e2113770119. https://doi.org/10.1073/pnas.2113770119.

(12) Hausinger, R. P. Fe(II)/α-Ketoglutarate-Dependent Hydroxylases and Related Enzymes. *Crit. Rev. Biochem. Mol. Biol.* **2004**, *39* (1), 21–68. https://doi.org/10.1080/10409230490440541.

(13) Herr, C. Q.; Hausinger, R. P. Amazing Diversity in Biochemical Roles of Fe(II)/2-Oxoglutarate Oxygenases. *Trends Biochem. Sci.* **2018**, *43* (7), 517–532. https://doi.org/10.1016/J.TIBS.2018.04.002.

(14) Mitchell, A. J.; Weng, J.-K. Unleashing the Synthetic Power of Plant Oxygenases: From Mechanism to Application. *Plant Physiol.* **2019**, *179* (3), 813–829. https://doi.org/10.1104/pp.18.01223.

(15) Peters, C.; Buller, R. Industrial Application of 2-Oxoglutarate-Dependent Oxygenases. *Catalysts* **2019**, *9* (3), 221. https://doi.org/10.3390/catal9030221.

(16) Dunham, N. P. MECHANISTIC INVESTIGATION OF THE DIVERSE IRON AND 2-OXOGLUTARATE-DEPENDENT OXYGENASE SUPERFAMILY, Pennsylvania State University, 2018.

(17) Bollinger Jr., J. M.; Chang, W.; Matthews, M. L.; Martinie, R. J.; Boal, A. K.; Krebs, C. CHAPTER 3 Mechanisms of 2-Oxoglutarate-Dependent Oxygenases: The Hydroxylation Paradigm and Beyond. In *2-Oxoglutarate-Dependent Oxygenases*; The Royal Society of Chemistry, 2015; pp 95–122. https://doi.org/10.1039/9781782621959-00095.

(18) Martinez, S.; Hausinger, R. P. Catalytic Mechanisms of Fe(II)- and 2-Oxoglutarate-Dependent Oxygenases. *J. Biol. Chem.* **2015**, *290* (34), 20702–20711. https://doi.org/10.1074/JBC.R115.648691.

(19) Cui, Q.; Du, R.; Liu, M.; Rong, L. Lignans and Their Derivatives from Plants as Antivirals. *Molecules*. MDPI AG January 1, 2020. https://doi.org/10.3390/molecules25010183.

(20) Moss, G. P. Nomenclature of Lignans and Neolignans (IUPAC Recommendations 2000). **2000**, *72* (8), 1493–1523. https://doi.org/doi:10.1351/pac200072081493.

(21) Hirano, T.; Gotoh, M.; Oka, K. Natural Flavonoids and Lignans Are Potent Cytostatic Agents against Human Leukemic HL-60 Cells. *Life Sci.* **1994**, *55* (13), 1061–1069. https://doi.org/10.1016/0024-3205(94)00641-5.

(22) Yamauchi, S.; Ina, T.; Kirikihira, T.; Masuda, T. Synthesis and Antioxidant Activity of Oxygenated Furofuran Lignans. *Biosci. Biotechnol. Biochem.* **2004**, *68* (1), 183–192. https://doi.org/10.1271/bbb.68.183.

(23) Saleem, M.; Kim, H. J.; Ali, M. S.; Lee, Y. S. An Update on Bioactive Plant Lignans. *Nat. Prod. Rep.* **2005**, *22* (6), 696. https://doi.org/10.1039/b514045p.

(24) Hano, C. F.; Dinkova-Kostova, A. T.; Davin, L. B.; Cort, J. R.; Lewis, N. G. Editorial: Lignans: Insights Into Their Biosynthesis, Metabolic Engineering, Analytical Methods and Health Benefits. *Front. Plant Sci.* **2021**, *11*. https://doi.org/10.3389/fpls.2020.630327.

(25) Pan, J.-Y.; Chen, S.-L.; Yang, M.-H.; Wu, J.; Sinkkonen, J.; Zou, K. An Update on Lignans: Natural Products and Synthesis. *Nat. Prod. Rep.* **2009**, *26* (10), 1251. https://doi.org/10.1039/b910940d.

(26) Zakon, S. J. DISCOVERY OF PODOPHYLLUM RESIN. *AMA. Arch. Derm. Syphilol.* **1952**, *65* (5), 620–622. https://doi.org/10.1001/archderm.1952.01530240112022.

(27) Shen, S.; Tong, Y.; Luo, Y.; Huang, L.; Gao, W. Biosynthesis, Total Synthesis, and Pharmacological Activities of Aryltetralin-Type Lignan Podophyllotoxin and Its Derivatives. *Nat. Prod. Rep.* **2022**, *39* (9), 1856–1875. https://doi.org/10.1039/D2NP00028H.

(28) Yildiz, H.; Van Den Neste, E.; P. Defour, J.; Danse, E.; Yombi, J. . Adult Haemophagocytic Lymphohistiocytosis: A Review. *QJM An Int. J. Med.* **2022**, *115* (4), 205–213. https://doi.org/10.1093/qjmed/hcaa011.

(29) Satake, H.; Koyama, T.; Bahabadi, S.; Matsumoto, E.; Ono, E.; Murata, J. Essences in Metabolic Engineering of Lignan Biosynthesis. *Metabolites* **2015**, *5* (2), 270–290. https://doi.org/10.3390/metabo5020270.

(30) Satake, H.; Ono, E.; Murata, J. Recent Advances in the Metabolic Engineering of Lignan Biosynthesis Pathways for the Production of Transgenic Plant-Based Foods and Supplements. *J. Agric. Food Chem.* **2013**, *61* (48), 11721–11729. https://doi.org/10.1021/jf4007104.

(31) Chaurasia, O. P.; Ballabh, B.; Tayade, A.; Kumar, R.; Kumar, G. P.; Singh, S. B.

Podophyllum L.: An Endergered and Anticancerous Medicinal Plant–An Overview. **2012**.

(32) GUERRAM, M.; JIANG, Z.-Z.; ZHANG, L.-Y. Podophyllotoxin, a Medicinal Agent of Plant Origin: Past, Present and Future. *Chin. J. Nat. Med.* **2012**, *10* (3), 161–169. https://doi.org/10.3724/SP.J.1009.2012.00161.

(33) Suzuki, S.; Umezawa, T. Biosynthesis of Lignans and Norlignans. *J. Wood Sci.* **2007**, *53* (4), 273–284. https://doi.org/10.1007/s10086-007-0892-x.

(34) Dixon, R. A.; Achnine, L.; Kota, P.; Liu, C.-J.; Reddy, M. S. S.; Wang, L. The Phenylpropanoid Pathway and Plant Defence-a Genomics Perspective. *Mol. Plant Pathol.* **2002**, *3* (5), 371–390. https://doi.org/10.1046/j.1364-3703.2002.00131.x.

(35) Zhou, R.; Jackson, L.; Shadle, G.; Nakashima, J.; Temple, S.; Chen, F.; Dixon, R. A. Distinct Cinnamoyl CoA Reductases Involved in Parallel Routes to Lignin in Medicago Truncatula. *Proc. Natl. Acad. Sci.* **2010**, *107* (41), 17803–17808. https://doi.org/10.1073/pnas.1012900107.

(36) Pan, H.; Zhou, R.; Louie, G. V.; Mühlemann, J. K.; Bomati, E. K.; Bowman, M. E.; Dudareva, N.; Dixon, R. A.; Noel, J. P.; Wang, X. Structural Studies of Cinnamoyl-CoA Reductase and Cinnamyl-Alcohol Dehydrogenase, Key Enzymes of Monolignol Biosynthesis. *Plant Cell* **2014**, *26* (9), 3709–3727. https://doi.org/10.1105/tpc.114.127399.

(37) Bhattacharyya, D.; Hazra, S.; Banerjee, A.; Datta, R.; Kumar, D.; Chakrabarti, S.; Chattopadhyay, S. Transcriptome-Wide Identification and Characterization of CAD Isoforms Specific for Podophyllotoxin Biosynthesis from Podophyllum Hexandrum. *Plant Mol. Biol.* **2016**, *92* (1–2), 1–23. https://doi.org/10.1007/s11103-016-0492-5.

(38) Vogt, T. Phenylpropanoid Biosynthesis. *Mol. Plant* **2010**, *3* (1), 2–20. https://doi.org/10.1093/mp/ssp106.

(39) Padmakshan, D.; Timokhin, V. I.; Lu, F.; Schatz, P. F.; Vanholme, R.; Boerjan, W.; Ralph, J. Synthesis of Hydroxycinnamoyl Shikimates and Their Role in Monolignol Biosynthesis. *Holzforschung* **2022**, *76* (2), 133–144. https://doi.org/10.1515/hf-2021-0149.

(40) Liu, X.; Zhao, C.; Gong, Q.; Wang, Y.; Cao, J.; Li, X.; Grierson, D.; Sun, C. Characterization of a Caffeoyl-CoA O-Methyltransferase-like Enzyme Involved in Biosynthesis of Polymethoxylated Flavones in Citrus Reticulata. *J. Exp. Bot.* **2020**, *71* (10), 3066–3079. https://doi.org/10.1093/jxb/eraa083.

(41) Davin, L. B.; Wang, H.-B.; Crowell, A. L.; Bedgar, D. L.; Martin, D. M.; Sarkanen, S.; Lewis, N. G. Stereoselective Bimolecular Phenoxy Radical Coupling by an Auxiliary (Dirigent) Protein Without an Active Center. *Science (80-.).* **1997**, *275* (5298), 362–367. https://doi.org/10.1126/science.275.5298.362.

(42) Zoclanclounon, Y. A. B.; Rostás, M.; Chung, N.-J.; Mo, Y.; Karlovsky, P.; Dossa, K. Characterization of Peroxidase and Laccase Gene Families and In Silico Identification of Potential Genes Involved in Upstream Steps of Lignan Formation in Sesame. *Life* **2022**, *12* (8), 1200. https://doi.org/10.3390/life12081200.

(43) Pickel, B.; Constantin, M.-A.; Pfannstiel, J.; Conrad, J.; Beifuss, U.; Schaller, A. An Enantiocomplementary Dirigent Protein for the Enantioselective Laccase-Catalyzed Oxidative Coupling of Phenols. *Angew. Chemie Int. Ed.* **2010**, *49* (1), 202–204.

(44) Lopes, N. P.; Yoshida, M.; Kato, M. J. Biosynthesis of Tetrahydrofuran Lignans in Virola Surinamensis. *Rev. Bras. Ciências Farm.* **2004**, *40* (1), 53–57. https://doi.org/10.1590/S1516-93322004000100009.

(45) Dong, Y. Q.; Qiang, T. Y.; Liu, J. S.; Li, B.; Wei, X. P.; Qi, Y. D.; Liu, H. T.; Zhang, B.

G. Identification and Characterization of DIR Gene Family in Schisandra Chinensis. *Zhongguo Zhongyao Zazhi* **2021**, *46* (20), 5270–5277. https://doi.org/10.19540/j.cnki.cjcmm.20210723.101.

(46) Halls, S. C.; Lewis, N. G. Secondary and Quaternary Structures of the (+)-Pinoresinol-Forming Dirigent Protein. *Biochemistry* **2002**, *41* (30), 9455–9461. https://doi.org/10.1021/bi0259709.

(47) Kim, S. S.; Sattely, E. S. Dirigent Proteins Guide Asymmetric Heterocoupling for the Synthesis of Complex Natural Product Analogues. *J. Am. Chem. Soc.* **2021**, *143* (13), 5011–5021. https://doi.org/10.1021/jacs.0c13164.

(48) Fujita, M.; Gang, D. R.; Davin, L. B.; Lewis, N. G. Recombinant Pinoresinol-Lariciresinol Reductases from Western Red Cedar (Thuja Plicata) Catalyze Opposite Enantiospecific Conversions. *J. Biol. Chem.* **1999**, *274* (2), 618–627. https://doi.org/10.1074/jbc.274.2.618.

(49) Moinuddin, S. G. A.; Youn, B.; Bedgar, D. L.; Costa, M. A.; Helms, G. L.; Kang, C.; Davin, L. B.; Lewis, N. G. Secoisolariciresinol Dehydrogenase: Mode of Catalysis and Stereospecificity of Hydride Transfer in Podophyllum Peltatum. *Org. Biomol. Chem.* **2006**, *4* (5), 808–816. https://doi.org/10.1039/b516563f.

(50) Walsh, C. T. Tailoring Enzyme Strategies and Functional Groups in Biosynthetic Pathways. *Natural Product Reports*. Royal Society of Chemistry October 21, 2022, pp 326–386. https://doi.org/10.1039/d2np00048b.

(51) Jia, K.-Z.; Zhu, L.-W.; Qu, X.; Li, S.; Shen, Y.; Qi, Q.; Zhang, Y.; Li, Y.-Z.; Tang, Y.-J. Enzymatic O -Glycosylation of Etoposide Aglycone by Exploration of the Substrate Promiscuity for Glycosyltransferases. *ACS Synth. Biol.* **2019**, *8* (12), 2718–2725.

https://doi.org/10.1021/acssynbio.9b00318.

(52) Marques, J. V; Kim, K.-W.; Lee, C.; Costa, M. A.; May, G. D.; Crow, J. A.; Davin, L. B.; Lewis, N. G. Next Generation Sequencing in Predicting Gene Function in Podophyllotoxin Biosynthesis. *J. Biol. Chem.* **2013**, *288* (1), 466–479. https://doi.org/10.1074/jbc.M112.400689.

(53) Kawai, Y.; Ono, E.; Mizutani, M. Evolution and Diversity of the 2–Oxoglutarate-Dependent Dioxygenase Superfamily in Plants. *Plant J.* **2014**, *78* (2), 328–343. https://doi.org/https://doi.org/10.1111/tpj.12479.

(54) Sakakibara, N.; Suzuki, S.; Umezawa, T.; Shimada, M. Biosynthesis of Yatein in Anthriscus Sylvestris. *Org. Biomol. Chem.* **2003**, *1* (14), 2474. https://doi.org/10.1039/b304411d.

(55) Anarat-Cappillino, G.; Sattely, E. S. The Chemical Logic of Plant Natural Product Biosynthesis. *Curr. Opin. Plant Biol.* **2014**, *19*, 51–58. https://doi.org/10.1016/j.pbi.2014.03.007.

(56) Chang, W.; Yang, Z.-J.; Tu, Y.-H.; Chien, T.-C. Reaction Mechanism of a Nonheme Iron Enzyme Catalyzed Oxidative Cyclization via C–C Bond Formation. *Org. Lett.* **2019**, *21* (1), 228–232. https://doi.org/10.1021/acs.orglett.8b03670.

(57) Xiang, H.; Ferla, S.; Varricchio, C.; Brancale, A.; Brown, N. L.; Black, G. W.; Turner, N. J.; Castagnolo, D. Biocatalytic and Chemo-Enzymatic Synthesis of Quinolines and 2-Quinolones by Monoamine Oxidase (MAO-N) and Horseradish Peroxidase (HRP) Biocatalysts. *ACS Catal.* **2023**, *13* (5), 3370–3378. https://doi.org/10.1021/acscatal.2c05902.

(58) Zhang, H.-Q.; Yan, C.-X.; Xiao, J.; Wang, Y.-W.; Peng, Y. Recent Advances in the Total

Synthesis of 2,7′-Cyclolignans. *Org. Biomol. Chem.* **2022**, *20* (8), 1623–1636. https://doi.org/10.1039/D1OB02457D.

(59) Ting, C. P.; Maimone, T. J. C-H Bond Arylation in the Synthesis of Aryltetralin Lignans: A Short Total Synthesis of Podophyllotoxin. *Angew. Chemie Int. Ed.* **2014**, *53* (12), 3115–3119. https://doi.org/10.1002/anie.201311112.

(60) Schultz, B. J.; Kim, S. Y.; Lau, W.; Sattely, E. S. Total Biosynthesis for Milligram-Scale Production of Etoposide Intermediates in a Plant Chassis. *J. Am. Chem. Soc.* **2019**, *141* (49), 19231–19235. https://doi.org/10.1021/jacs.9b10717.

(61) Li, J.; Zhang, X.; Renata, H. Asymmetric Chemoenzymatic Synthesis of (−)-Podophyllotoxin and Related Aryltetralin Lignans. *Angew. Chemie Int. Ed.* **2019**, *58* (34), 11657–11660. https://doi.org/10.1002/anie.201904102.

(62) Xiang, J.-C.; Fung, C.; Wang, Q.; Zhu, J. Taming the Radical Cation Intermediate Enabled One-Step Access to Structurally Diverse Lignans. *Nat. Commun.* **2022**, *13* (1), 3481. https://doi.org/10.1038/s41467-022-31000-4.

(63) Decembrino, D.; Raffaele, A.; Knöfel, R.; Girhard, M.; Urlacher, V. B. Synthesis of (−)−deoxypodophyllotoxin and (−)−epipodophyllotoxin via a Multi-Enzyme Cascade in E. Coli. *Microb. Cell Fact.* **2021**, *20* (1), 183. https://doi.org/10.1186/s12934-021-01673-5.

(64) Chern, J.; Lu, C.-P.; Fang, Z.; Chang, C.-M.; Hua, K.-F.; Chen, Y.-T.; Ng, C. Y.; Chen, Y.-L. S.; Lam, Y.; Wu, S.-H. Affinity-Driven Covalent Modulator of the Glyceraldehyde-3-Phosphate Dehydrogenase (GAPDH) Cascade. *Angew. Chemie Int. Ed.* **2018**, *57* (24), 7040–7045. https://doi.org/10.1002/anie.201801618.

(65) Duan, S.; Huang, S.; Gong, J.; Shen, Y.; Zeng, L.; Feng, Y.; Ren, W.; Leng, Y.; Hu, Y.

Design and Synthesis of Novel Arctigenin Analogues for the Amelioration of Metabolic Disorders. *ACS Med. Chem. Lett.* **2015**, *6* (4), 386–391. https://doi.org/10.1021/acsmedchemlett.5b00007.

(66) Kiralj, R.; Ferreira, M. M. C.; Donate, P. M.; da Silva, R.; Albuquerque, S. Conformational Study of (8α,8‘β)-Bis(Substituted Phenyl)-Lignano-9,9‘-Lactones by Means of Combined Computational, Database Mining, NMR, and Chemometric Approaches. *J. Phys. Chem. A* **2007**, *111* (28), 6316–6333. https://doi.org/10.1021/jp066746m.

(67) Cambie, R.; Craw, P.; Rutledge, P.; Woodgate, P. Oxidative Coupling of Lignans. III. Non-Phenolic Oxidative Coupling of Deoxypodorhizon and Related Compounds. *Aust. J. Chem.* **1988**, *41* (6), 897. https://doi.org/10.1071/CH9880897.

(68) Wilson, S. R.; Augelli, C. E. THE CARROLL REARRANGEMENT: 5-DODECEN-2-ONE. *Org. Synth.* **1990**, *68*, 210. https://doi.org/10.15227/orgsyn.068.0210.

(69) Kim, Y.; You, Y.-J.; Nam, N.-H.; Ahn, B.-Z. 2,3-Dibenzylbutyrolactones and 1,2,3,4-Tetrahydro-2-Naphthoic Acid Γnes: Structure and Activity Relationship in Cytotoxic Activity. *Arch. Pharm. Res.* **2002**, *25* (3), 240–249. https://doi.org/10.1007/BF02976621.

(70) Tang, H.; Wu, M.-H.; Lin, H.-Y.; Han, M.-R.; Tu, Y.-H.; Yang, Z.-J.; Chien, T.-C.; Chan, N.-L.; Chang, W. Mechanistic Analysis of Carbon–Carbon Bond Formation by Deoxypodophyllotoxin Synthase. *Proc. Natl. Acad. Sci.* **2022**, *119* (1). https://doi.org/10.1073/pnas.2113770119.

(71) Maya, A. B. S.; Pérez-Melero, C.; Mateo, C.; Alonso, D.; Fernández, J. L.; Gajate, C.; Mollinedo, F.; Peláez, R.; Caballero, E.; Medarde, M. Further Naphthylcombretastatins. An Investigation on the Role of the Naphthalene Moiety. *J. Med. Chem.* **2005**, *48* (2),

556–568. https://doi.org/10.1021/jm0310737.

(72) Pérez-Melero, C.; Maya, A. B. .; del Rey, B.; Peláez, R.; Caballero, E.; Medarde, M. A New Family of Quinoline and Quinoxaline Analogues of Combretastatins. *Bioorg. Med. Chem. Lett.* **2004**, *14* (14), 3771–3774. https://doi.org/10.1016/j.bmcl.2004.04.098.

(73) Albertson, A. K. F.; Lumb, J.-P. The Lignans. In *Recent Advances in Polyphenol Research*; John Wiley & Sons, Ltd: Chichester, UK, 2019; pp 1–70. https://doi.org/10.1002/9781119427896.ch1.

APPENDICES

Appendix A.1 ^{1}H-NMR (1)

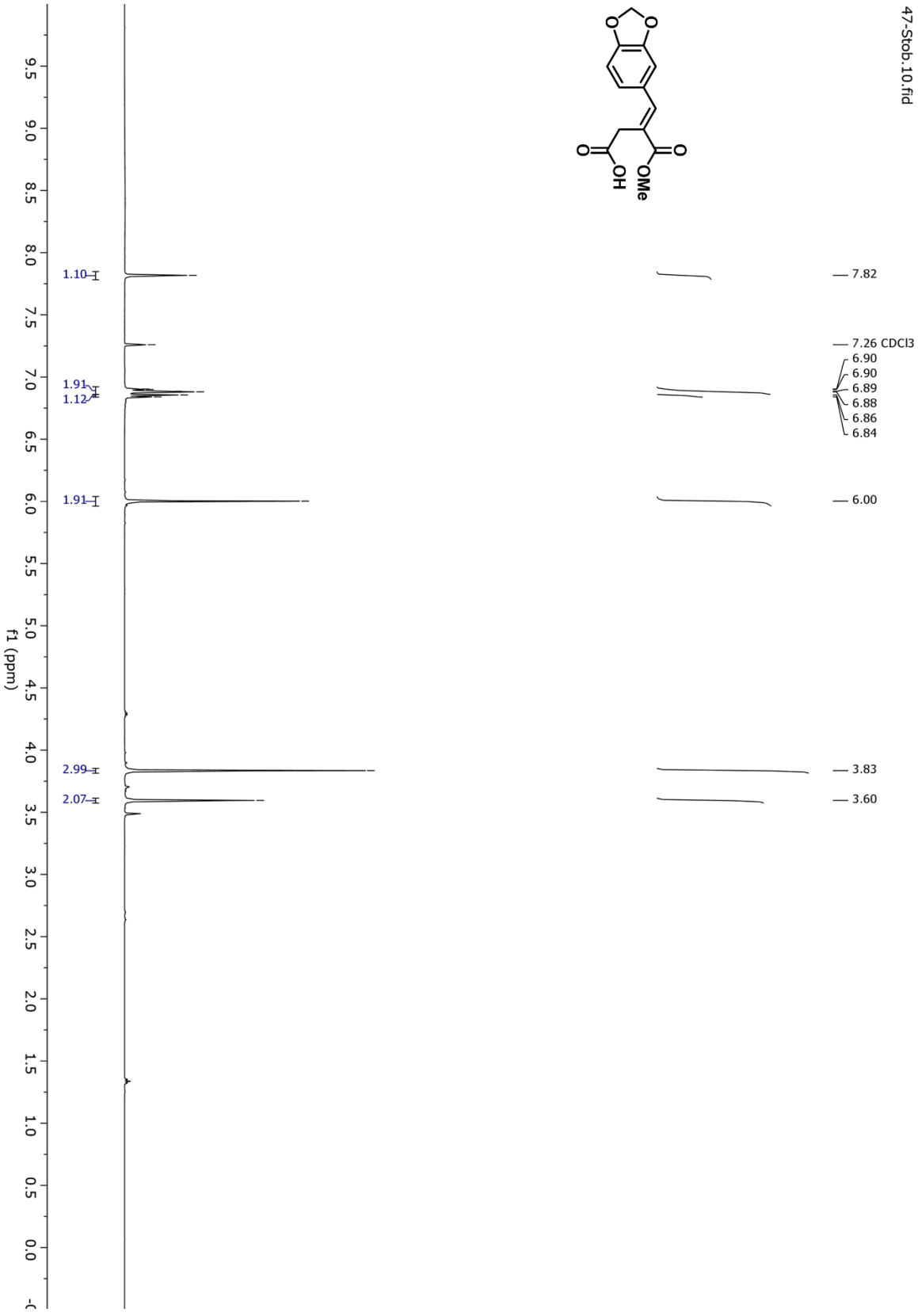

^{13}C-NMR (1)

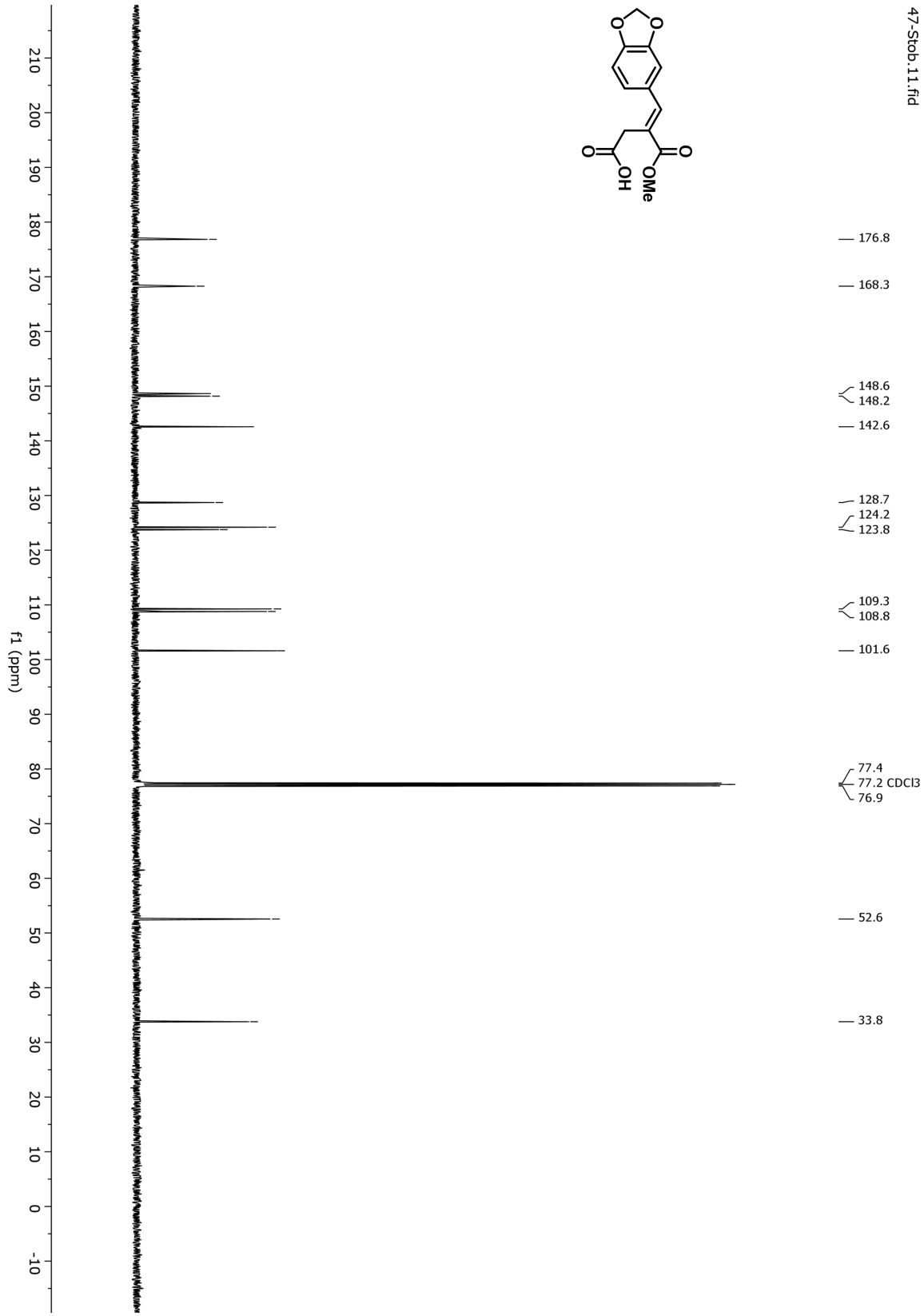
47-Stob.11.fid
176.8
168.3
148.6
148.2
142.6
128.7
124.2
123.8
109.3
108.8
101.6
77.4
77.2 CDCl3
76.9
52.6
33.8
f1 (ppm)
OH
OMe

Appendix A.2 ^{1}H-NMR (2)

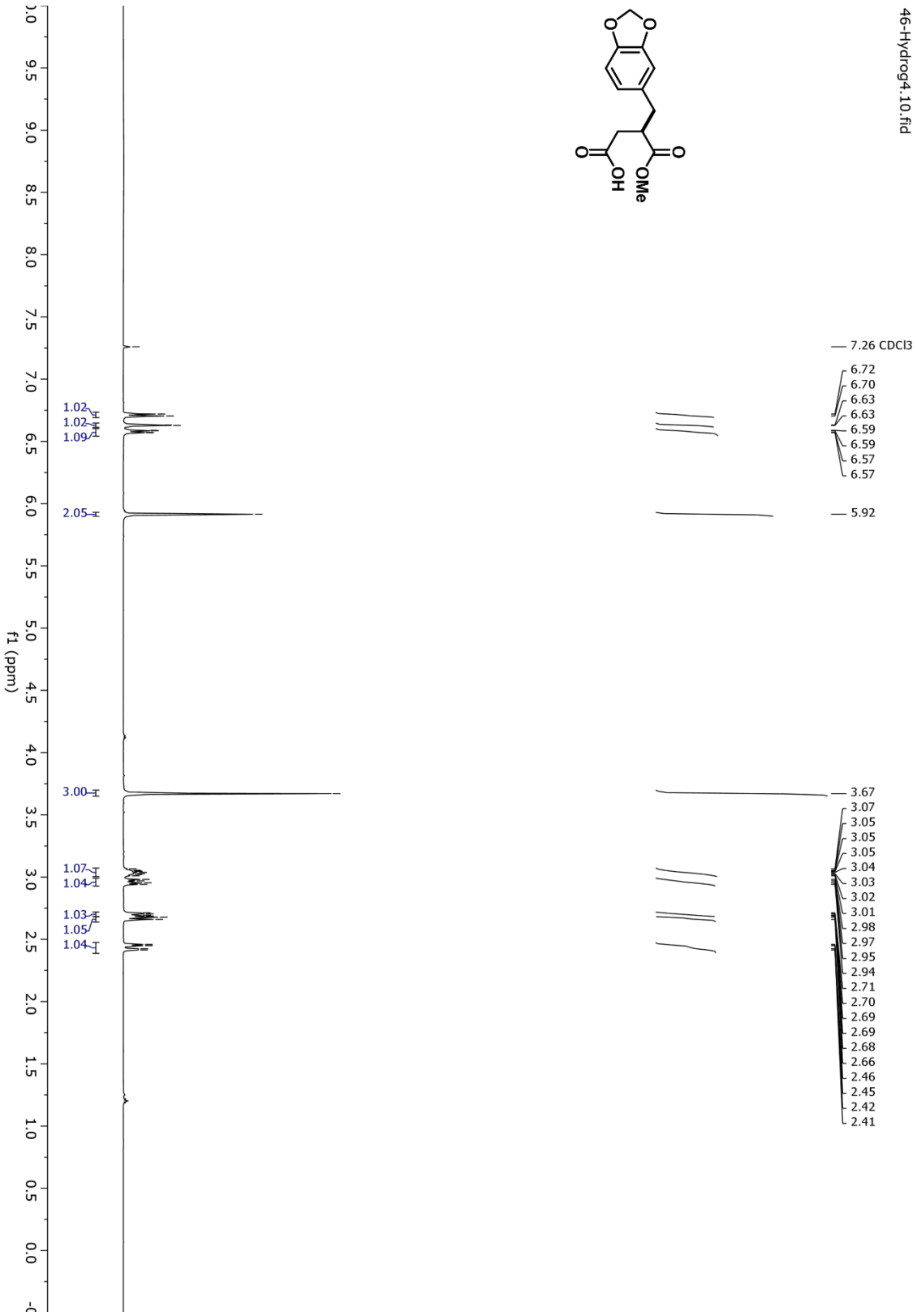

^{13}C-NMR (2)

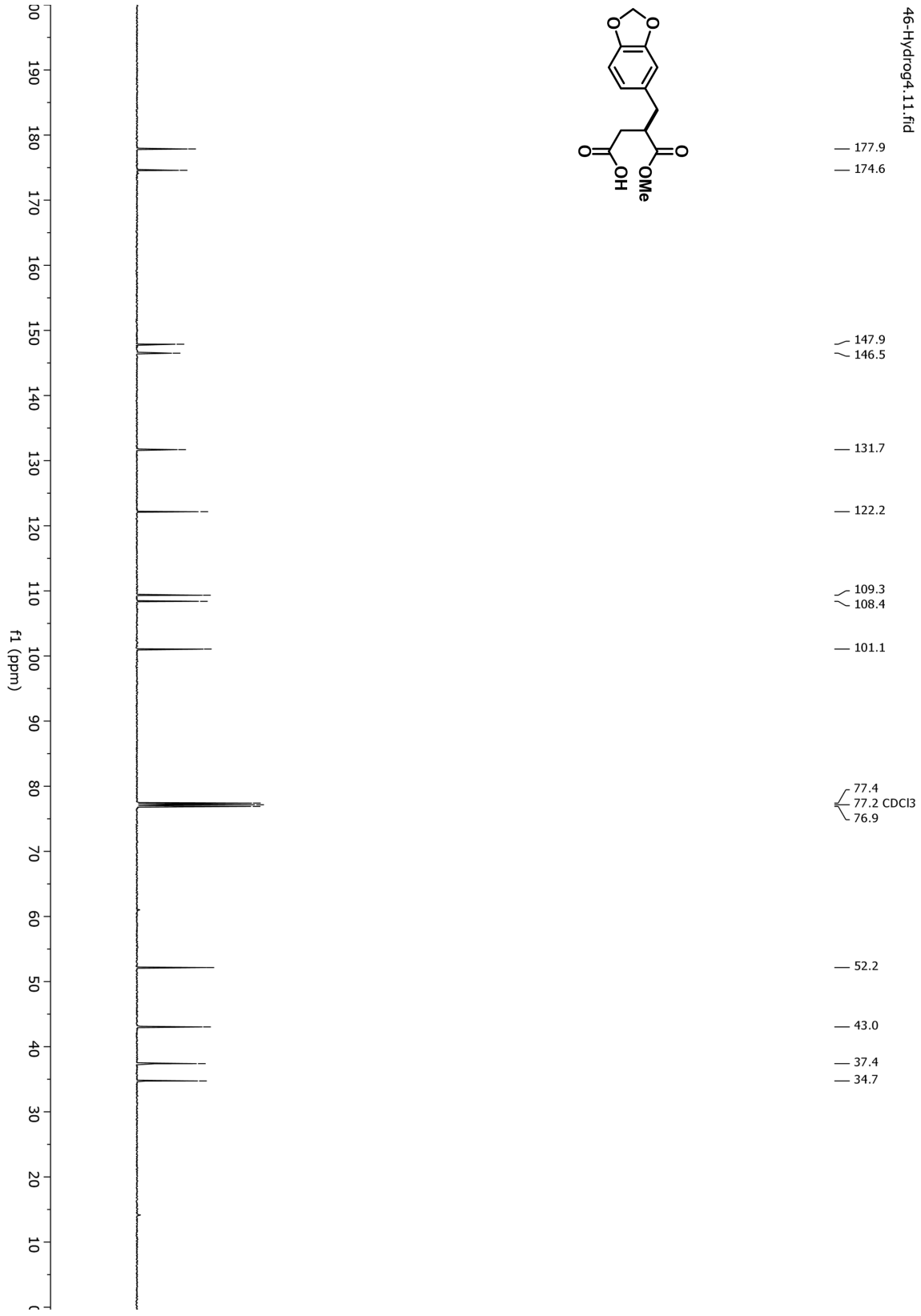
46-Hydrog4.11.fid
177.9
174.6
147.9
146.5
131.7
122.2
109.3
108.4
101.1
77.4
77.2 CDCl3
76.9
52.2
43.0
37.4
34.7
f1 (ppm)
OH
OMe

Appendix A.3 ^{1}H-NMR (3)

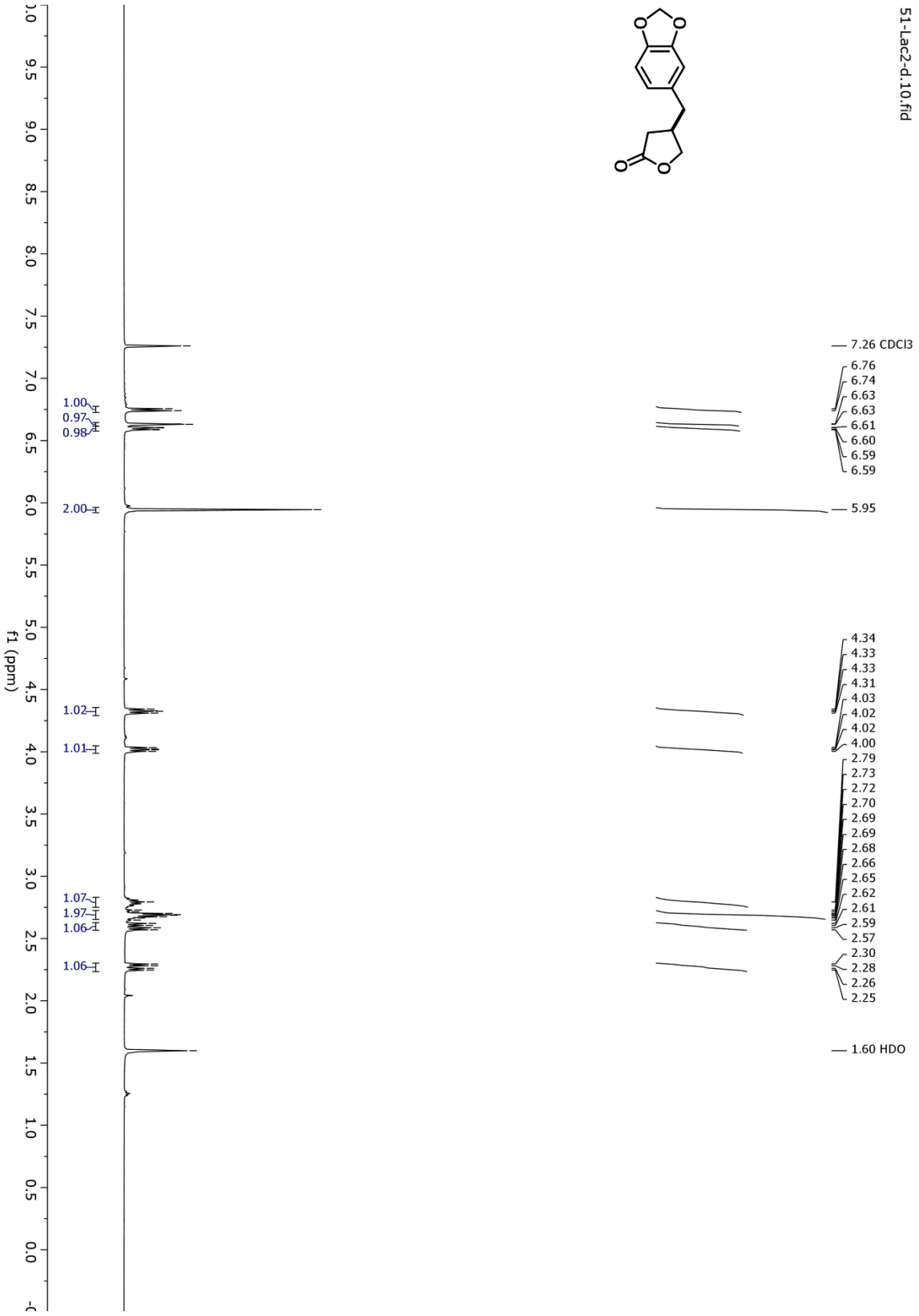

^{13}C-NMR (3)

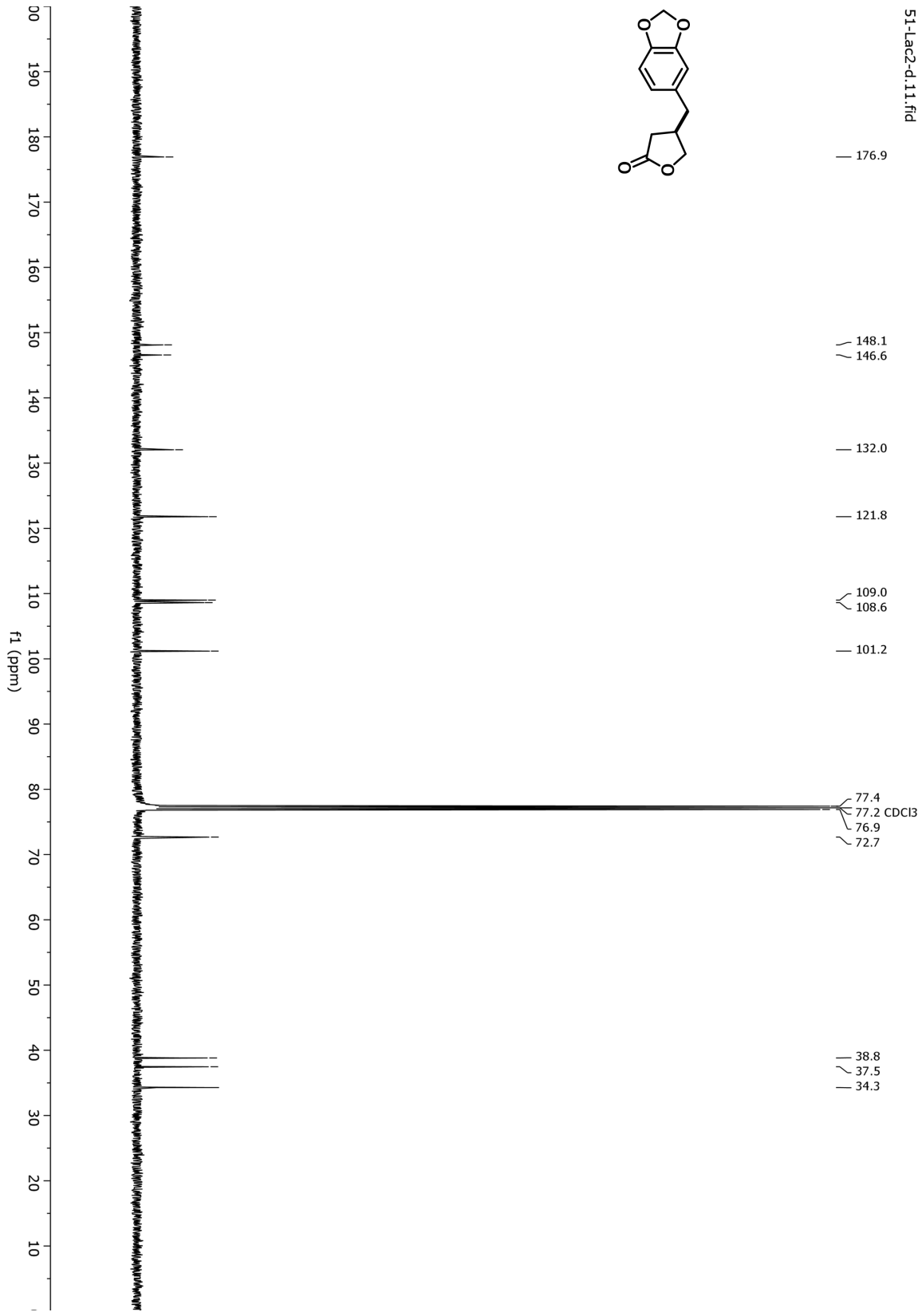
51-Lac2-d.11.fid
176.9
148.1
146.6
132.0
121.8
109.0
108.6
101.2
77.4
77.2 CDCl3
76.9
72.7
38.8
37.5
34.3
f1 (ppm)

Appendix A.4 ^{1}H-NMR (4)

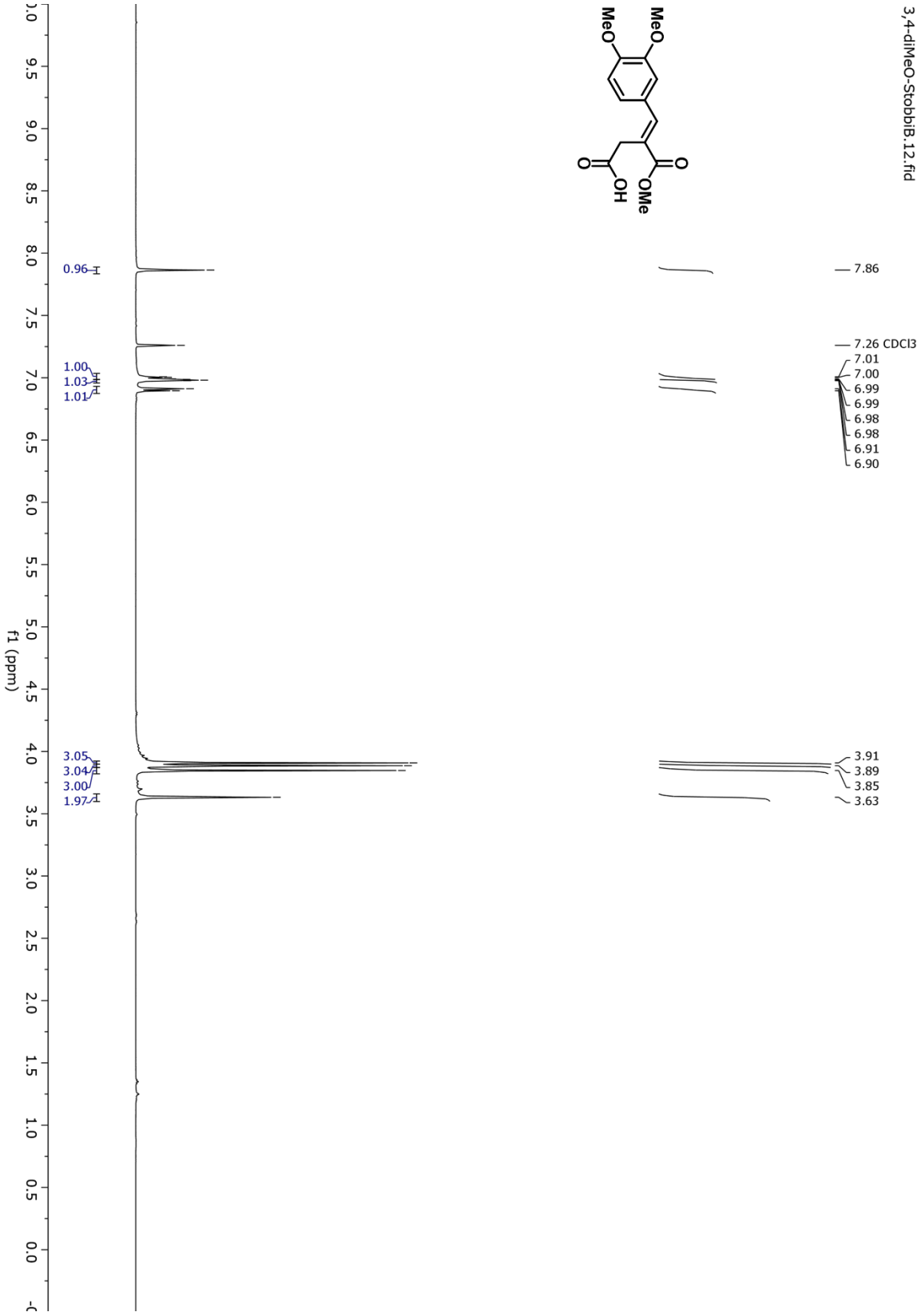

^{13}C-NMR (4)

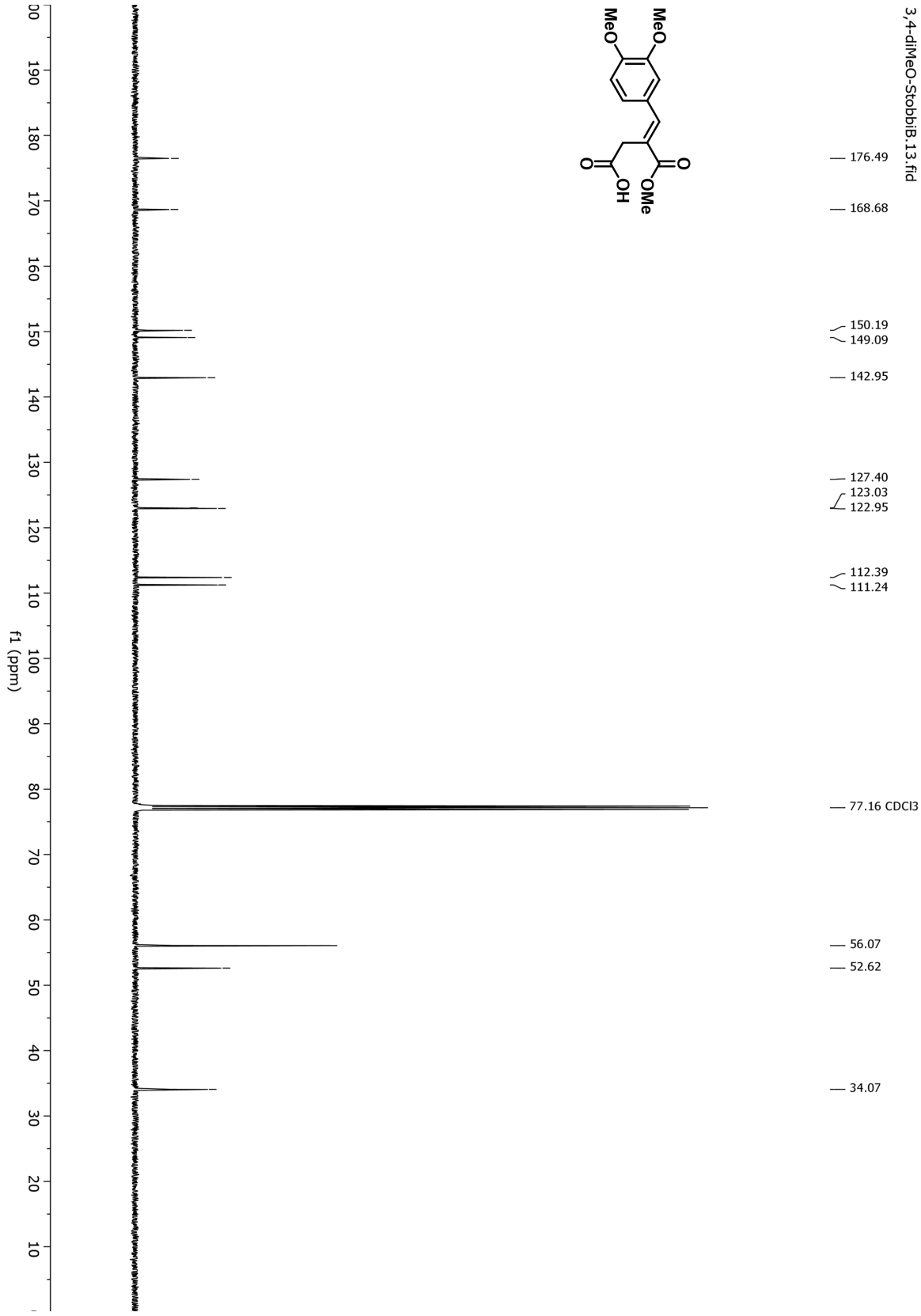
3,4-diMeO-StobbiB.13.fid
MeO
MeO
O
OH
O
OMe
176.49
168.68
150.19
149.09
142.95
127.40
123.03
122.95
112.39
111.24
77.16 CDCl3
56.07
52.62
34.07
f1 (ppm)

Appendix A.5 ^{1}H-NMR (5)

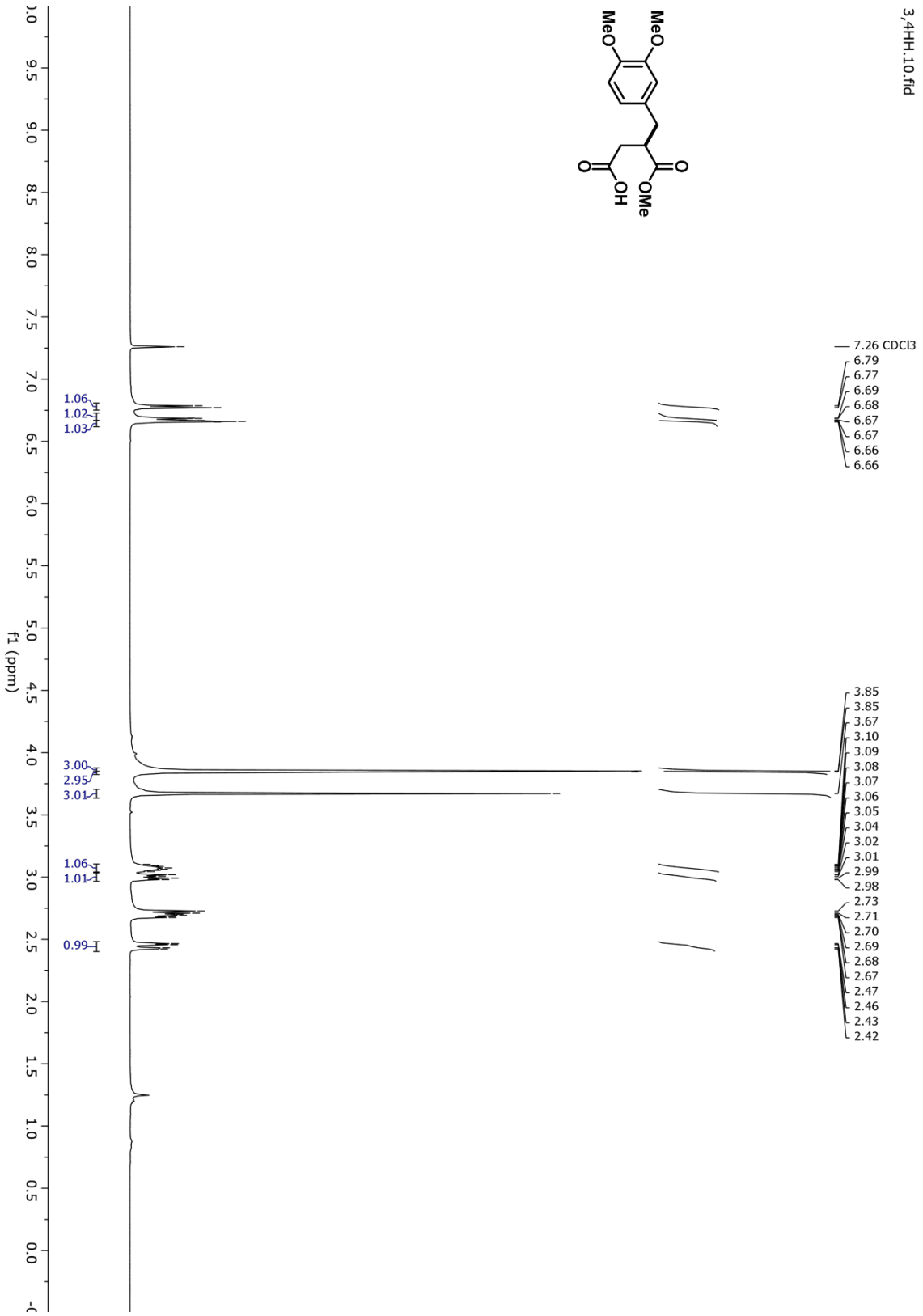

^{13}C-NMR (5)

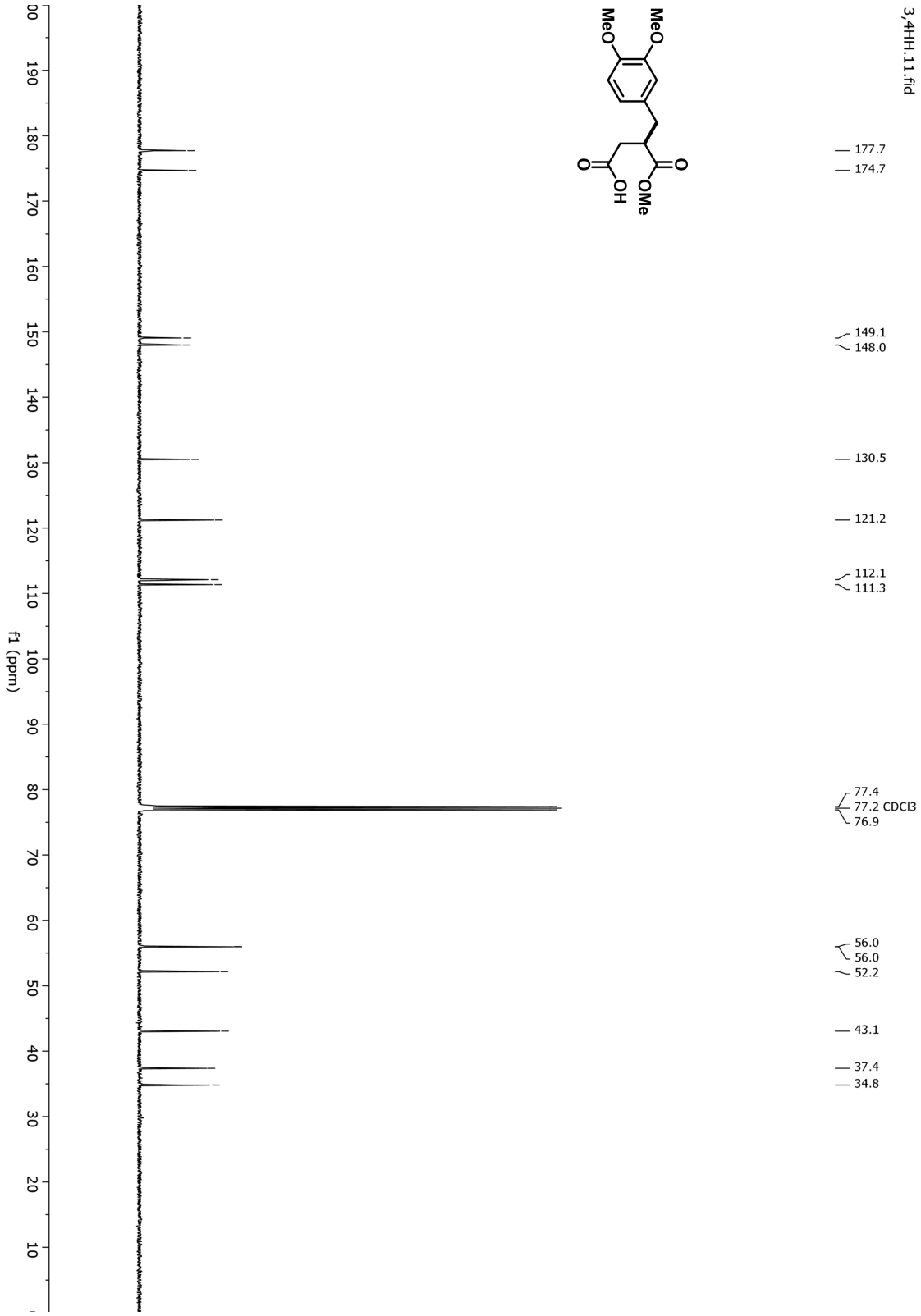
3,4HH.11.fid
MeO
MeO
OH
O
OMe
O
177.7
174.7
149.1
148.0
130.5
121.2
112.1
111.3
77.4
77.2 CDCl3
76.9
56.0
56.0
52.2
43.1
37.4
34.8
f1 (ppm)

Appendix A.6 ^{1}H-NMR (6)

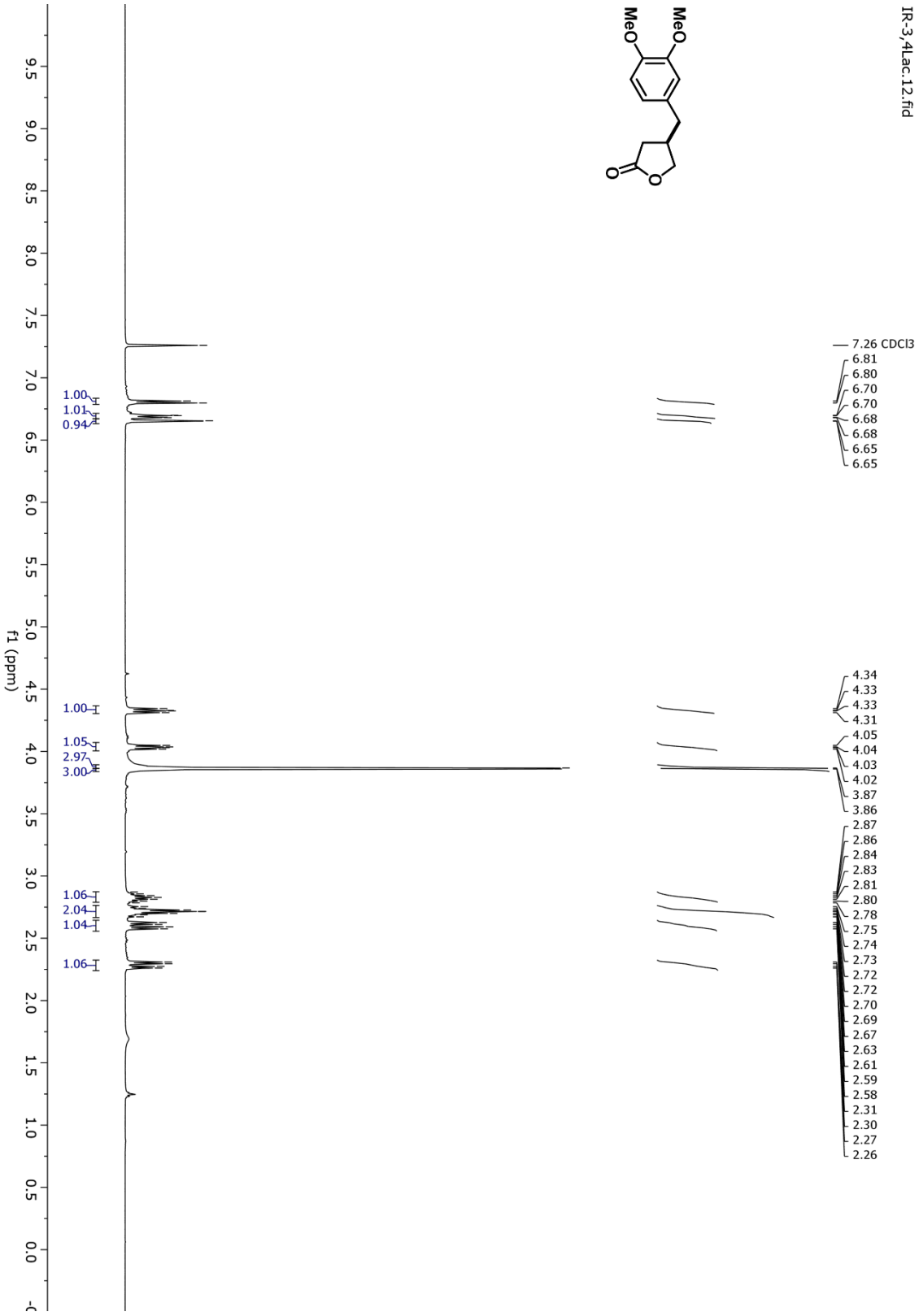

^{13}C-NMR (6)

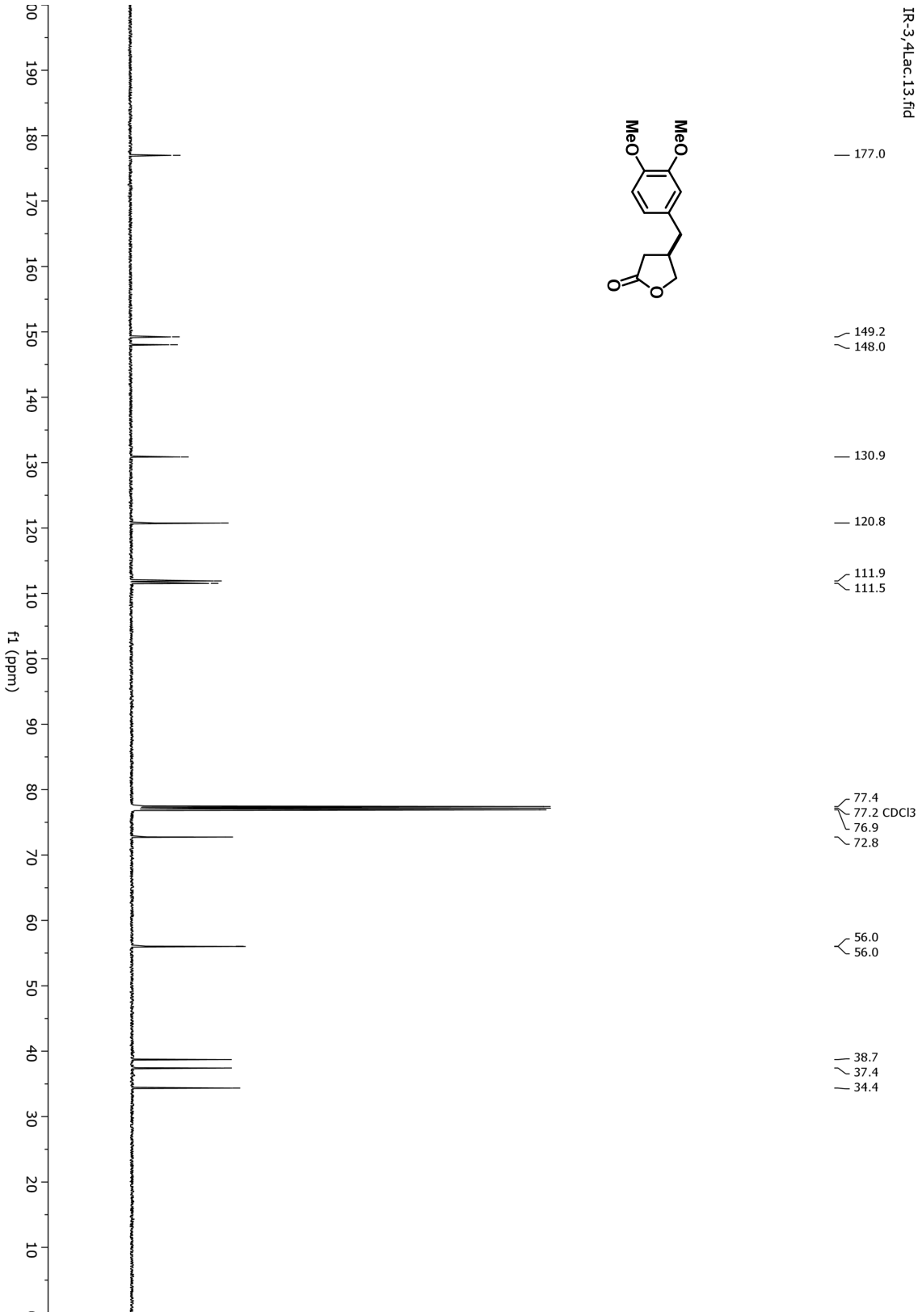
IR-3,4Lac.13.fid
MeO
MeO
O
O
177.0
149.2
148.0
130.9
120.8
111.9
111.5
77.4
77.2 CDCl3
76.9
72.8
56.0
56.0
38.7
37.4
34.4
f1 (ppm)

Appendix A.7 ^{1}H-NMR (7)

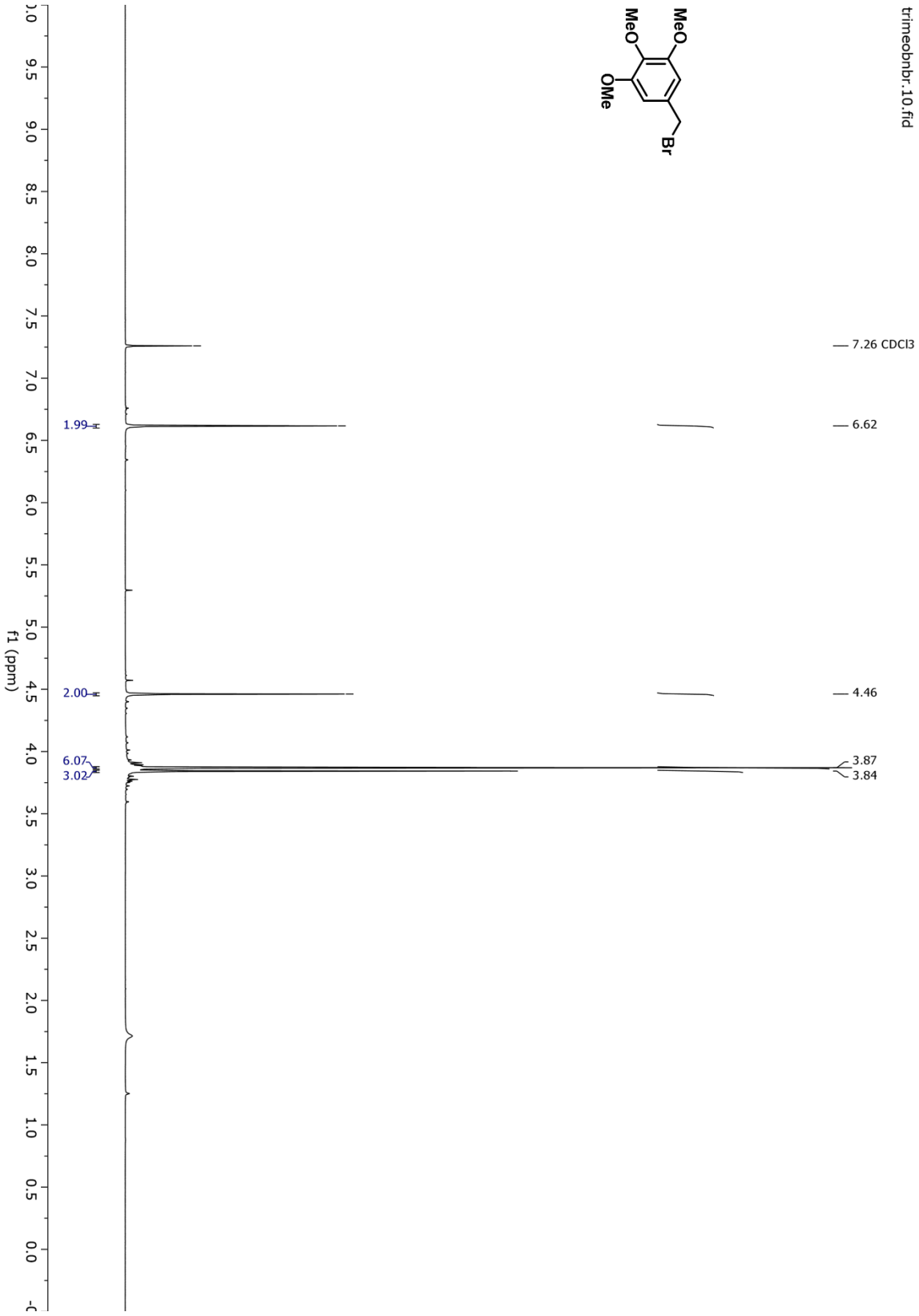

^{13}C-NMR (7)

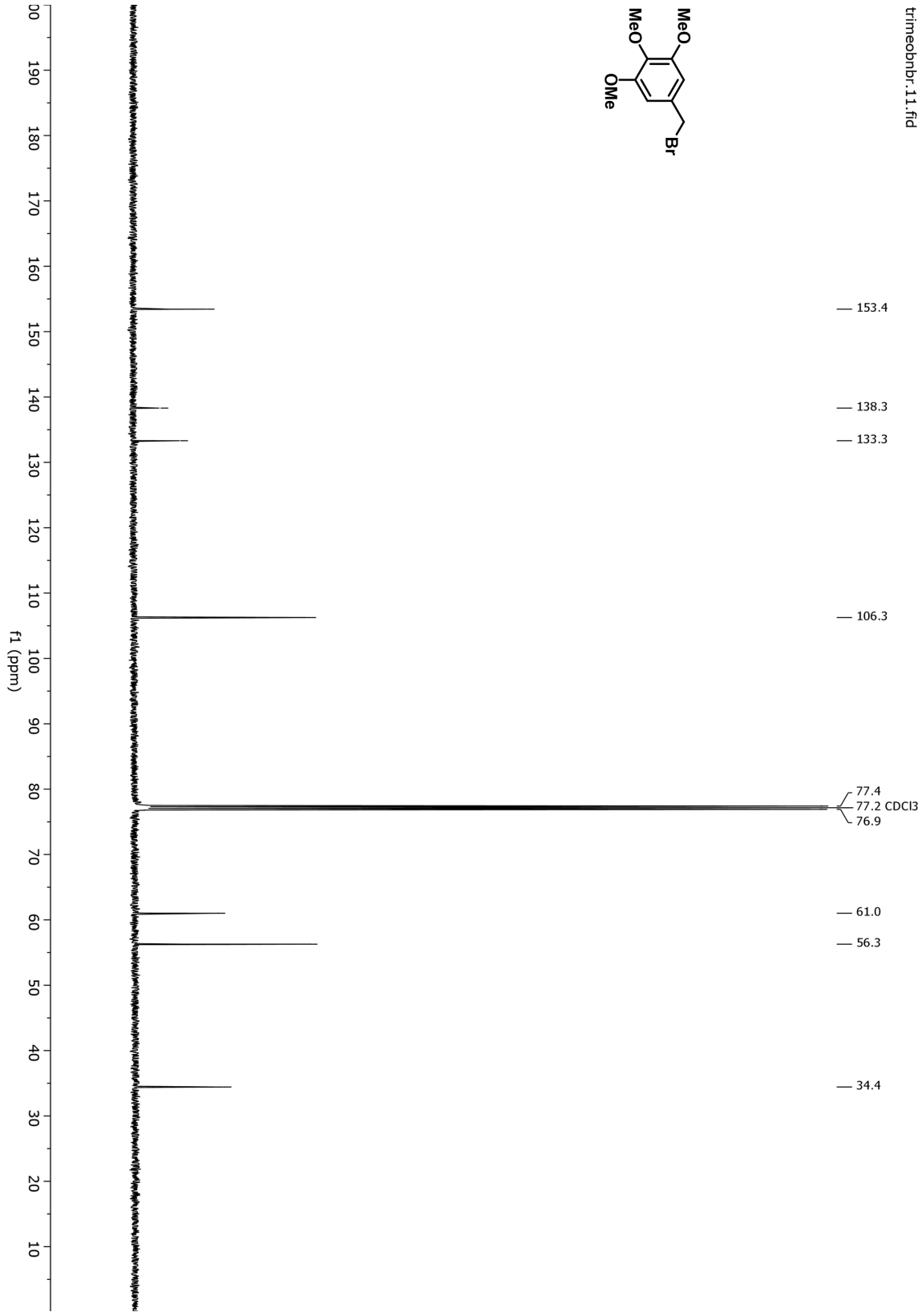
trimeobnbr.11.fid
MeO
MeO
OMe
Br
153.4
138.3
133.3
106.3
77.4
77.2 CDCl3
76.9
61.0
56.3
34.4
f1 (ppm)

Appendix A.8 ^{1}H-NMR (8)

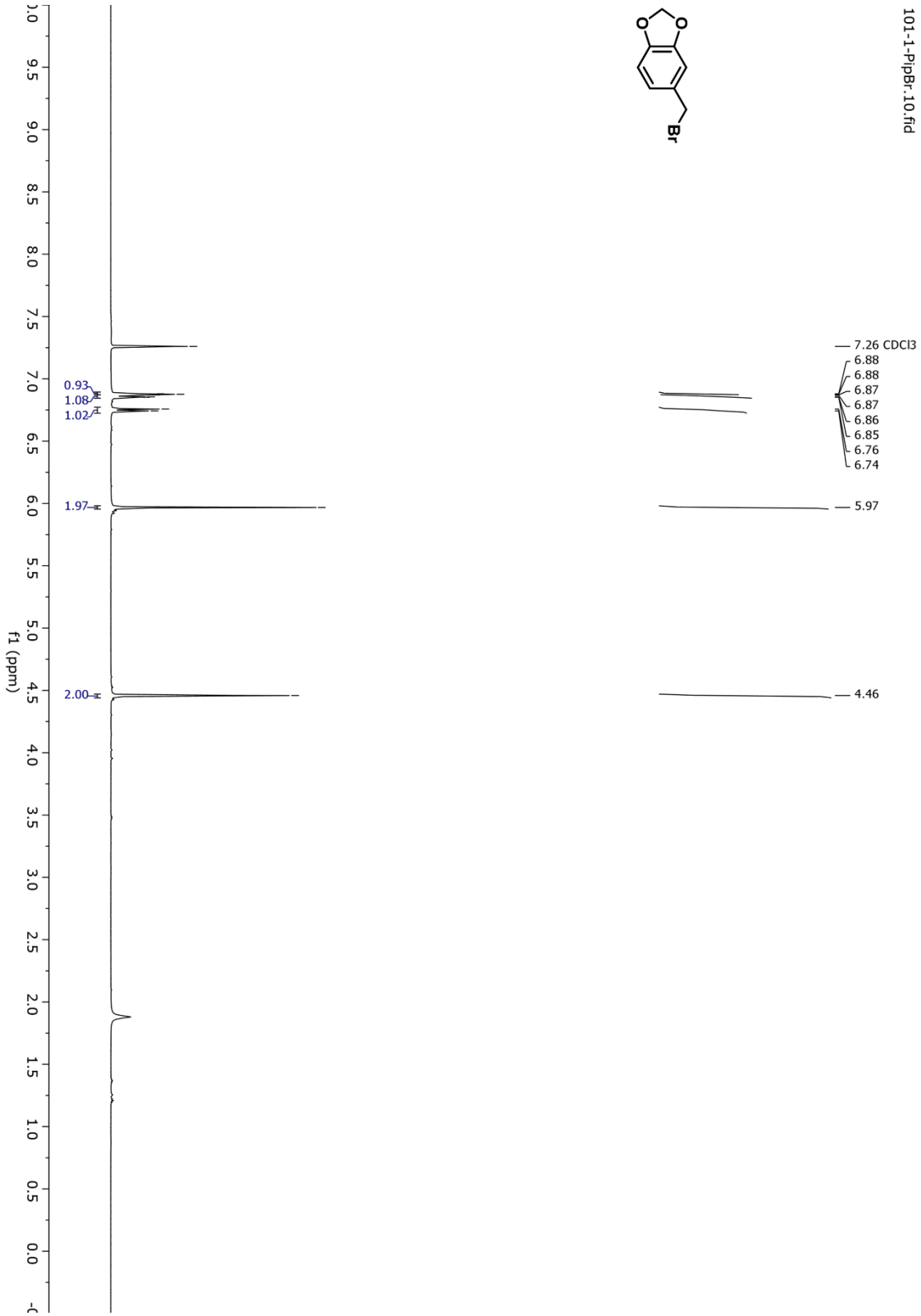

^{13}C-NMR (8)

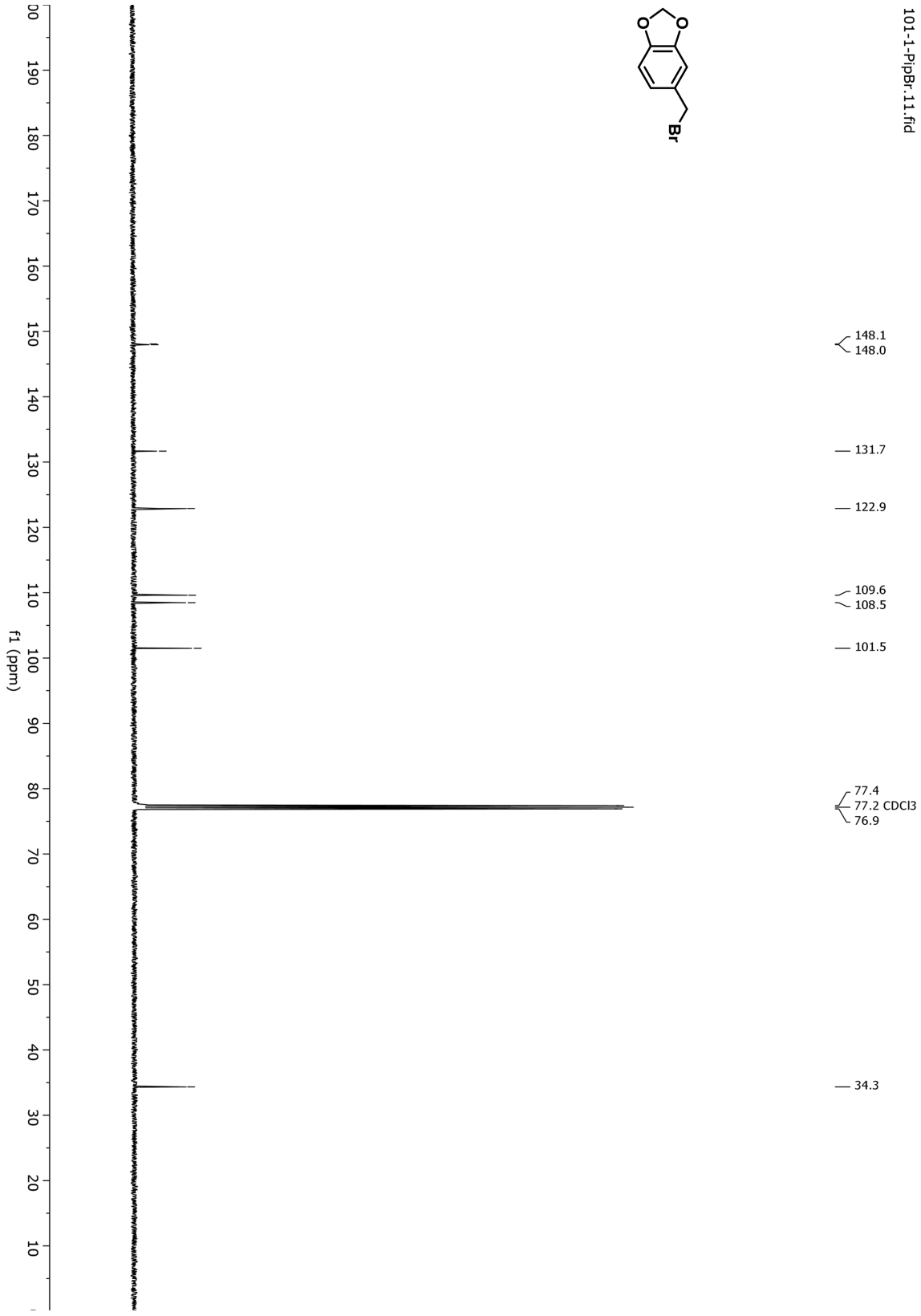
101-1-PipBr.11.fid
148.1
148.0
131.7
122.9
109.6
108.5
101.5
77.4
77.2 CDCl3
76.9
34.3
f1 (ppm)
Br

Appendix A.9 ^{1}H-NMR (9)

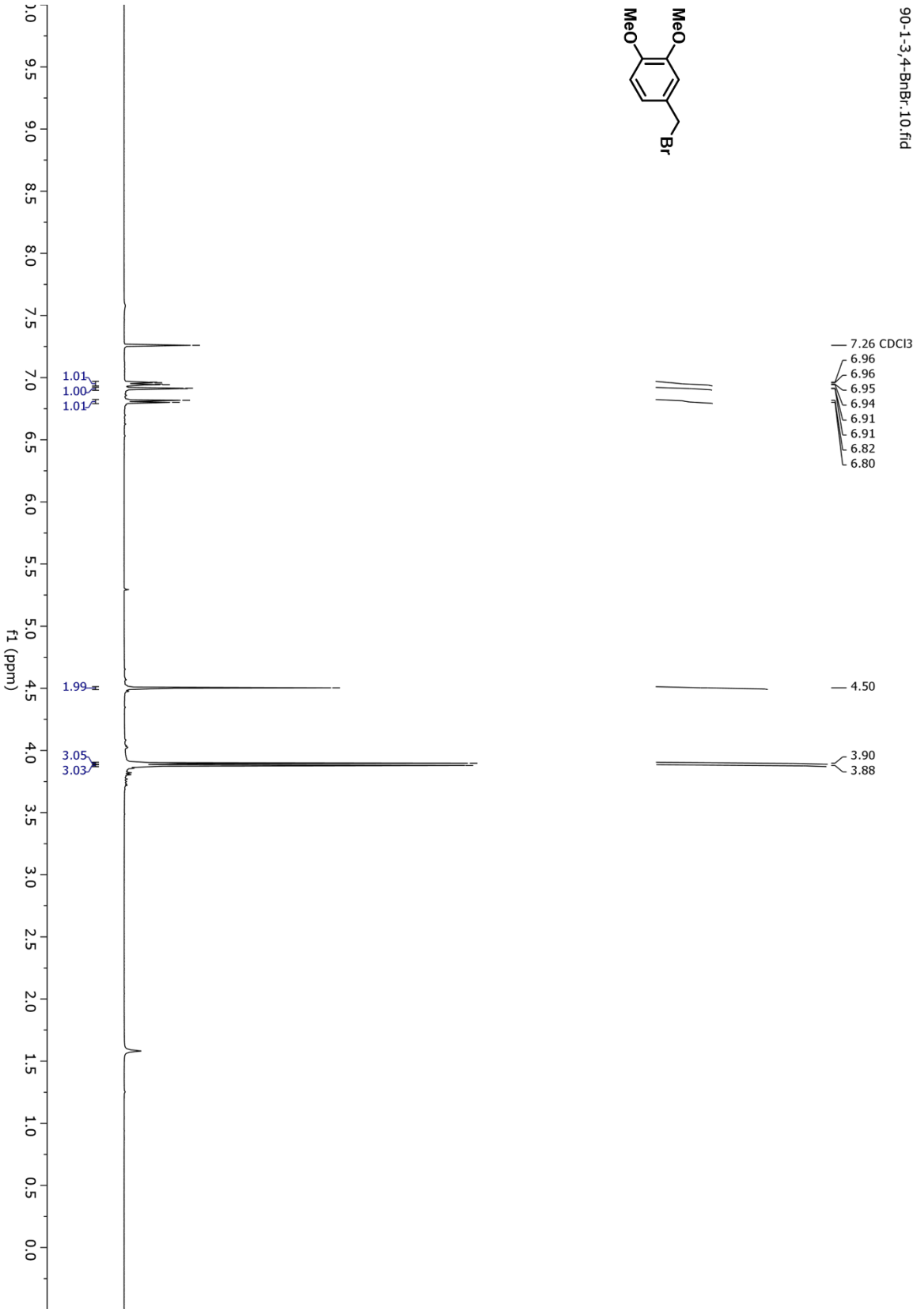

^{13}C-NMR (9)

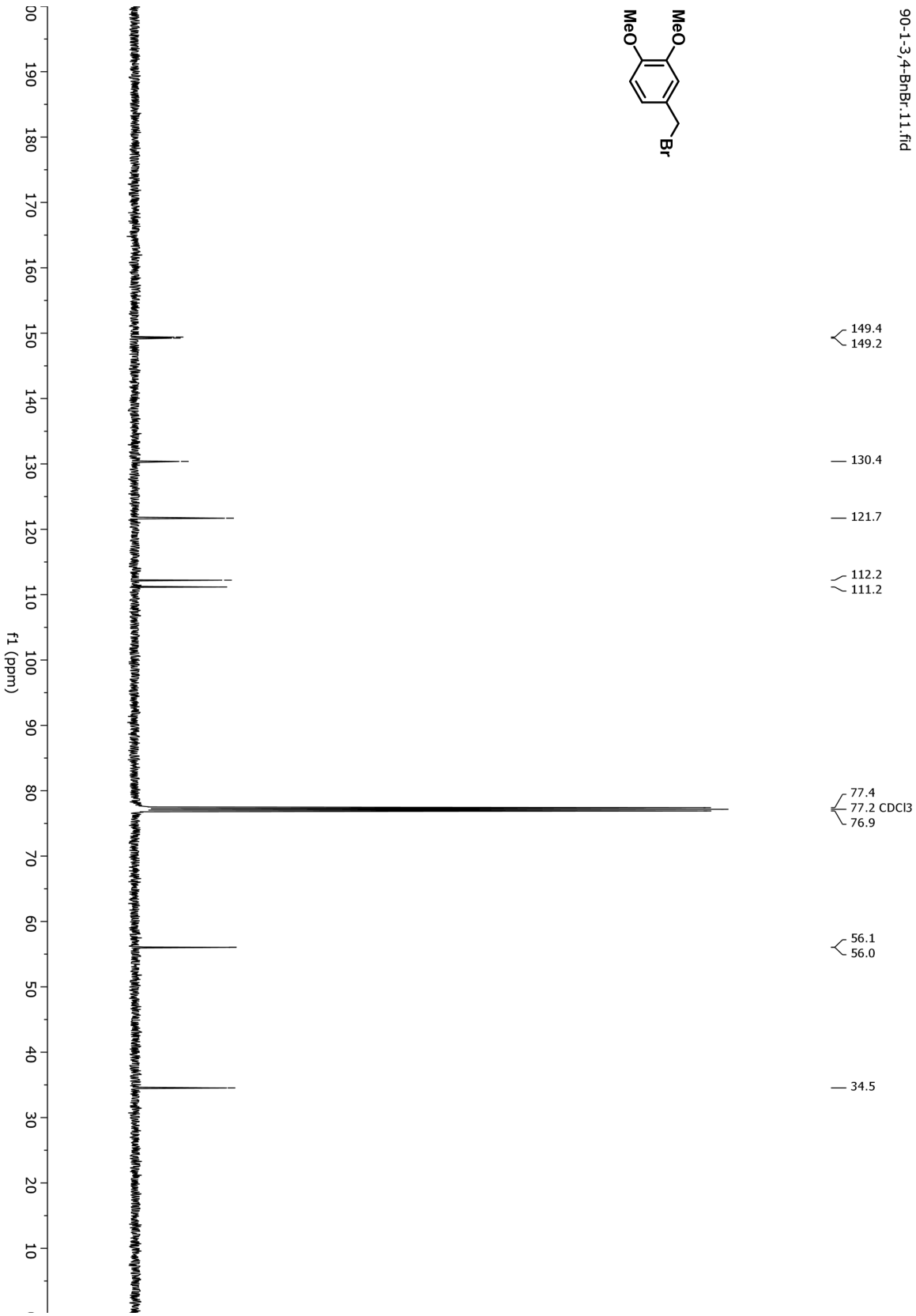
90-1-3,4-BnBr.11.fid
MeO
MeO
Br
149.4
149.2
130.4
121.7
112.2
111.2
77.4
77.2 CDCl3
76.9
56.1
56.0
34.5
f1 (ppm)

Appendix A.10 ^{1}H-NMR (10)

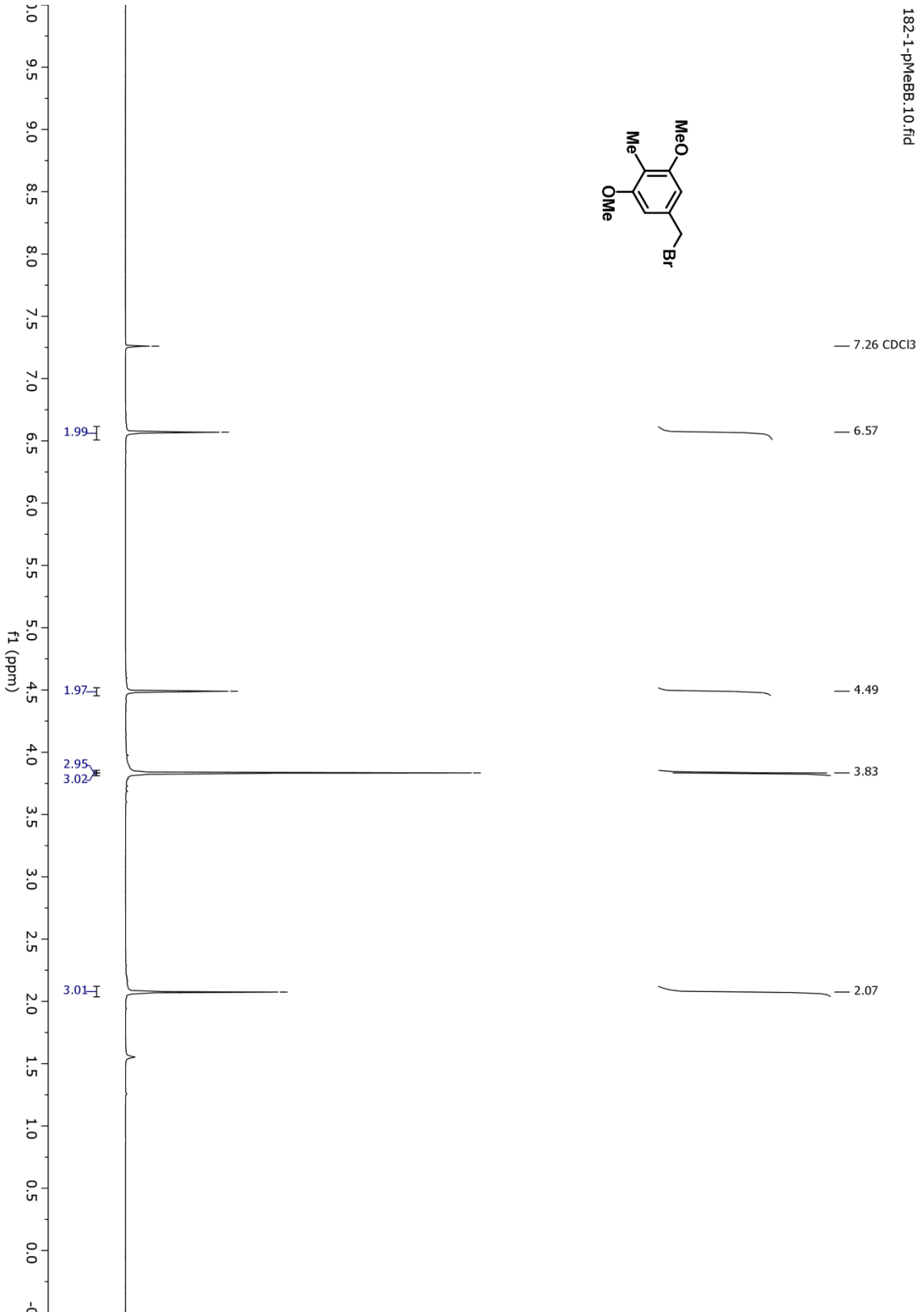

^{13}C-NMR (10)

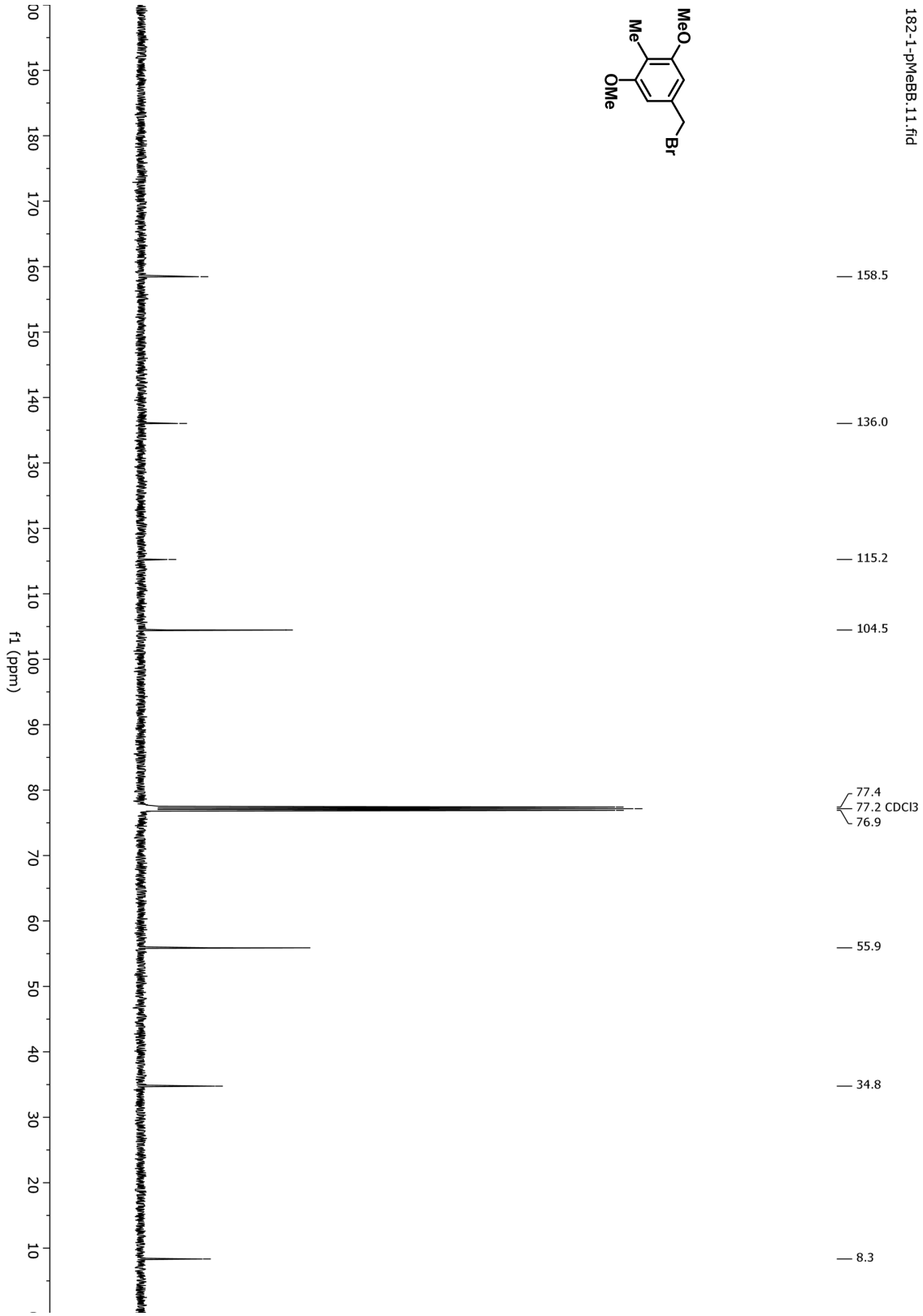
MeO
Me
OMe
Br
182-1-pMeBB.11.fid
158.5
136.0
115.2
104.5
77.4
77.2 CDCl3
76.9
55.9
34.8
8.3
f1 (ppm)

Appendix A.11 ^{1}H-NMR (11)

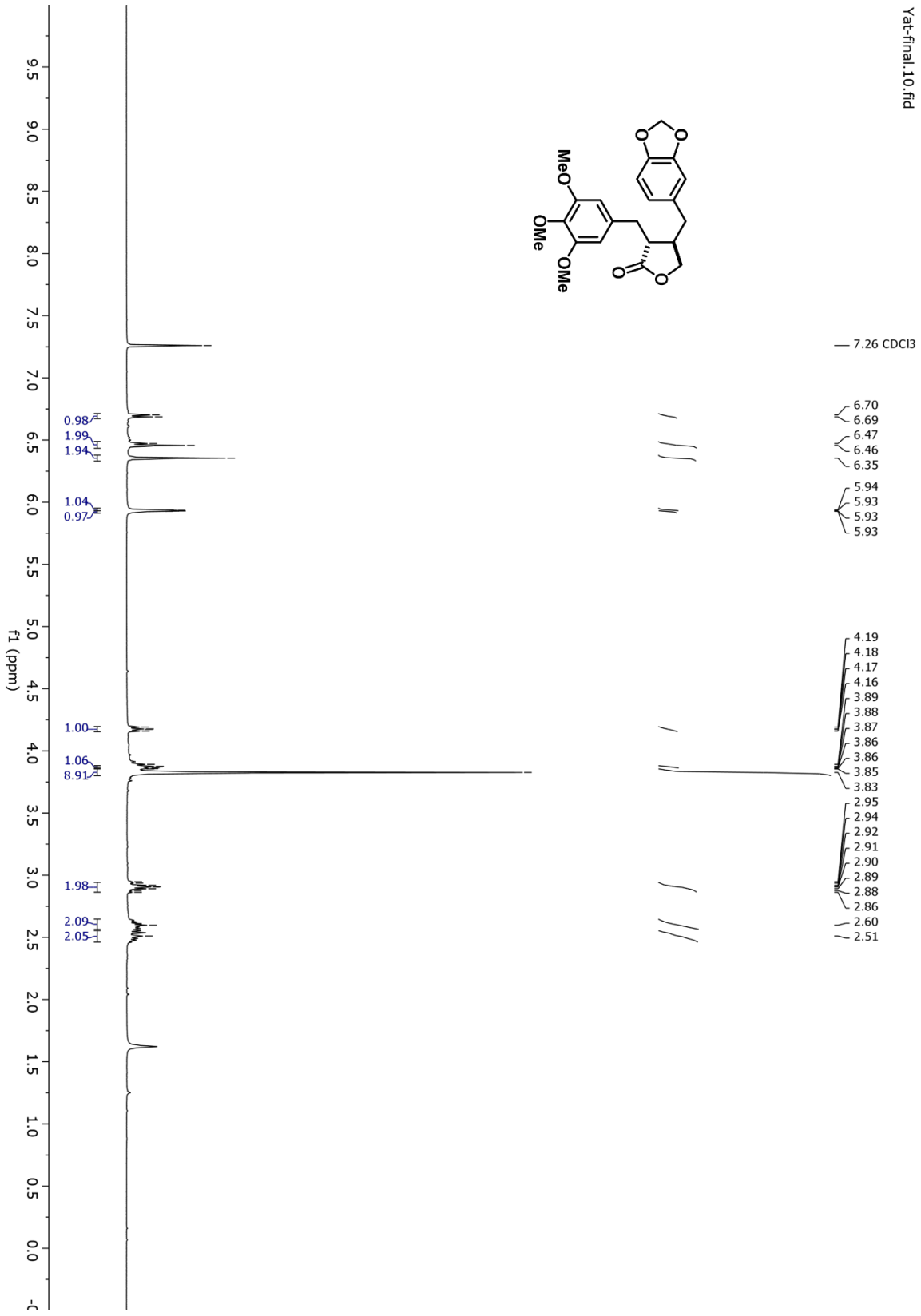

^{13}C-NMR (11)

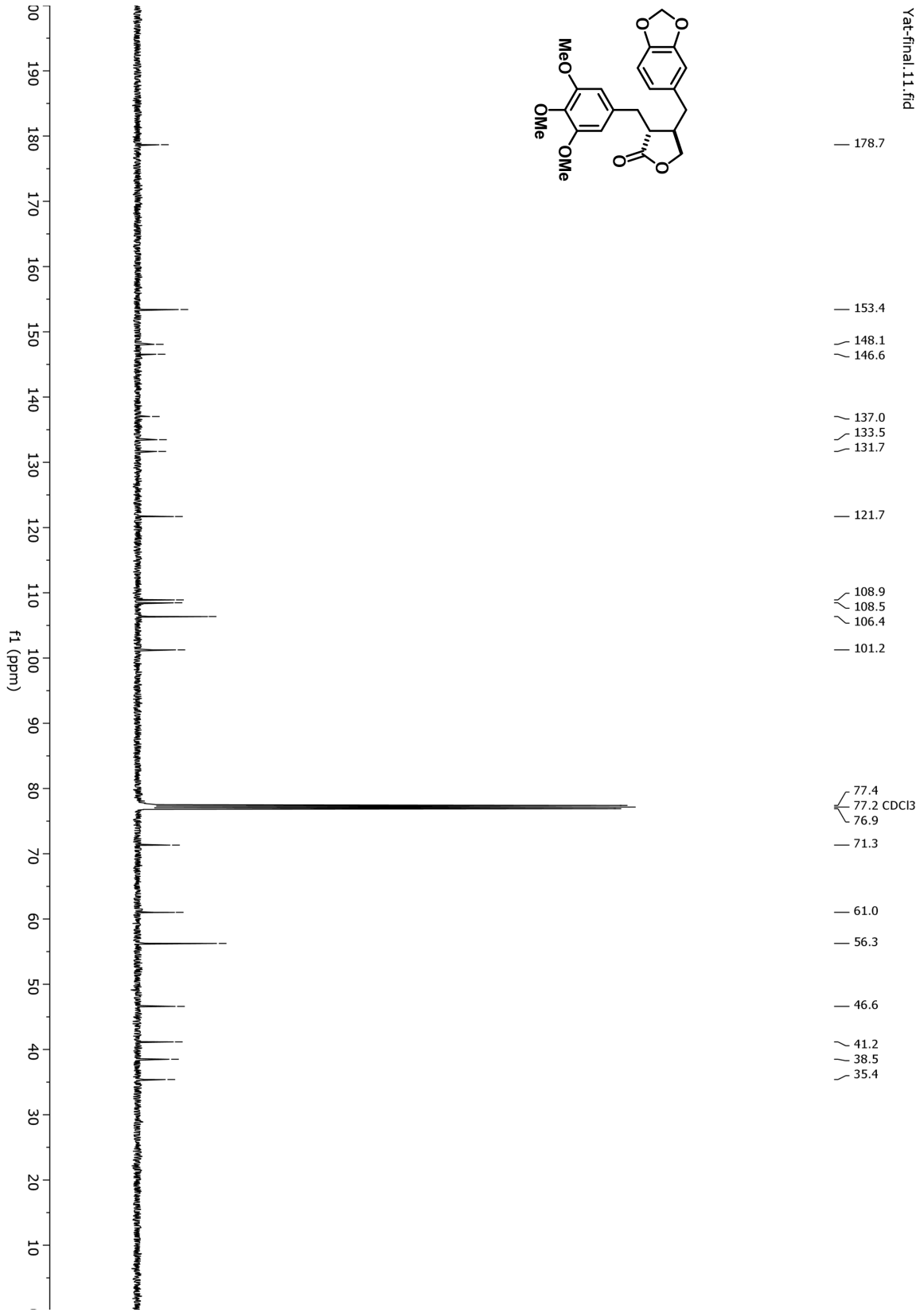
Yat-final.11.fid
MeO
OMe
OMe
178.7
153.4
148.1
146.6
137.0
133.5
131.7
121.7
108.9
108.5
106.4
101.2
77.4
77.2 CDCl3
76.9
71.3
61.0
56.3
46.6
41.2
38.5
35.4
f1 (ppm)

Appendix A.12 ^{1}H-NMR (12)

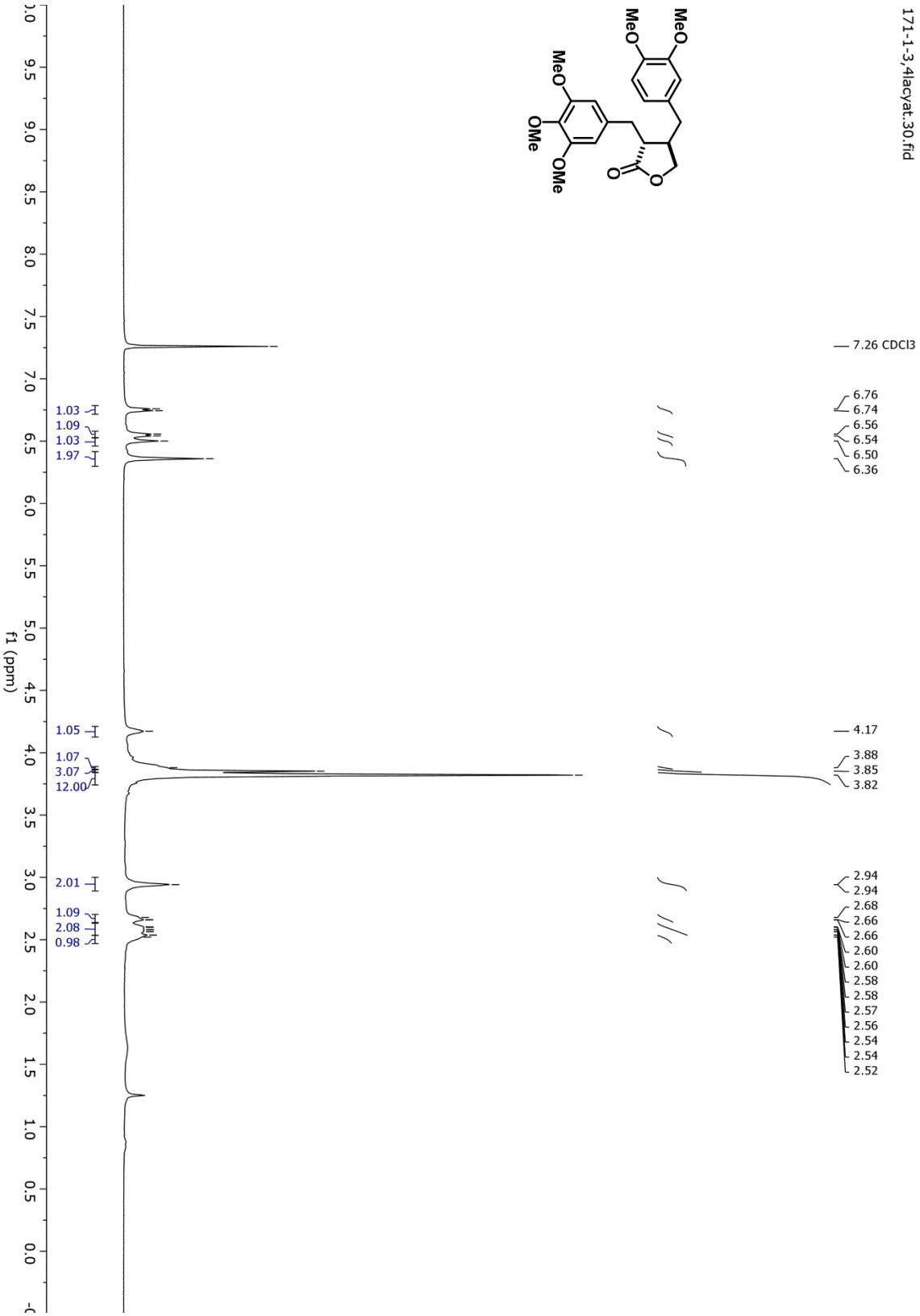

^{13}C-NMR (12)

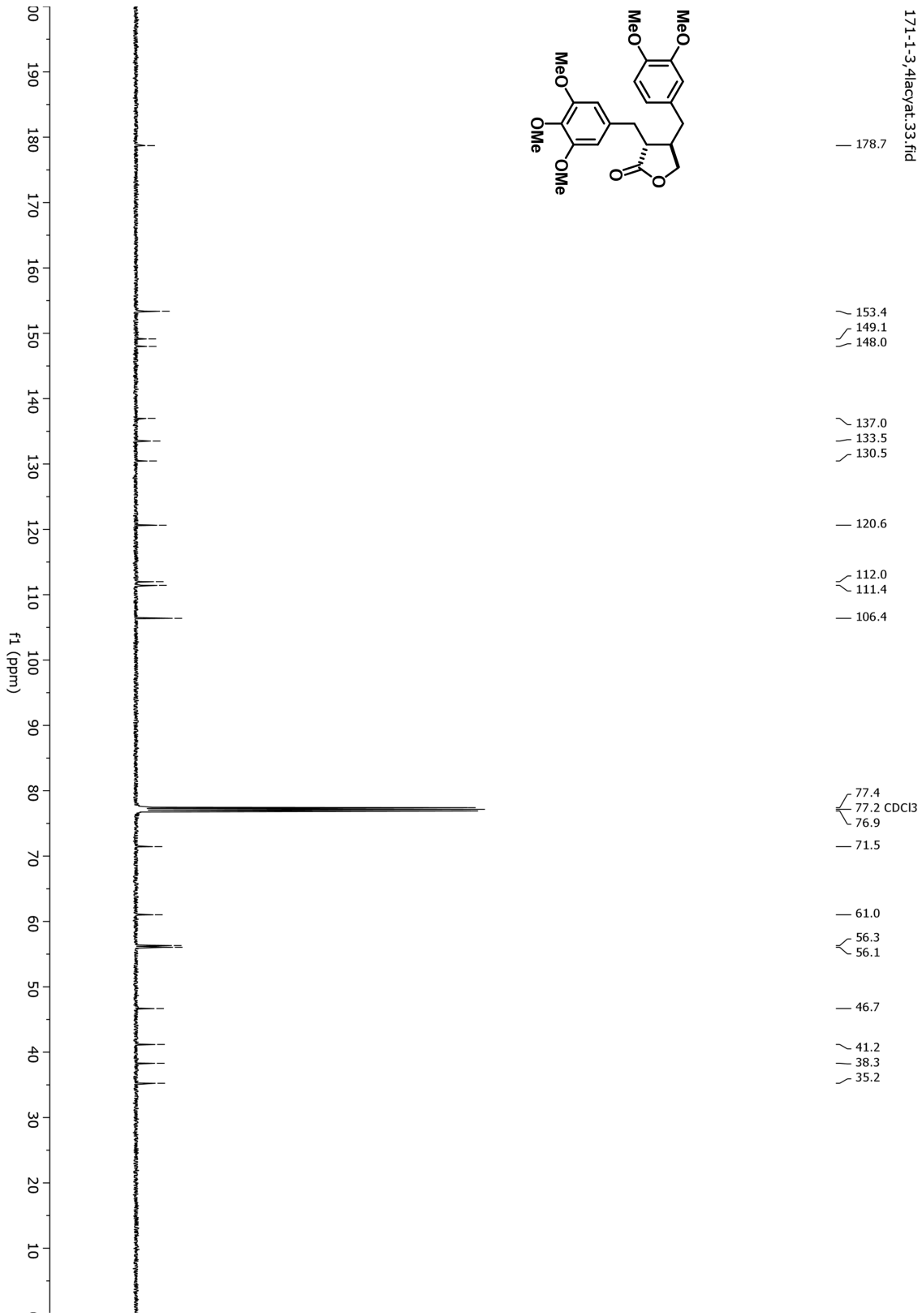
171-1-3,4lacyat.33.fid
MeO
MeO
MeO
OMe
OMe
O
O
178.7
153.4
149.1
148.0
137.0
133.5
130.5
120.6
112.0
111.4
106.4
77.4
77.2 CDCl3
76.9
71.5
61.0
56.3
56.1
46.7
41.2
38.3
35.2
f1 (ppm)

Appendix A.13 ^{1}H-NMR (13)

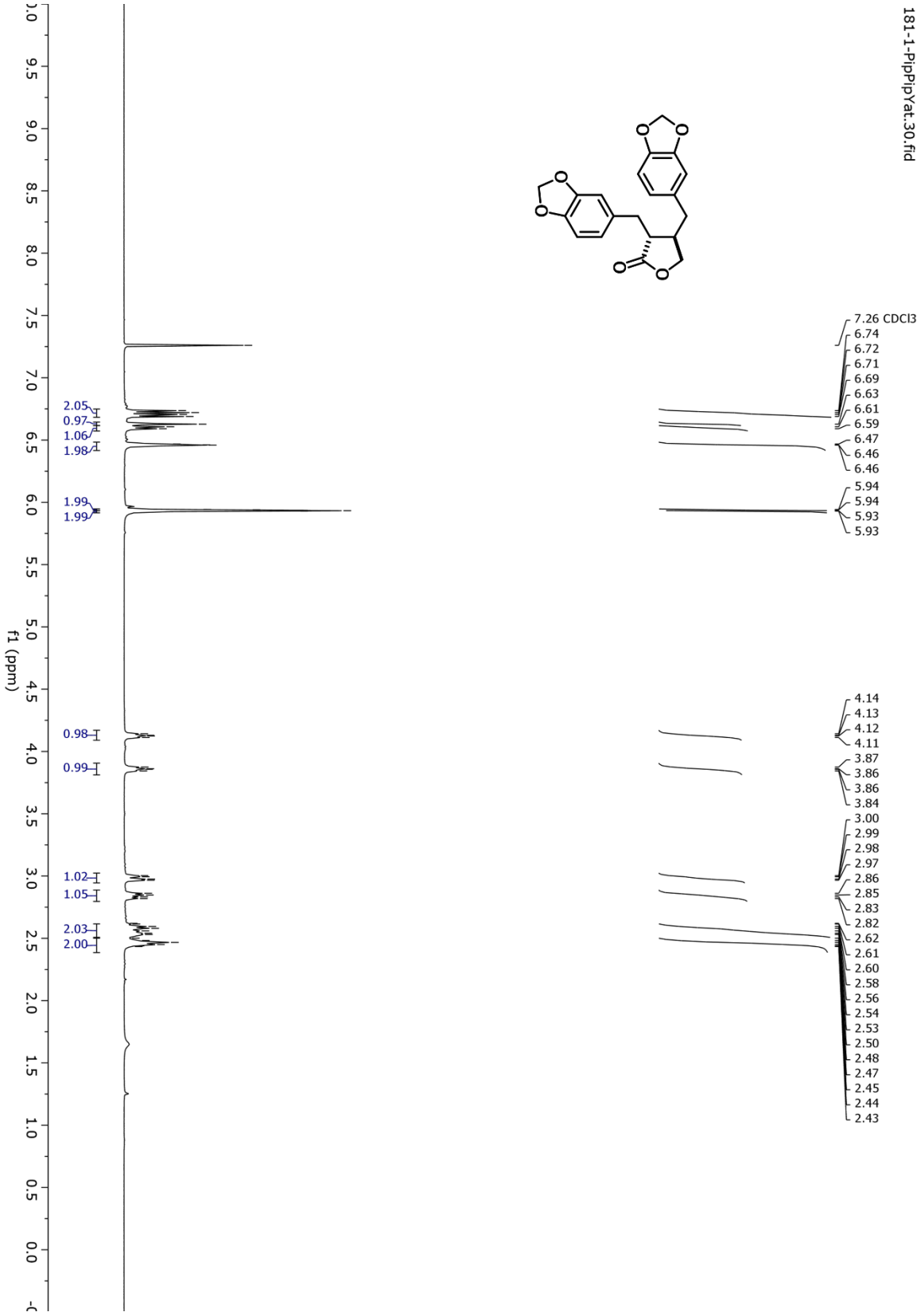

^{13}C-NMR (13)

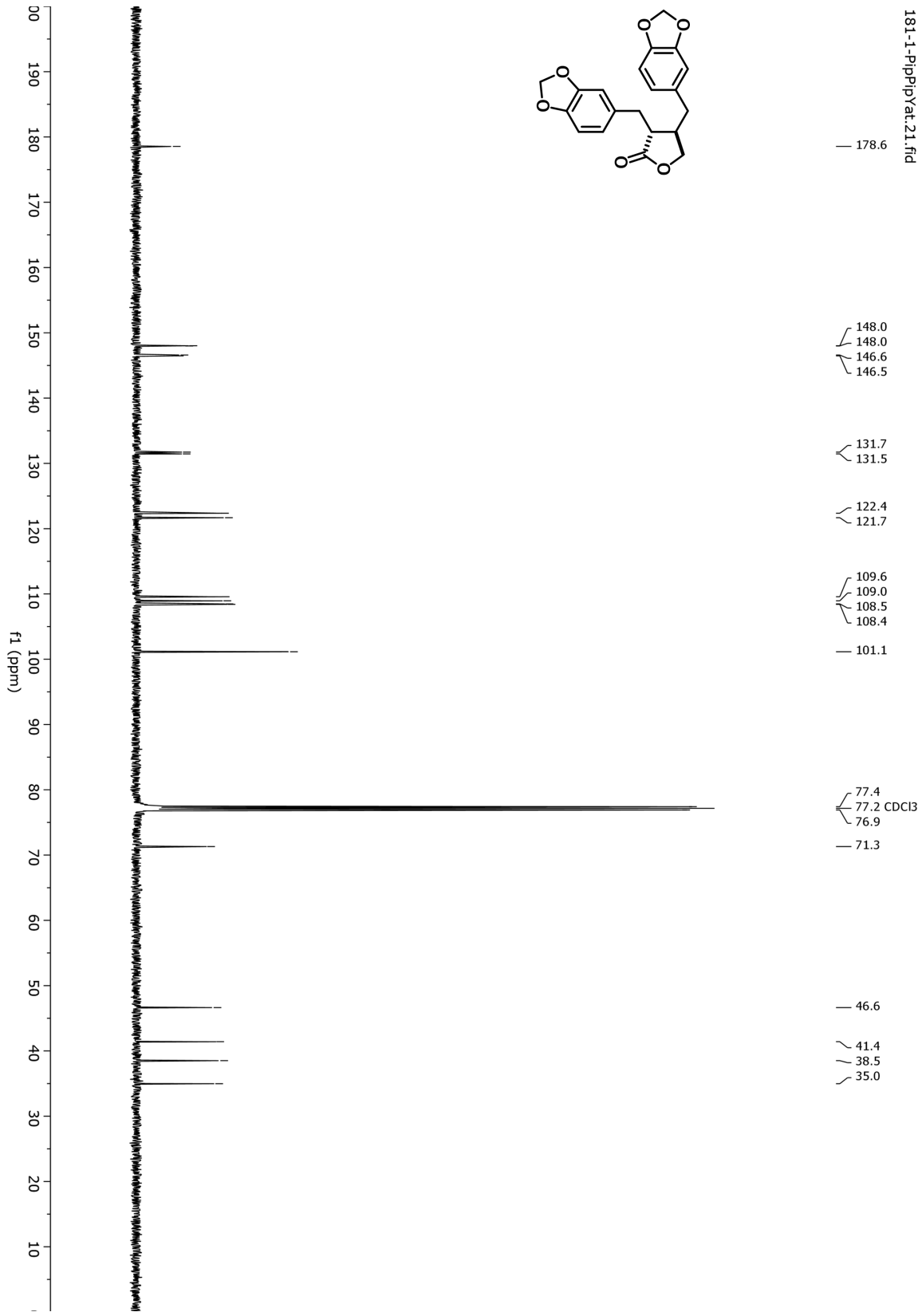
181-1-PipPipYat.21.fid
178.6
148.0
148.0
146.6
146.5
131.7
131.5
122.4
121.7
109.6
109.0
108.5
108.4
101.1
77.4
77.2 CDCl3
76.9
71.3
46.6
41.4
38.5
35.0
f1 (ppm)

Appendix A.14 ^{1}H-NMR (14)

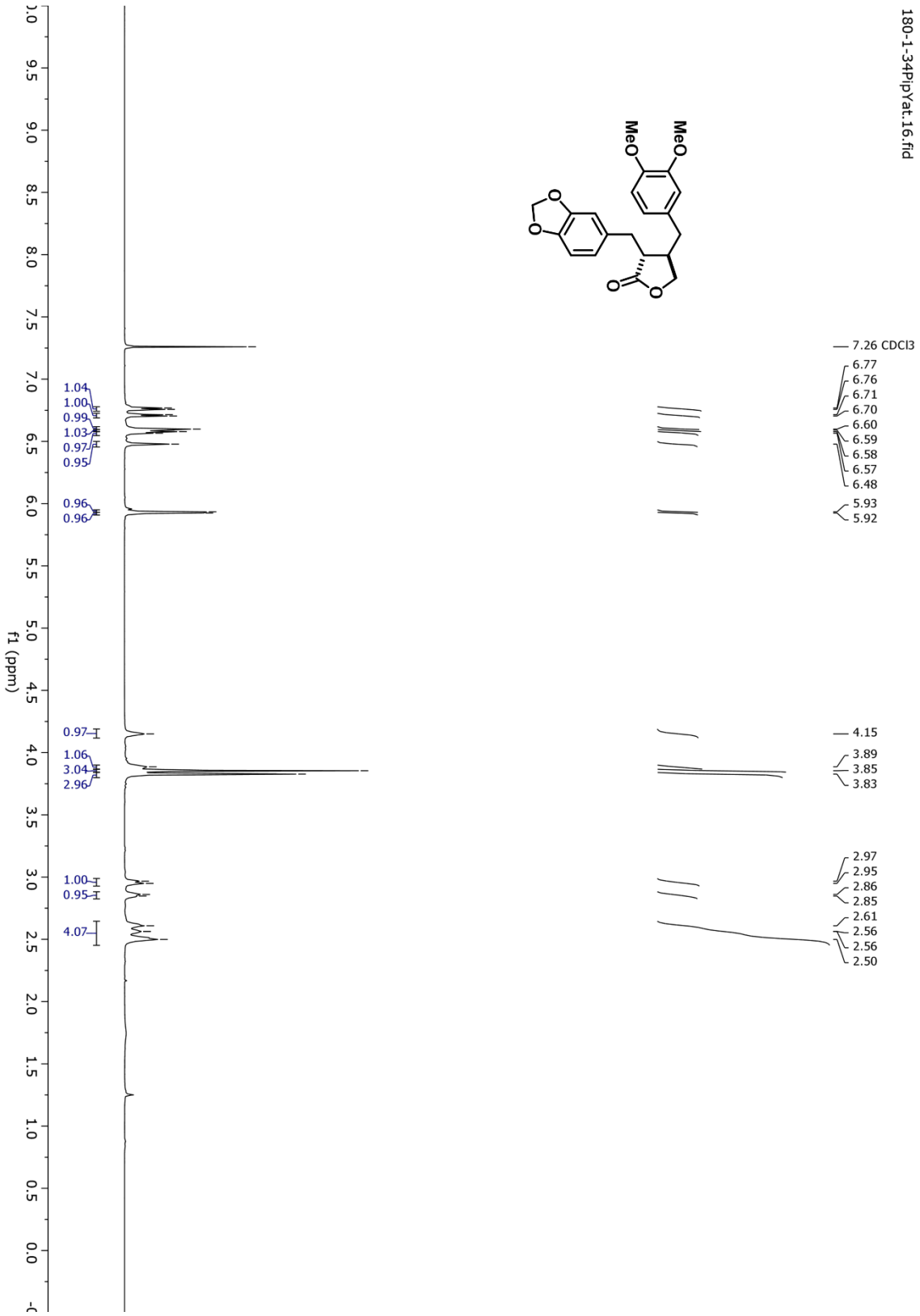

^{13}C-NMR (14)

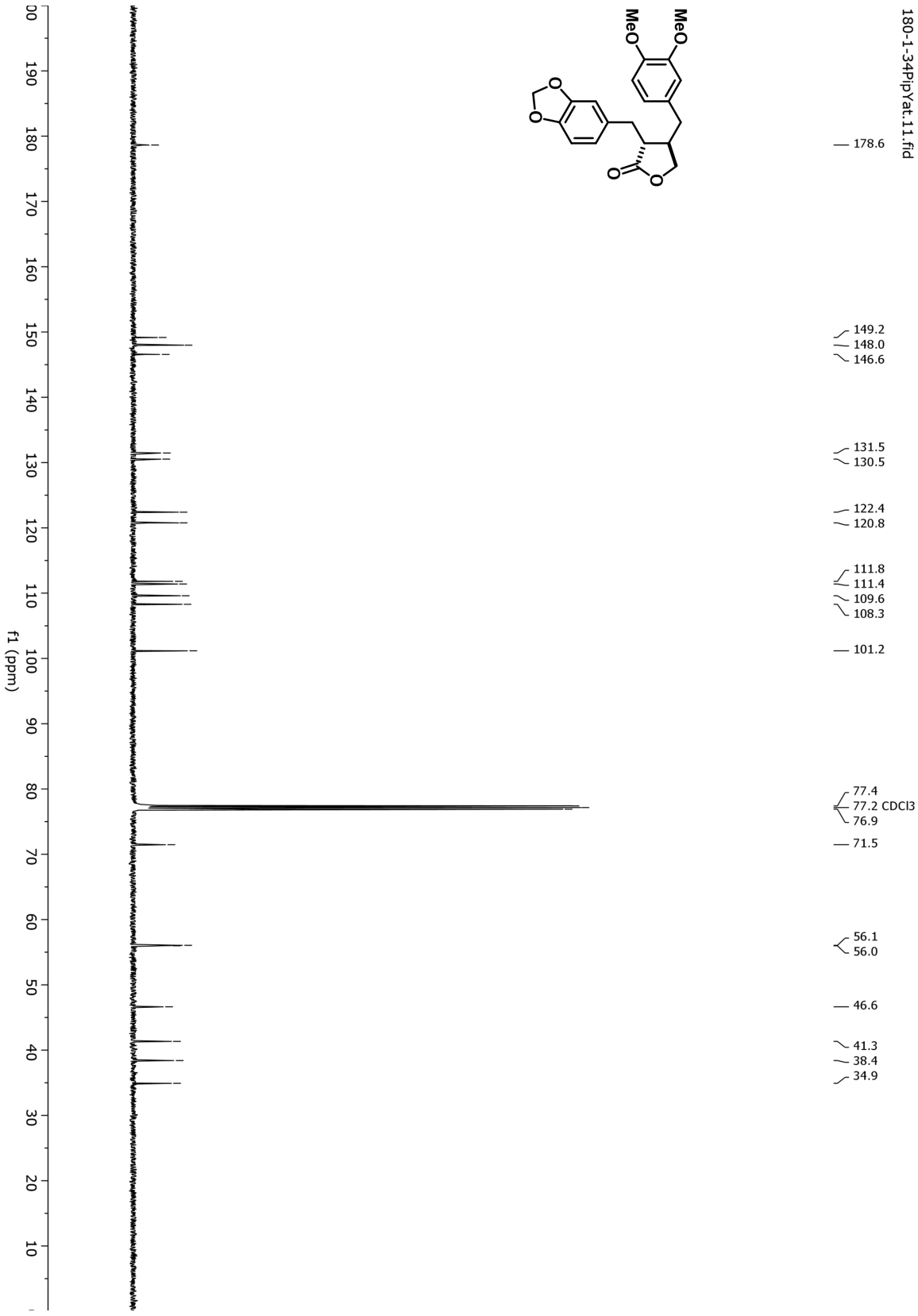
180-1-34PipYat.11.fid
MeO
MeO
O
O
O
O
178.6
149.2
148.0
146.6
131.5
130.5
122.4
120.8
111.8
111.4
109.6
108.3
101.2
77.4
77.2 CDCl3
76.9
71.5
56.1
56.0
46.6
41.3
38.4
34.9
f1 (ppm)

Appendix A.15 ^{1}H-NMR (15)

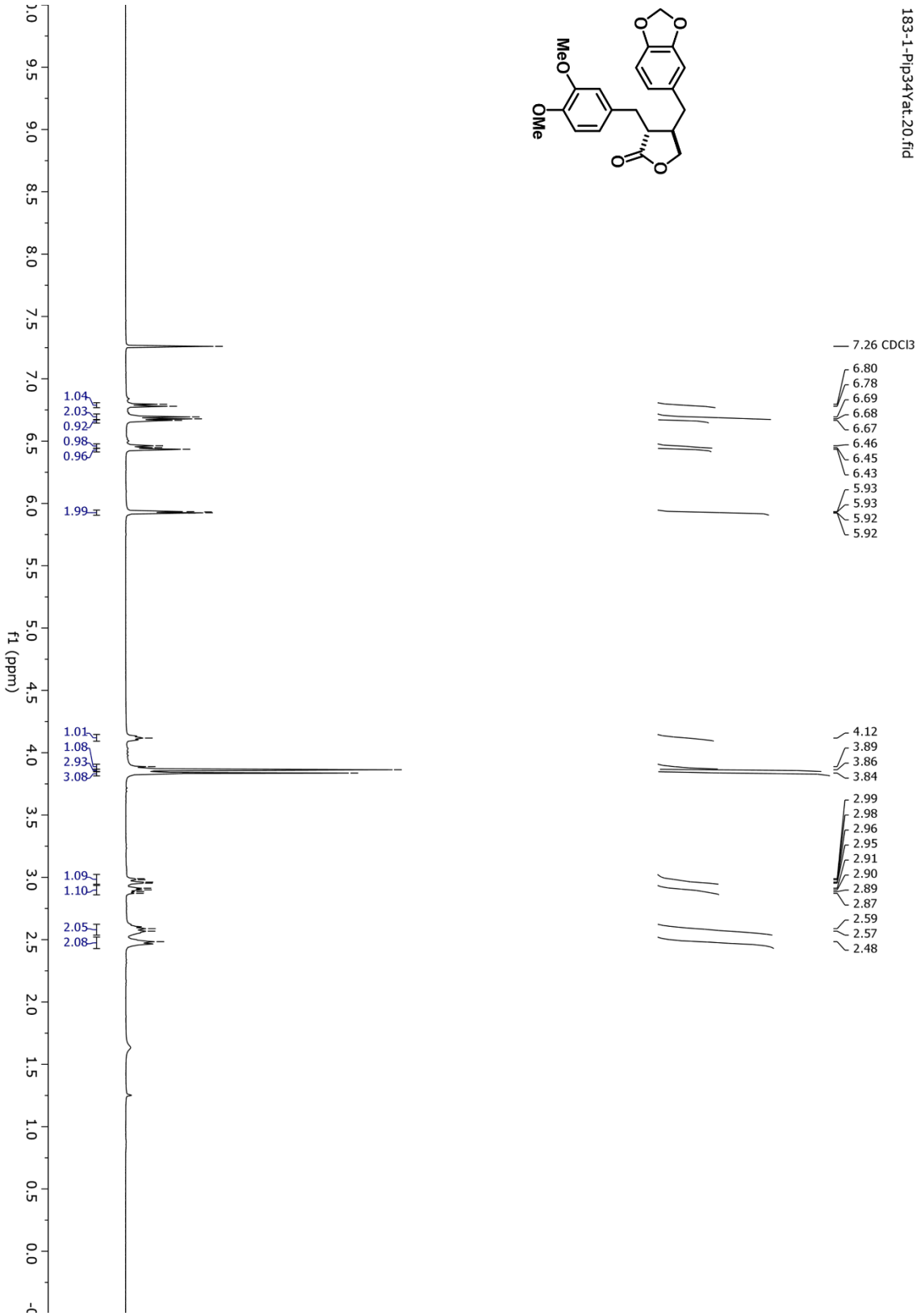

^{13}C-NMR (15)

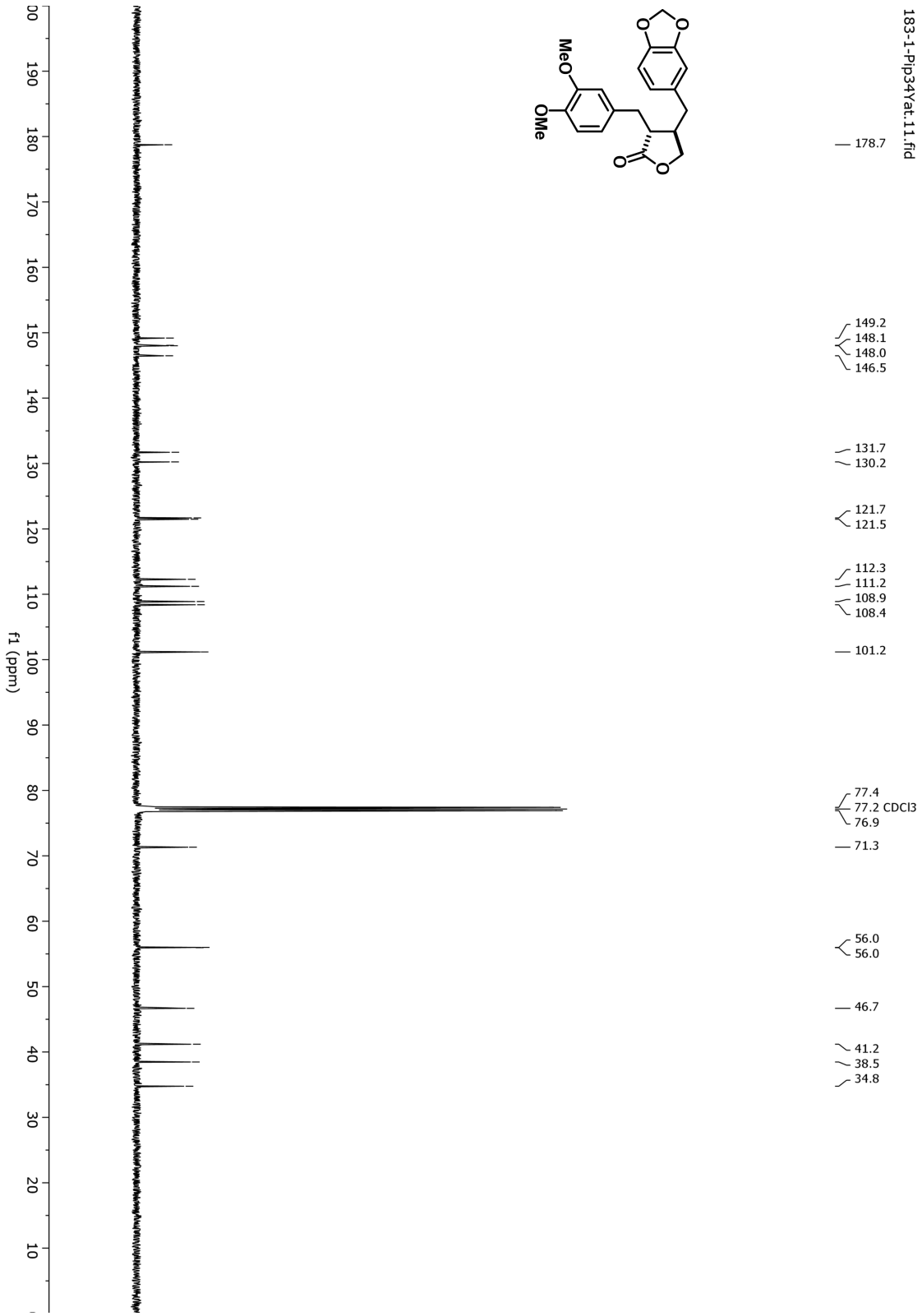
183-1-Pip34Yat.11.fid
MeO
OMe
178.7
149.2
148.1
148.0
146.5
131.7
130.2
121.7
121.5
112.3
111.2
108.9
108.4
101.2
77.4
77.2 CDCl3
76.9
71.3
56.0
56.0
46.7
41.2
38.5
34.8
f1 (ppm)

Appendix A.16 ^{1}H-NMR (16)

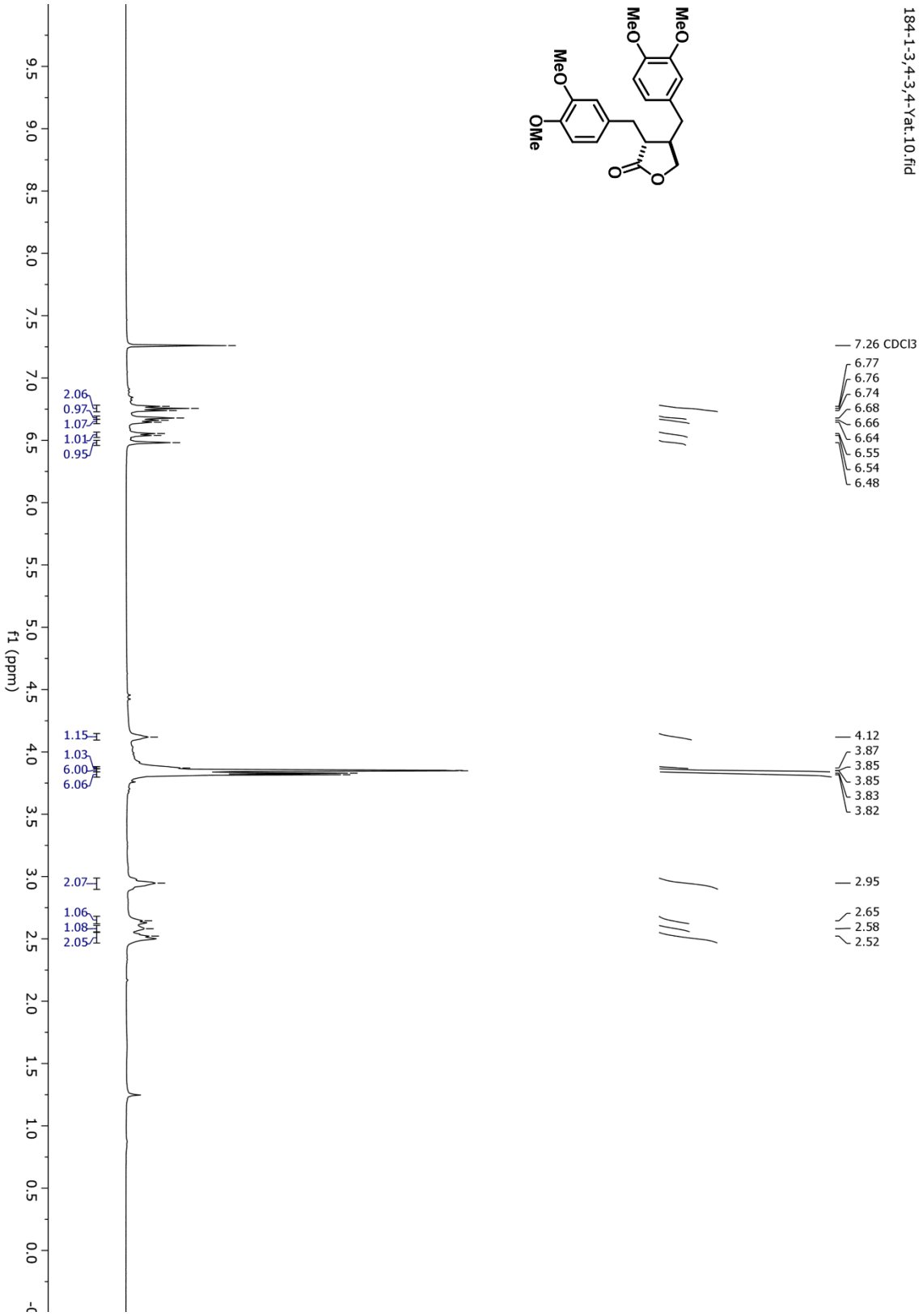

^{13}C-NMR (16)

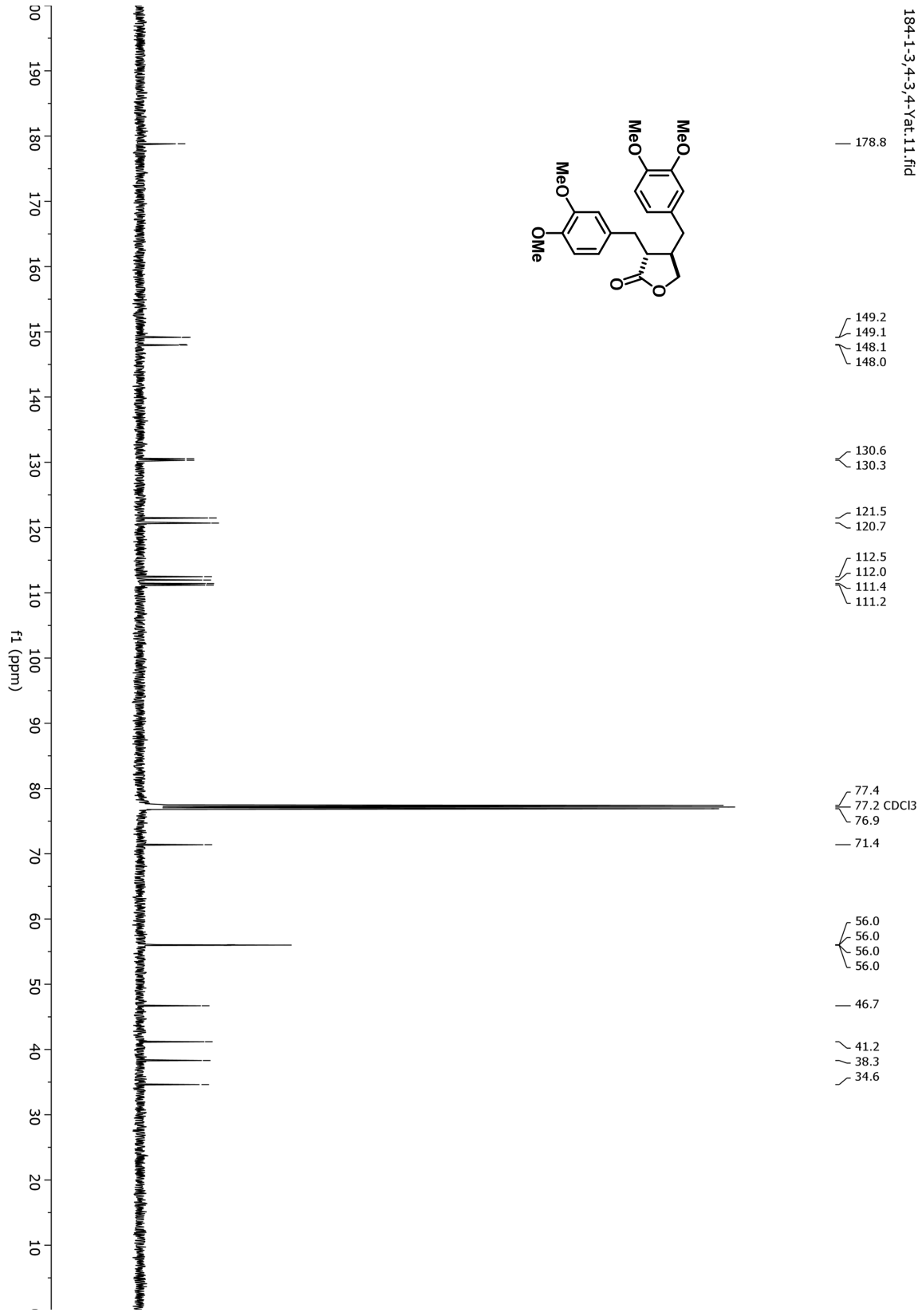
184-1-3,4-3,4-Yat.11.fid
MeO
MeO
MeO
OMe
O
O
178.8
149.2
149.1
148.1
148.0
130.6
130.3
121.5
120.7
112.5
112.0
111.4
111.2
77.4
77.2 CDCl3
76.9
71.4
56.0
56.0
56.0
56.0
46.7
41.2
38.3
34.6
f1 (ppm)

Appendix A.17 ^{1}H-NMR (17)

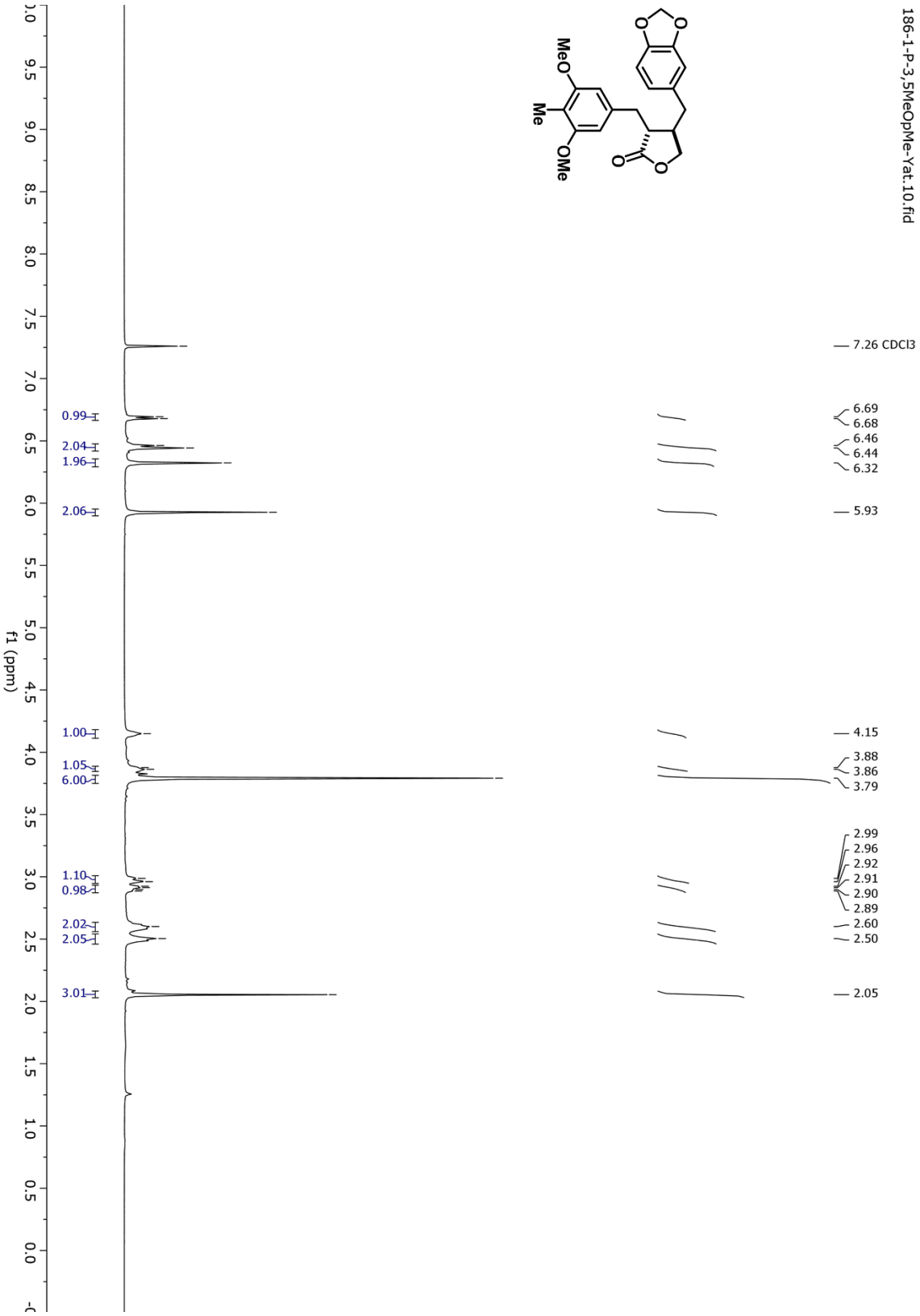

^{13}C-NMR (17)

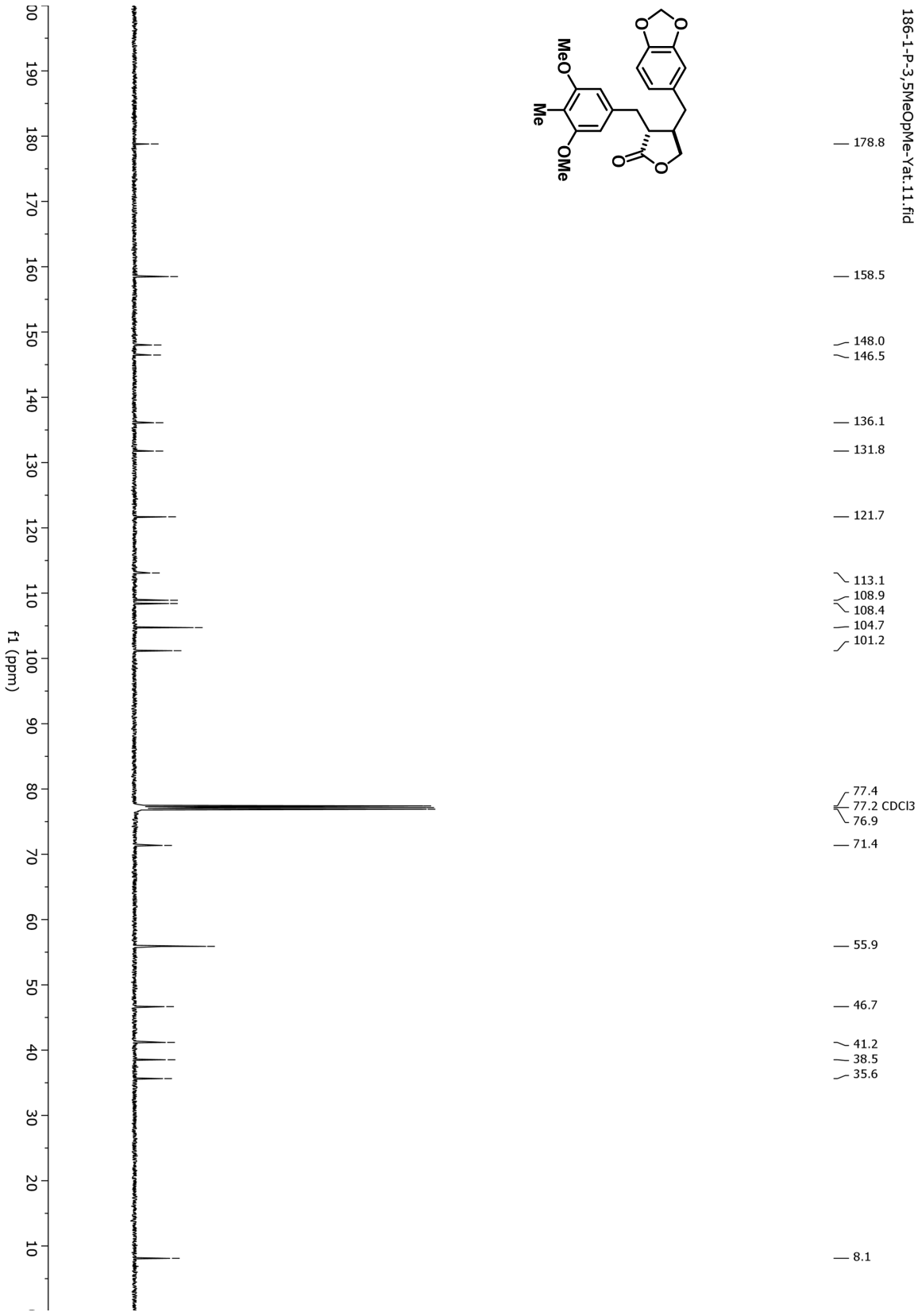
MeO
Me
OMe
O
O
O
O
186-1-P-3,5MeOpMe-Yat.11.fid
178.8
158.5
148.0
146.5
136.1
131.8
121.7
113.1
108.9
108.4
104.7
101.2
77.4
77.2 CDCl3
76.9
71.4
55.9
46.7
41.2
38.5
35.6
8.1
f1 (ppm)

Appendix A.18 Numbered Compounds

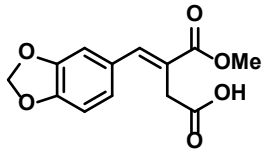

1

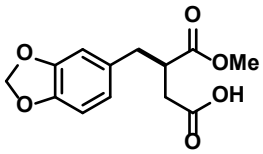

2

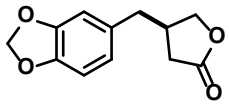

3

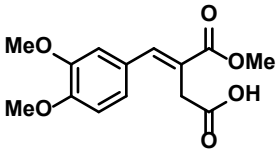

4

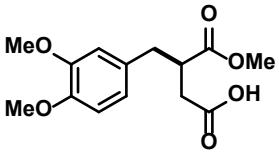

5

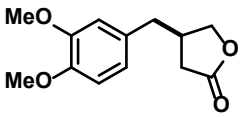

6

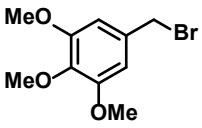

7

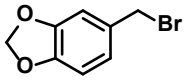

8

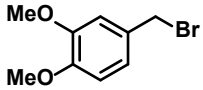

9

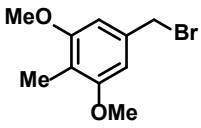

10

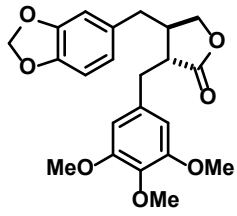

11

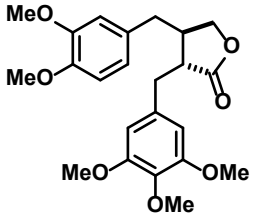

12

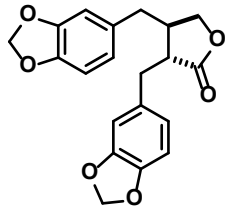

13

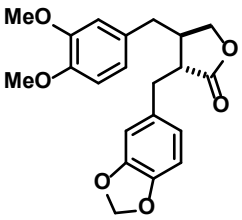

14

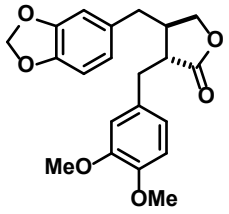

15

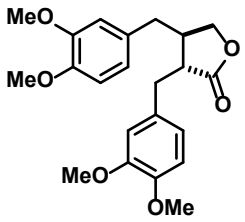

16

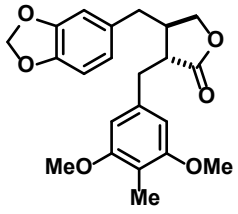

17

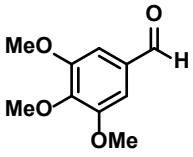

18

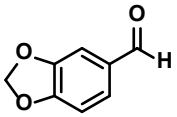

19

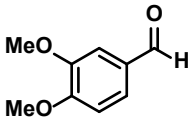

20

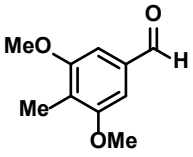

21

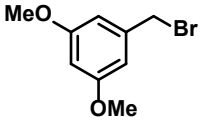

22